Higher-order linked interpolation in moderately thick plate and facet shell finite elements

Ribarić, Dragan

University of Rijeka,

Faculty of Civil Engineering

Dragan Ribarić

Higher-Order Linked Interpolation in Moderately Thick Plate and Facet Shell Finite Elements

Doctoral Thesis

°

Gordan Jelenić

Supervisor

Rijeka, October 2012.

Dragan Ribarić

Higher-Order Linked Interpolation in Moderately Thick Plate and Facet Shell Finite Elements

Doctoral Thesis

Contents:

In memory of

Ph.D. Sergio Blažić (1939. -2000.)

Danijel Šverko (1936. – 2005.)

Grateful to

Jasna and Marin,

my wife and son.

Acknowledgement. *The results shown here have been obtained within the scientific project No 114-0000000-3025: 'Improved accuracy in non-linear beam elements with finite 3D rotations' financially supported by the Ministry of Science, Education and Sports of the Republic of Croatia.*

1. Abstract

In here proposed thesis, the use of higher-order linked interpolation in the design of plate and facet shell finite elements is analysed for elastic behavior. In the Timoshenko (thick) beam elements linked interpolation completely eliminates the shear-locking problem and is capable of returning the exact result for arbitrary polynomial loading. Here, the basis for development of higher-order Mindlin plate and shell elements is found in the analogy between the Timoshenko beam theory and the Mindlin plate theory. The aim of the proposed thesis is to validate the approach not only on low-order elements, which has been already extensively studied by various authors, but also on higher-order elements to improve the accuracy of the method and to demonstrate that they are competitive to other elements from literature. The results obtained on standard test examples are compared and numerically assessed against the reference results from literature and from the finite-element programme *FEAP*, using various mesh densities and various order of interpolation. On this basis, the new family of facet shell elements are also developed, analysed, compared and assessed against the elements from literature.

Key words: Finite element method, Mindlin plate theory, linked interpolation, higher-order elements, shell elements.

Sažetak

U ovoj dizertaciji, analizirana je primjena vezane interpolacije višeg reda u modeliranju ploča i ravnih ljuski za elastična ponašanja modela konstrukcija. Kod Timošenkovih (srednje debelih) grednih elemenata vezana interpolacija u potpunosti eliminira problem 'shear-lockinga' i sposobna je proizvesti točno rješenje za proizvoljno polinomno opterećenje. Polazište za razvoj elemenata za Mindlinove ploče i ravne ljuske je u analogije između Timošenkove teorije greda i Mindlinove teorije ploča. Cilj je predložene teme da afirmira pristup ne samo na elementima nižeg reda, što je već često primjenjeno kod različitih autora, nego i na elementima višeg reda kako bi se povećala točnost metode, te dokazala kompetitivnost naspram drugih elemenata iz literature. Dobiveni rezultati na standardnim primjerima uspoređeni su s referentnim rezultatima iz literature, te s rezultatima iz *FEAP* programa (Finite Element Analysis Program), na mrežama različite gustoće, te uz pomoć interoplacija različitog reda. Na toj osnovi razvijeni konačni elementi primjenjeni su i na ravne ljuske, te uspoređeni sa sličnim elementima iz literature u cilju njihova vrednovanja.

Ključne riječi: metoda konačnih elemenata, Mindlinova teorija ploča, vezana interpolacija, elementi višeg reda, elementi za ljuske.

2. Introduction

The subject of bending of plates and its extension to shells was one of the first to which the finite element method was applied in the early 1960s [1]. In contrast to the problem of bending of beams and frames, which was thoroughly theoretically studied and the solution methods developed, bending of plates could be analytically solved only in a limited number of simple boundary situations, and even then most often formed as a series of polynomial or trigonometric functions. And yet, plates and shells are very interesting structural types, because they often make the most natural choice that can efficiently cover operational hollow spaces. However, the plate and especially the shell forms are very seldom geometrically simple. For this reason, appropriate solution methods for arbitrary shaped planes and domes with arbitrary supporting conditions were being extensively developed throughout the 20th century. An efficient solution method was found quite early in the finite element technique [1], but only introducing the computer technology made it possible to solve the practical problems with sufficient accuracy.

Plates and shells belong to a particular class of 3D bodies for which two dimensions are dominant comparable to the third one (thickness) and either belong to a plane (plates) or are curved in one or two directions (shells). The third dimension is very small compared to the other two dimensions, so that the stresses across the thickness may be represented with the stress resultants in form of in-and out-of-plane forces and bending moments.

The finite element method as the most desirable method for solving the plate and shell problems is a procedure based on dividing a continuum into a set of segments ('finite elements') [1]. The elements are assumed to be interconnected at the discrete number of nodal points placed on their boundaries and in their interior. The displacements and, in plates and shells, the rotations of these nodal points are the basic unknown parameters of the problem. A set of functions should be chosen to define uniquely the displacement and rotations fields within each element and on its boundaries in term of the nodal displacements and rotations. These functions must define uniquely the state of strain within the element and together with the constitutive properties of the material they also uniquely define the state of stress throughout the element. A system of the resulting forces acting at the nodes is determined from this stress state that balances the boundary and any distributed loads, resulting in a system of equations from which the nodal parameters can be obtained. The concept is quite simple, but many difficulties have been met with and overcome in its application and the research in modeling plates and shells has remained active to the present day.

In this thesis, we propose a new idea for developing the plate and shell elements by introducing a family of interpolation functions for displacement fields of arbitrary order with special capabilities that follow from the beam element analysis and involve the displacement parameters as well as the rotational parameters at the nodal points.

The idea of linking the displacement field to the rotations of the cross-sections has been often studied and thoroughly investigated and exploited in finite-element applications of the Mindlin moderately thick plate theory [1-16]. It has been found out

that the idea on its own cannot eliminate the problem of shear locking even though this result may be achieved for the Timoshenko beam elements [1, 17-23]. Different improvements have been proposed by different authors, which involve adjusted material parameters [24] or the assumed or enhanced strain concepts [2,14,15,25] or are based on the use of mixed and hybrid approaches [3,6,7,9,11,12].

The elements designed to solve the Kirchhoff plate problem [1,26,27] have the whole deformation expressed with just one unknown field, namely the lateral displacement of the plate mid-surface w. In the Kirchhoff theory, there are no shear strains and as a result any interpolation of this field has to satisfy C_1 continuity, because the strains within the element are expressed via the second derivatives of w. The determination of suitable shape functions is thus relatively demanding and slope continuity is required on the interfaces between adjacent elements. With this, mathematical and computational difficulties rise disproportionately fast.

On the other hand, the elements designed to solve the Mindlin plate problem [1,3,7] in which the sear strains in the direction orthogonal to the mid-surface do exist and are assumed as constant through the thickness, have both the displacement w and the rotations θ_x and θ_y interpolated. As a result the strains are expressed using just the first derivatives of these fields. C_0 continuity for shape functions is then sufficient but locking effects are usually observed for the thin limit cases, in which the rotations are expected to approach the first derivatives of the displacement field.

Various element types have been developed to overcome these difficulties resulting in new techniques and algorithms [8-16]. As examples, some of these elements will be described here in more detail.

For the thin-plate problems, the DKT–elements (discrete Kirchhoff theory elements) [e.g. 10] have to be mentioned for their efficiency. In defining their deformation, both the nodal displacement and the rotations are used as the parameters for interpolation, like in the Mindlin plate elements. At first, both the vertex nodes and the mid-side nodes are considered, but then the mid-side node parameters are eliminated from the final stiffness matrix by constraining shear strain to zero (the Kirchhoff assumption [2]) at certain discrete points (usually the Gauss integration points). Both triangular and quadrilateral elements can be modeled in this way. Various types of DKT-elements can be constructed depending on the position of the constraint points and on the parameters to be eliminated [1].

The early Mindlin plate elements are isoparametric quadrilaterals [1], in which the same integration is used to define both the geometry and deformation and with C_0 continuity they are able to describe constant strain states necessary for consistency of the model. These elements tend to lock when approaching thin limit (when the thickness-to-span ratio tends to zero) if a lowest order integration is applied. An improvement is observed if reduced quadrature is selectively applied in integration of the shear terms [1].

Another approach to eliminating the shear-locking problems is the so-called mixed formulation. In the mixed formulation [1], together with the displacement and rotation

fields, the shear force is interpolated independently and discontinuously over the element edges. By imposing stationarity of an appropriately defined functional, a mixed element matrix is formed with the displacement-based parameters and the shear-force parameters. The latter may be eliminated to form the condensed element stiffness matrix. To perform the condensation, certain conditions have to be fulfilled: the matrix block associated with the shear force must approach zero in the thin limit situation and the so-called count conditions [1,3,7] have to hold: the sum of the displacement and rotation parameters has to be greater than the number of the shear-force parameters and the number of shear-force parameters has to be greater than the number of the displacement parameters in an element. It turns out that the reduced selective integration is equivalent to the mixed form with a discontinuous shear force [26].

Using mixed formulation, a new class of elements has been designed introducing additional 'bubble modes' for the rotation field [1]. These 'bubble modes' can be interpreted as enhanced strain modes in shear and bending [3,7] and they are useful in satisfying the mixed count conditions, making this class of elements very robust.

Introducing linked interpolation [3,6,7,12,24,28] in the form presented in this thesis on the basic triangles and quadrilaterals, together with the bubble modes, another class of mixed elements may be derived, which has excellent performance compared to the above element classes. Examples of this class of elements are the Auricchio and Taylor *T3BL*, *T3-LIM* and *Q4-LIM* elements presented in detail in 5.4.2.

There also exist other approaches aimed at removing the shear-locking problem and improving accuracy of the solution in general. Tessler and Hughes [24], for instance, introduce a correction coefficient to adjust the shear energy in order to remove locking. With their technique, however, the correction coefficient becomes a new user-defined parameter without a proper physical justification.

In the so-called assumed strain approaches (see e.g. Ibrahimbegović [2] and Chen and Cheung [14-16]) the shear strain is deliberately interpolated on its own in order to provide the required lower order distribution than that obtained from the kinematic equations. This technique is effectively capable of reproducing the results of the mixed approaches, even though it lacks the proper mathematical background present in those approaches.

A related method evolves from the so-called enhanced strain technique of Simo and Rifai [25], designed to offer a variational basis stemming from the three-field Hu-Washizu functional. There also exist various hybrid approaches (see e.g. de Ubertini and Miranda's [9]) in which the stress resultants (and sometimes also the stress-couple resultants) are prescribed in a way which satisfies the differential equilibrium equation within an element.

In this thesis we generalise the ideas given in [18] to the plate problem. Remaining firmly in the framework of the standard displacement-based design technique, we shall derive the families of triangular and quadrilateral thick plate and shell elements by extending the higher-order linked interpolation functions developed for the Timoshenko beams. Within this approach, the kinematic and constitutive equations of

the problem are satisfied in the strong sense, while the equilibrium equations are satisfied in the weak sense with the unknown displacement and rotation fields as the only interpolated quantities. Even though the Mindlin theory of thick plates may be regarded as a 2D generalisation of the Timoshenko theory of thick beams, the differential equations of equilibrium for thick plates cannot be solved in terms of a finite number of parameters and so, in contrast to beams, there does not exist an exact finite-element interpolation.

In contrast to most of the existing displacement-based approaches, which base their developments on constraining the shape functions for the displacement and the rotation fields so as to produce a required distribution of the shear strains [8,10,24,29], here we extend the higher-order linked interpolation functions developed for the Timoshenko beam to the plate structures and investigate the results and their relationships with the known approaches. For example, in [1,3,30] such interpolation has been used to formulate three-node triangular and four-node quadrilateral thick plate elements, while in [2,6] a six-node triangular and an eight-node quadrilateral elements have been proposed. A family of triangular elements designed in this way has been proposed in [8].

Generalizing this idea to arbitrary curvilinear quadrilateral and triangular shapes (on higher order elements) is non-trivial and special care needs to be taken for such elements to satisfy the standard patch tests. We present a manner in which these new elements may be properly developed, which involves additional internal displacement

degrees of freedom as in [29] and we conduct some numerical tests which demonstrate the potential of this approach, in particular for the higher-order elements.

After presenting briefly the Timoshenko beam theory an the Mindlin plate theory in Section 3, in Section 4 we present the family of interpolation functions for the Timoshenko beam elements and specifically analyse the solution for two-, three- and four-node beam elements and appropriate load conditions.

In Section 5 we present the families of triangular and quadrilateral plate elements beginning with the basic triangular three-node element and the quadrilateral four-node element, for which the constant shear strain condition imposed on the element edges is known to lead to an interpolation for the displacement field which is dependent not only on the nodal displacements, but also on the nodal rotations around the in-plane normal directions to the element edges. The same result may be obtained by generalising the linked interpolation for beams [18] to 2D situations. This approach enables a straightforward generalisation of the linked-interpolation beam concept to higher-order triangular plate elements leading to additional internal degrees of freedom which do not exist in the beam elements. The matrix element formulation is presented in a general form. We next compare the presented elements with some similar elements from literature. As an alternative, for instance, imposing a shear-strain distribution of a specified order over the element domain may be achieved following the approach presented in [8] where a family of displacement-based linked-interpolation triangular elements has been derived which, in contrast, does not involve internal degrees of freedom. The patch test is considered as very important for testing

the consistency of elements, ensuring convergence of the finite element solution problem. The necessary condition for convergence is to satisfy constant bending state over the element domain in the mesh limit, and all the presented elements satisfy this condition independently of the patch geometry set. However, all the higher-order elements satisfy even the more rigorous constant shear test exactly. In Section 5 we also conduct numerical tests on the standard benchmark examples for thick plates. A detailed analysis is given for the square, rhombic and circular plate examples both for the thick and for the thin plate.

In Section 6 we explore the possibilities of merging the plate elements developed in Section 5 with the membrane in-plane effects, forming moderately thick facet shell triangular and quadrilateral elements. Some test examples are run with using the developed elements and compared with the SHELL element from FEAP programme of R.L.Taylor [1].

The three-node and four-node elements are very simple to describe in a structural model compared to the higher order elements with ten or sixteen nodes for this reason and thus they are widely used in practical problems. With this in mind, in Section 7 we present an idea of enriching the basic low-order elements with the bubble functions coming from higher order interpolations for displacements and rotations. The new enriched elements are incompatible with adjacent elements except at the nodal points, but they do not contain zero-energy modes and are extremely accurate in describing deformation and stress even in otherwise difficult tests. The numerical results for this type of elements are also given in section 7.

This thesis is concluded by summarising the most important findings in section 8.

3. Differential equations of beam and plate theories

Here we want to outline the differences between beam and plate theories when they are developed just on bending deformations or expanded to the effects of shear and how they can be solved with discretisation techniques via finite element method.

3.1. Timoshenko beam theory

When describing a beam theory a coordinate system must be introduced first. The *x*-coordinate is taken along the length of the beam, *z*-coordinate along the thickness or height of the beam and *y*-coordinate along the width of the beam. The displacements (*u, v, w*) correspond to global coordinates (*x, y, z*) and it is assumed that *v* displacement is always equal to zero, i.e. the applied loading and geometry are such to produce displacements only in *x* and *z* directions.

The simplest beam theory assumes that

$$u(x,z) = -z\frac{dw_0}{dx} \qquad \text{and} \qquad w(x,z) = w_0(x), \tag{1}$$

where w_0 is the transverse deflection of the point $(x,0)$ on the mid-plane of the beam. The displacement field (1) implies plane normal section to remain plane and normal to the deformed line of the mid-plane of the beam (see Fig. 1.a). This theory is called the Euler-Bernoulli beam theory (sometimes just Bernoulli theory) and in it the transverse shear and normal strains are neglected. What follows is that the rotation of the section

can be expressed as:

$$\theta(x) = \frac{u(x,z)}{z} = -\frac{dw_0}{dx} \qquad \text{and} \qquad \gamma(x) = \frac{dw_0}{dx} + \theta(x) = 0 \tag{2}$$

at every beam section.

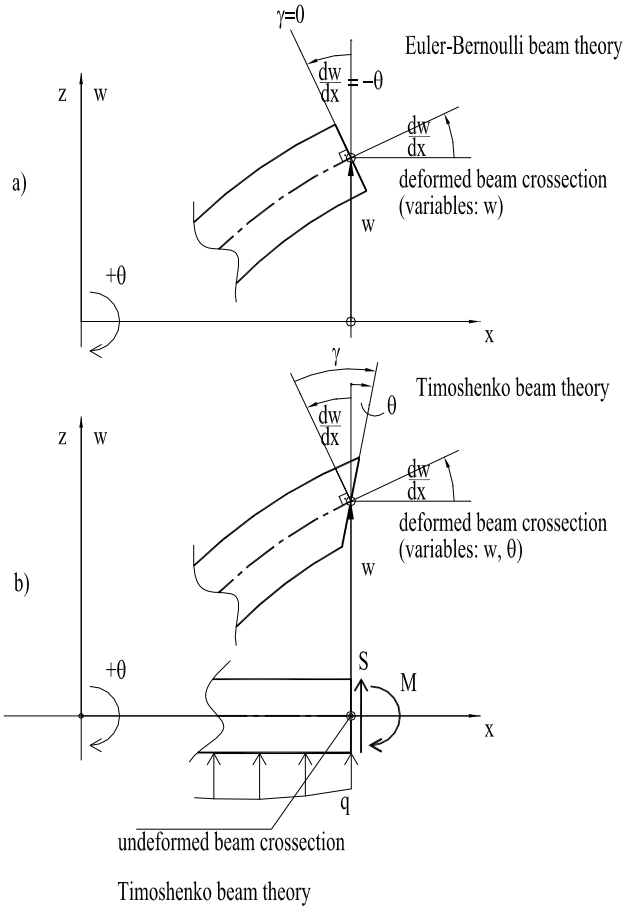

Fig. 1: *Initial and deformed configuration of a thin and of a moderately thick beam*

In contrast to the Bernoulli beam theory, in the Timoshenko beam theory the cross section of a beam also remains planar after the deformation, but not necessarily

orthogonal to the beam centroidal axis at the mid-plane so the horizontal displacement of the point depends on the rotation of the cross section (see Fig. 1.b):

$$u(x,z) = z\theta(x) \qquad \text{and} \qquad w(x,z) = w_0(x)\,. \tag{3}$$

This departure from orthogonality is the shear angle

$$\gamma(x) = \frac{dw_0}{dx} + \theta(x) = w' + \theta\,,$$

where the dash (') indicates a differentiation with respect to the co-ordinate *x*.

After defining the bending moment as a cross-sectional stress-couple resultant with respect to the mid-surface of the section:

$$M(x) = \int_A z\sigma_{xx} dA$$

and the shear force as a shear stress resultant over the section:

$$S(x) = \int_A \tau_{zx} dA\,,$$

equilibrium condition can be expressed as

$$-\frac{dM(x)}{dx} + S(x) = 0 \qquad \text{and} \qquad \frac{dS(x)}{dx} = -q(x)\,. \tag{4}$$

In the latest expression *q(x)* is a distributed transverse load that acts on the centroidal

axis of the beam.

Let the stress resultants M and S be linearly dependent on curvature (change of cross-sectional rotation) and shear angle via

$$M = EI\theta' \quad \text{and} \quad S = GA_s\gamma\,, \tag{5}$$

where EI and GA_s are the bending and shear stiffness, respectively. Introducing (5) into (4) results in the following differential equations:

$$EI\theta''' = -q \quad \text{and} \quad GA_s(w''+\theta') = -q\,. \tag{6}$$

In the case of Euler-Bernoulli theory, where assumptions (2) hold, equations (6) can be expressed as

$$-EIw^{IV} = -q \tag{6a}$$

Here, the index *'IV'* denotes the fourth derivative of the transverse displacement of the centroidal axis with respect to the position on the beam (x-coordinate).

As the Euler-Bernoulli theory is just the limiting case of the Timoshenko theory when γ is approaching to zero, the solution of equations (6) should hold in both cases. Actually, (6) has the following closed-form solution for a polynomial loading q of order n-4 [18]:

$$\theta = \sum_{i=1}^{n} I_i \theta_i \quad \text{and} \quad w = \sum_{i=1}^{n} I_i w_i - \frac{L}{n} \prod_{j=1}^{n} N_j \sum_{i=1}^{n} (-1)^{i-1} \binom{n-1}{i-1} \theta_i , \tag{7}$$

where L is the beam length, θ_i and w_i are the values of the displacements and the rotations at the n nodes equidistantly spaced between the beam ends, I_i are the standard Lagrangen polynomials of order n-1, and $N_j = \frac{x}{L}$ for j=1 and $N_j = 1 - \frac{n-1}{j-1}\frac{x}{L}$ otherwise. In the natural co-ordinate system (bi-unit beam segment domain from ξ_L=-1 to ξ_R=1) with $\xi = \frac{2x}{L} - 1$ the displacement solution reads $w = \sum_{i=1}^{n} I_i w_i - \frac{L}{n} \sum_{i=1}^{n} \frac{\xi - \xi_i}{2} I_i \theta_i$.

3.2. Mindlin plate theory

The plate theories can be based on the same assumptions as the beam theories (whether transverse shear deformation effects are neglected or not). If they are neglected, the theory is a classical plate theory or the Kirchhoff theory [27]. The plate is assumed to be of a uniform thickness h with a mid-surface lying in the horizontal co-ordinate plane and a distributed loading q assumed to act on the plate mid-surface in the direction perpendicular to it. The displacement field is assumed as:

$$u(x,y,z) = -z\frac{dw_0}{dx}, \quad v(x,y,z) = -z\frac{dw_0}{dy} \quad \text{and} \quad w(x,z) = w_0(x), \tag{8}$$

where (*u, v, w*) are the displacement components along the (*x, y, z*) coordinate directions, respectively, and w_0 is the transverse deflection of a point on the mid-surface (i.e. *z=0*). As with the beams, the displacement field (8) implies that straight lines normal to the *xy*-plane before deformation remain straight and normal to the mid-surface after deformation. This assumption (the Kirchhoff assumption) neglects both the transverse shear and in-plane effects and deformation is entirely caused by in-plane stretching due to bending.

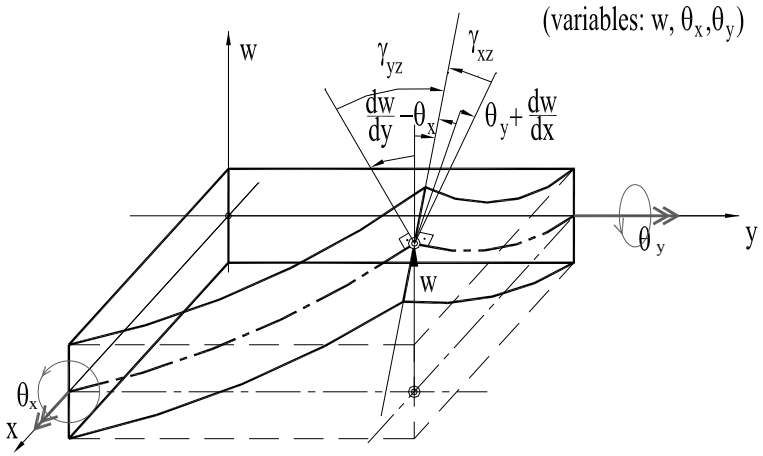

Fig. 2: *Initial and deformed configuration of a moderately thick - Mindlin plate*

There is a number of shear deformation plate theories [31]. The simplest is the first-order shear deformation plate theory also known as the Mindlin plate theory, which is closely related to the Timoshenko beam theory and may be regarded as its generalisation to two-dimensional problems. The displacement field is expressed as:

$$u(x,y,z) = z\theta_y(x,y)\,, \quad v(x,y,z) = -z\theta_x(x,y) \quad \text{and} \quad w(x,z) = w_0(x)\,, \qquad (9)$$

where θ_x and θ_y denote rotations about x and y axes, respectively (Fig. 2).

The changes of the angles which the vertical fibres close with the mid-surface are the shear angles (Fig. 2):

$$\boldsymbol{\Gamma} = \begin{Bmatrix} \gamma_{xz} \\ \gamma_{yz} \end{Bmatrix} = \begin{Bmatrix} \theta_y + \dfrac{\partial w}{\partial x} \\ -\theta_x + \dfrac{\partial w}{\partial y} \end{Bmatrix} = \begin{bmatrix} 0 & 1 \\ -1 & 0 \end{bmatrix} \begin{Bmatrix} \theta_x \\ \theta_y \end{Bmatrix} + \begin{Bmatrix} \dfrac{\partial}{\partial x} \\ \dfrac{\partial}{\partial y} \end{Bmatrix} w = \mathbf{e}\boldsymbol{\theta} + \nabla w \tag{10}$$

while the curvatures (the fibre's changes of rotations) are

$$\boldsymbol{\kappa} = \begin{Bmatrix} \kappa_x \\ \kappa_y \\ \kappa_{xy} \end{Bmatrix} = \begin{Bmatrix} \dfrac{\partial \theta_y}{\partial x} \\ -\dfrac{\partial \theta_x}{\partial y} \\ \dfrac{\partial \theta_y}{\partial y} - \dfrac{\partial \theta_x}{\partial x} \end{Bmatrix} = \begin{bmatrix} 0 & \dfrac{\partial}{\partial x} \\ -\dfrac{\partial}{\partial y} & 0 \\ -\dfrac{\partial}{\partial x} & \dfrac{\partial}{\partial y} \end{bmatrix} \begin{Bmatrix} \theta_x \\ \theta_y \end{Bmatrix} = \mathbf{L}\boldsymbol{\theta} \tag{11}$$

where $\boldsymbol{\theta}$ is the rotation vector with components θ_x and θ_y around the respective horizontal global co-ordinate axes, w is the transverse displacement field, $\boldsymbol{\Gamma}$ is the shear strain vector and $\boldsymbol{\kappa}$ is the curvature vector, ∇w is a gradient on the displacement field and $\mathbf{L}$ is a differential operator on the rotation field (see e.g. [3]). Let us consider a linear elastic material with

$$\mathbf{M}=\begin{Bmatrix} M_x \\ M_y \\ M_{xy} \end{Bmatrix}=\frac{Eh^3}{12(1-\nu^2)}\begin{bmatrix} 1 & \nu & 0 \\ \nu & 1 & 0 \\ 0 & 0 & \frac{1-\nu}{2} \end{bmatrix}\begin{Bmatrix} \frac{\partial \theta_y}{\partial x} \\ -\frac{\partial \theta_x}{\partial y} \\ \frac{\partial \theta_y}{\partial y}-\frac{\partial \theta_x}{\partial x} \end{Bmatrix}=\mathbf{D}_\mathbf{b}\boldsymbol{\kappa}=\mathbf{D}_\mathbf{b}\mathbf{L}\boldsymbol{\theta} \qquad (12)$$

$$\mathbf{S}=\begin{Bmatrix} S_x \\ S_y \end{Bmatrix}=kGh\begin{bmatrix} 1 & 0 \\ 0 & 1 \end{bmatrix}\begin{Bmatrix} \gamma_{xz} \\ \gamma_{yz} \end{Bmatrix}=\mathbf{D}_\mathbf{s}\boldsymbol{\Gamma}=\mathbf{D}_\mathbf{s}(\mathbf{e}\boldsymbol{\theta}+\nabla w)\ , \qquad (13)$$

where M_x, M_y, and M_{xy} are the bending and twisting moments (stress-couple resultants) around the respective co-ordinate axes, S_x and S_y are the shear-stress resultants, E and G are the Young and shear moduli, while ν and k are Poisson's coefficient and the shear correction factor (usually set to 5/6). The differential equations of equilibrium are

$$\frac{\partial M_x}{\partial x}+\frac{\partial M_{xy}}{\partial y}=S_x\,,\quad \frac{\partial M_{xy}}{\partial x}+\frac{\partial M_y}{\partial y}=S_y\,,\quad \frac{\partial S_x}{\partial x}+\frac{\partial S_y}{\partial y}=-q\,. \qquad (14)$$

Substituting (12) and (13) in (14), results in the differential equations

$$\frac{Eh^3}{12(1-\nu^2)}\left(\frac{\partial^2}{\partial x^2}+\frac{\partial^2}{\partial y^2}\right)\left(\frac{\partial \theta_y}{\partial x}-\frac{\partial \theta_x}{\partial y}\right)=-q\,,$$

$$kGh\left[\frac{\partial}{\partial x}\left(\theta_y+\frac{\partial w}{\partial x}\right)-\frac{\partial}{\partial y}\left(\theta_x-\frac{\partial w}{\partial y}\right)\right]=-q$$

$$\frac{Eh^3}{12(1-\nu^2)}\left[\frac{\partial^3\theta_y}{\partial x^3}+\frac{\partial^3\theta_x}{\partial y^3}-\upsilon\left(\frac{\partial^3\theta_x}{\partial x^2\partial y}+\frac{\partial^3\theta_y}{\partial x\partial y^2}\right)\right]-kGh\left[\frac{\partial}{\partial x}\left(\theta_y+\frac{\partial w}{\partial x}\right)+\frac{\partial}{\partial y}\left(\theta_x-\frac{\partial w}{\partial y}\right)\right]=0$$

,

which now cannot be solved in terms of a finite number of parameters as before.

For example, if Kirchhoff assumptions (8) are assumed then:

$$\theta_y=-\frac{\partial w}{\partial x} \qquad \text{and} \qquad \theta_x=\frac{\partial w}{\partial y}$$

and the following differential equation is derived:

$$D\left(\frac{\partial^4 w}{\partial x^4}+2\frac{\partial^4 w}{\partial x^2\partial y^2}+\frac{\partial^4 w}{\partial y^4}\right)=q \qquad \text{with} \qquad D=\frac{Eh^3}{12\left(1-\nu^2\right)}$$

Again, the Kirchhoff theory is just the limiting case of the Mindlin theory when $\boldsymbol{\Gamma}$ is approaching to zero, so the obtained results in solving Mindlin plate equations should hold in both cases. As there is no exact solution in the general case for either of theories, we shell attempt to extend results (7) from Section 3.1 in order to derive more accurate Mindlin plate elements.

To do so, we shall need the functional of the total potential energy:

$$\Pi(w,\theta_x,\theta_y)=\frac{1}{2}\int(\mathbf{M}^T\boldsymbol{\kappa})dA+\frac{1}{2}\int(\mathbf{S}^T\boldsymbol{\Gamma})dA+\Pi_{ext}=\frac{1}{2}\int(\boldsymbol{\kappa}^T\mathbf{D}_\mathbf{b}\boldsymbol{\kappa})dA+\frac{1}{2}\int(\boldsymbol{\Gamma}^T\mathbf{D}_\mathbf{s}\boldsymbol{\Gamma})dA+\Pi_{ext}$$

, (15)

where the last term describes the potential energy of the distributed and boundary loading.

4. Solution of the Timoshenko beam problem using linked interpolation

Here we will present how exact beam element interpolations generally expressed as (7) can be applied to beams with two, three and four nodes and how after that, they can be used to form some trial interpolations for plate elements of the same order.

4.1. Two-node beam element

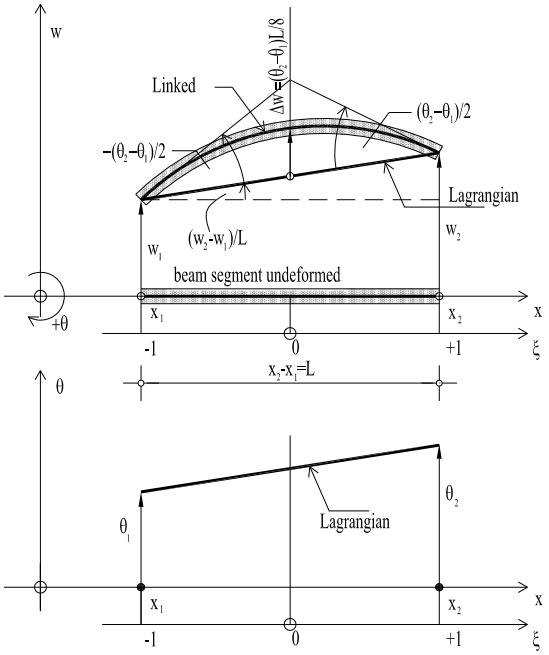

Fig. 3. *Interpolation functions for w and θ for a two-node beam element*

Two-node beam element (n=2) has 4 degrees of freedom (two displacements and two rotations) at the beam ends and the interpolations for transverse displacement and rotation follow from (7):

$$w = \frac{1-\xi}{2} w_1 + \frac{1+\xi}{2} w_2 - \frac{1-\xi}{2}\frac{1+\xi}{2}\frac{L}{2}(\theta_1 - \theta_2) = \sum_{i=1}^{2} I_i w_i - \frac{L}{2}\prod_{j=1}^{2} I_j(\theta_1 - \theta_2) \quad (16)$$

$$\theta = \frac{1-\xi}{2}\theta_1 + \frac{1+\xi}{2}\theta_2 = \sum_{i=1}^{2} I_i \theta_i \ , \quad (17)$$

with the argument ξ from the bi-unit parent domain from Fig. 3, $\xi = -1 + \frac{2}{L}(x - x_1)$ with $L=x_2-x_1$ and x_1, x_2 as the co-ordinates of the element end points.

In expressions above, we have, actually, an isoparametric mapping for the coordinate variable x

$$x = \frac{1-\xi}{2} x_1 + \frac{1-\xi}{2} x_2 = \sum_{i=1}^{2} I_i x_i \, .$$

From equations (16) and (17), the bending moment and the shear force in the beam cross section can be computed as

$$M = EI\frac{\theta_2 - \theta_1}{L} \quad (18)$$

and $$S = GA_s\left(\frac{w_2 - w_1}{L} + \frac{\theta_1 + \theta_2}{2}\right). \tag{19}$$

The bending moment is constant over the whole element in terms of parameters θ_1 and θ_2 and the corresponding shear force is also constant and equal to the shear force of the midpoint between nodes when just Lagrangean interpolation for w and θ is used. According to (18), for a constant moment, the shear force (19) should be zero for equilibrium reasons and it would be valid only if

$$w_2 - w_1 = -\frac{\theta_1 + \theta_2}{2} L \ , \tag{20}$$

meaning that the displacement change over the element is the integral of the rotational function over the element, which is a standard engineering result [19].

Since the displacement interpolation now also involves the rotational contributions, the displacement at the midpoint of the element is not just the mean value of the end-node displacements, but includes the additional hierarchical contribution Δw, shown in Fig. 3. Interpolations (16) and (17) are the exact solutions of the beam differential equations for a pure bending (equal and opposite moment loading at the boundaries).

4.2. Three-node beam element

For *n=3* the displacement field can be expressed using a third-order polynomial following the linked interpolation scheme with 3x2 parameters of freedom for the three-node beam element of Fig. 4:

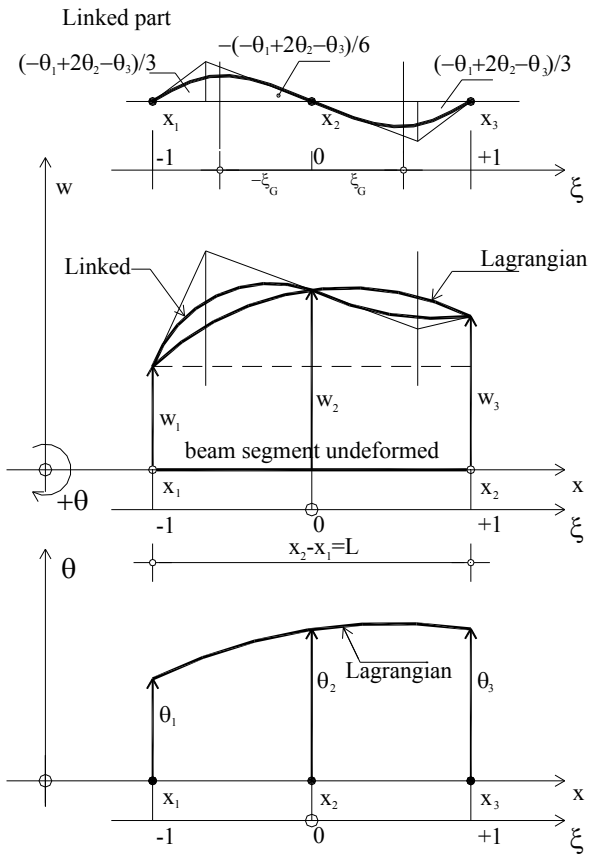

Fig. 4: *Interpolation functions for displacement w and rotation θ for a three-node beam element ($\xi_G=\pm\sqrt{3}/3$ are Gauss points)*

$$w=-\xi\left(\frac{1-\xi}{2}\right)w_1+4\left(\frac{1+\xi}{2}\right)\left(\frac{1-\xi}{2}\right)w_2+\left(\frac{1+\xi}{2}\right)\xi w_3-\left(\frac{1+\xi}{2}\right)\xi\left(\frac{1-\xi}{2}\right)\frac{L}{3}(-\theta_1+2\theta_2-\theta_3)=$$
$$=\sum_{i=1}^{3}I_i w_i-\frac{L}{3}\prod_{j=1}^{3}N_j(-\theta_1+2\theta_2-\theta_3), \tag{21}$$

$$\theta=-\xi\left(\frac{1-\xi}{2}\right)\theta_1+4\left(\frac{1+\xi}{2}\right)\left(\frac{1-\xi}{2}\right)\theta_2+\left(\frac{1+\xi}{2}\right)\xi\theta_3=\sum_{i=1}^{3}I_i\theta_i. \tag{22}$$

Using an isoparametric mapping for the coordinate variable x

$$x=-\xi\left(\frac{1-\xi}{2}\right)x_1+4\left(\frac{1+\xi}{2}\right)\left(\frac{1-\xi}{2}\right)x_2+\left(\frac{1+\xi}{2}\right)\xi x_3=\sum_{i=1}^{3}I_i x_i\ ,$$

the bending moment function can be derived as a linear function

$$M=EI\left(\frac{\theta_3-\theta_1}{L}-2\frac{-\theta_1+2\theta_2-\theta_3}{L}\xi\right). \tag{23}$$

The shear force is derived from (21) and (22) as a linear function too

$$S=GA_s\left[\frac{w_3-w_1}{L}+\frac{\Delta w}{2L}+\theta_2+\left(2\frac{w_1-2w_2+w_3}{L}+\frac{\theta_3-\theta_1}{2}\right)\xi\right]. \tag{24}$$

However, by equilibrium condition the shear force should be constant and the zero value scalar multiplying ξ leads to

$$w_2-\frac{w_1+w_3}{2}=-(\theta_1-\theta_3)\frac{L}{8}, \tag{25}$$

Which is actually the result obtained for the linked interpolation on a two-node beam

(see Fig. 3).

Interpolations (21) and (22) are the exact solutions of the beam differential equations for a linear moment state characteristic of the concentrated force loading.

4.3. Four-node beam element

By analogy, for *n=4* (four-node element shown in Fig. 5), the following expressions can be derived in a similar manner. The interpolation functions for displacements and rotations of the beam element are, with the linked part already incorporated in the formulation:

$$w = -\frac{9}{16}\left(\xi+\frac{1}{3}\right)\left(\xi-\frac{1}{3}\right)(\xi-1)w_1 + \frac{27}{16}(\xi+1)\left(\xi-\frac{1}{3}\right)(\xi-1)w_2 - \frac{27}{16}(\xi+1)\left(\xi+\frac{1}{3}\right)(\xi-1)w_3$$

$$+\frac{9}{16}(\xi+1)\left(\xi+\frac{1}{3}\right)\left(\xi-\frac{1}{3}\right)w_4 - \frac{9}{32}(\xi+1)\left(\xi+\frac{1}{3}\right)\left(\xi-\frac{1}{3}\right)(\xi-1)\frac{L}{4}(-\theta_1+3\theta_2-3\theta_3+\theta_4),$$

$$\theta = -\frac{9}{16}\left(\xi+\frac{1}{3}\right)\left(\xi-\frac{1}{3}\right)(\xi-1)\theta_1 + \frac{27}{16}(\xi+1)\left(\xi-\frac{1}{3}\right)(\xi-1)\theta_2 - \frac{27}{16}(\xi+1)\left(\xi+\frac{1}{3}\right)(\xi-1)\theta_3$$

$$+\frac{9}{16}(\xi+1)\left(\xi+\frac{1}{3}\right)\left(\xi-\frac{1}{3}\right)\theta_4, \qquad (26)$$

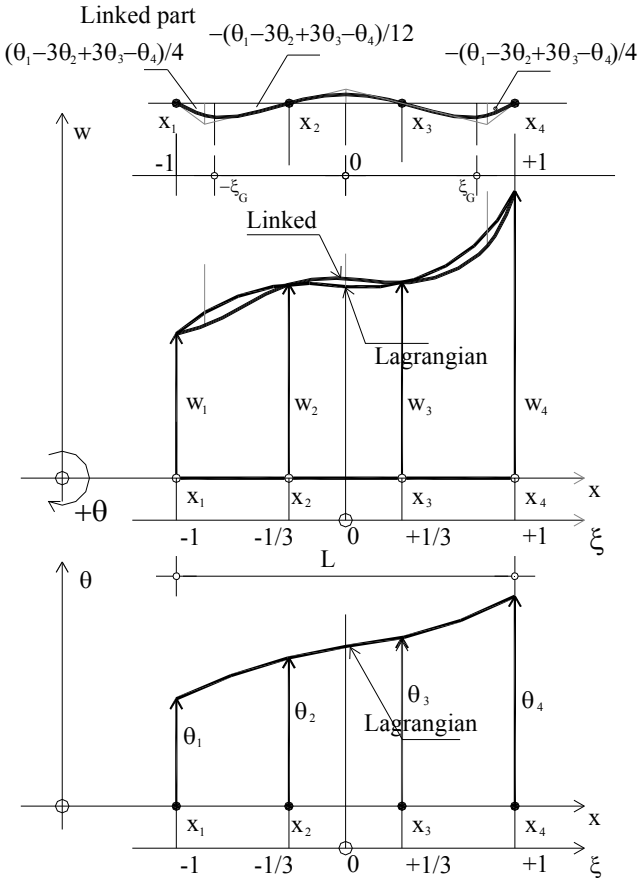

Fig. 5: *Interpolation functions for displacement w and rotation θ for a four-node beam element ($\xi_G=\pm\sqrt{3/5}$ and $\xi_G=0$ are Gauss points)*

or in an abbreviated form

$$w=\sum_{i=1}^{4} I_i w_i+\prod_{j=1}^{4} N_j \frac{L}{4}(\theta_1-3\theta_2+3\theta_3-\theta_4),$$
$$\theta=\sum_{i=1}^{4} I_i \theta_i. \tag{27}$$

The isoparametric mapping between the coordinate variable x and the natural

coordinate ξ now reads

$$x = -\frac{9}{16}\left(\xi+\frac{1}{3}\right)\left(\xi-\frac{1}{3}\right)(\xi-1)x_1 + \frac{27}{16}(\xi+1)\left(\xi-\frac{1}{3}\right)(\xi-1)x_2 - \frac{27}{16}(\xi+1)\left(\xi+\frac{1}{3}\right)(\xi-1)x_3,$$
$$+\frac{9}{16}(\xi+1)\left(\xi+\frac{1}{3}\right)\left(\xi-\frac{1}{3}\right)x_4 = \sum_{i=1}^{4} I_i x_i.$$

The bending moment can be derived from the rotation field:

$$M = EI\cdot\left(\frac{1}{8}\frac{\theta_1 - 27\theta_2 + 27\theta_3 - \theta_4}{L} + \frac{9}{4}\frac{\theta_1 - \theta_2 - \theta_3 + \theta_4}{L}\xi + \frac{27}{8}\frac{-\theta_1 + 3\theta_2 - 3\theta_3 + \theta_4}{L}\xi^2\right) \tag{28}$$

and the shear force can be derived from the displacement field derivative and the rotation field:

$$S = GA_s\left(\frac{1}{8}\frac{w_1 - 27w_2 + 27w_3 - w_4}{L} - \frac{1}{16}(\theta_1 - 9\theta_2 - 9\theta_3 + \theta_4)\xi\right) +$$
$$+GA_s\left(\frac{9}{4}\frac{w_1 - w_2 - w_3 + w_4}{L} - \frac{\theta_1 + 3\theta_2 - 3\theta_3 - \theta_4}{4}\right)\xi +$$
$$+GA_s\left(\frac{27}{8}\frac{-w_1 + 3w_2 - 3w_3 + w_4}{L} - \frac{9}{16}(-\theta_1 + \theta_2 + \theta_3 - \theta_4)\right)\xi^2. \tag{29}$$

The expression for the shear force would contain a cubic term, but for the linked expression in (27), which eliminates the scalar multiplying ξ^3 in a manner similar to those for the two-node and three-node elements.

For a quadratic expression of the bending moment in (28), the shear force must be

linear over the element for the equilibrium reasons. The factor multiplied by ξ^2 in (29) therefore vanishes if

$$(w_3 - w_2) + \frac{w_1 - w_4}{3} = \frac{L}{18}((\theta_4 - \theta_3) - (\theta_2 - \theta_1)) \,, \tag{30}$$

which would alternatively enable expressing an internal displacement in terms of the remaining displacements and rotations.

Again, the interpolation functions (27) are the exact solutions of the differential equations of Timoshenko's beam, if the beam element is subjected to a uniformly distributed load.

5. Linked-interpolation elements for Mindlin plates

5.1. Triangular plate elements

For triangle elements like the one from Fig. 6, the displacements and rotations are expressed in the so-called area coordinates which, for any interior point, make the ratio of the respective interior area to the area of the whole triangle 1-2-3.

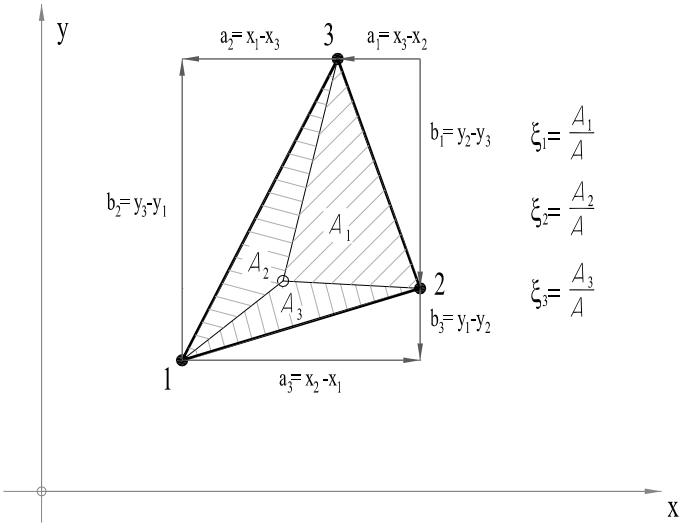

Fig. 6*: Three-node triangular plate element and its area coordinates of an interior point*

Because in two dimensions any point is uniquely defined by only two coordinates, the three coordinates ξ_1, ξ_2 and ξ_3 are not independent of each other and for any point within the domain they are related by the expression:

$$\xi_1 + \xi_2 + \xi_3 = 1.$$

The area coordinates of any point within the domain are transformed into the Cartesian coordinates as

$$x = \xi_1 x_1 + \xi_2 x_2 + \xi_3 x_3$$

$$y = \xi_1 y_1 + \xi_2 y_2 + \xi_3 y_3$$

and vice versa

$$\xi_1 = \frac{(x - x_3)b_1 + (y - y_3)a_1}{a_2 b_1 - a_1 b_2} = \frac{2A_1}{2A} = \frac{A_1}{A}$$

$$\xi_2 = \frac{(x - x_1)b_2 + (y - y_1)a_2}{a_3 b_2 - a_2 b_3} = \frac{A_2}{A}$$

$$\xi_3 = \frac{(x - x_2)b_3 + (y - y_2)a_3}{a_1 b_3 - a_3 b_1} = \frac{A_3}{A},$$

where $a_i = x_k - x_j$ and $b_i = y_j - y_k$ are the directed side-length projections along the coordinate axes and the indices *i*, *j*, and *k* denoting the triangle vertices are cyclic permutations of 1, 2 and 3. The area $A_i = \frac{1}{2}\left[(x - x_k)b_i - (y_k - y)a_i\right]$ denotes the area of the interior triangle whose one vertex is at the point (x, y) while the other two are the vertices j and k, while $A = \frac{1}{2}\left(a_j b_i - a_i b_j\right)$ is the area of the whole triangle (Fig. 6).

Note that the area co-ordinates ξ_1, ξ_2, ξ_3 are in fact the standard linear Lagrangean shape functions over a triangular domain.

5.1.1. Three-node triangular plate element

The linked interpolation as defined in (7) may be applied to2D situation in its original form written for arbitrary number of nodal points, but such a form would not be very illustrative. Instead we shall first apply the result given in (7) to a triangular element with three nodal points at the element vertices as in [8,12,15,24,28,30] (see Fig. 6).

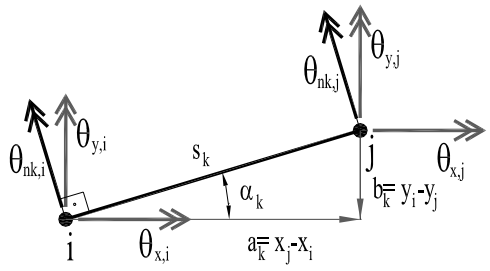

Fig. 7: *Triangular element's side and its rotation degrees of freedom*

If any triangle side k of length s_k (where $s_k^2=a_k^2+b_k^2$) is taken as a beam element (Fig. 7), the expressions for the displacement w and the rotation around the in-plane normal θ_n can be derived in linked form like in (16) and (17) but with area coordinates this time:

$$w=\xi_i w_i+\xi_j w_j-\xi_i\xi_j\frac{s_k}{2}\left(\theta_{ni}-\theta_{nj}\right)=\xi_i w_i+\xi_j w_j-\xi_i\xi_j\frac{s_k}{2}\left[\left(\theta_{yi}-\theta_{yj}\right)\cos\alpha_k-\left(\theta_{xi}-\theta_{xj}\right)\sin\alpha_k\right]$$
$$=\xi_i w_i+\xi_j w_j-\frac{1}{2}\xi_i\xi_j\left[\left(\theta_{xi}-\theta_{xj}\right)b_k+\left(\theta_{yi}-\theta_{yj}\right)a_k\right],$$

$$\theta_n=\xi_i\theta_{ni}+\xi_j\theta_{nj},$$

while $\xi_k=0$. Such interpolation provides constant moments and constant shear along the element side.

At each nodal point i (i=1, 2, 3) of an element there exist three degrees of freedom (displacements w_i, and rotations θ_{xi}, and θ_{yi} in the global coordinate directions). The linked interpolation for the displacement and rotation field over the whole triangular domain may be now proposed as:

$$w=\xi_1 w_1+\xi_2 w_2+\xi_3 w_3-\frac{1}{2}\xi_1\xi_2\left[\left(\theta_{x1}-\theta_{x2}\right)b_3+\left(\theta_{y1}-\theta_{y2}\right)a_3\right]-\frac{1}{2}\xi_2\xi_3\left[\left(\theta_{x2}-\theta_{x3}\right)b_1+\left(\theta_{y2}-\theta_{y3}\right)a_1\right]$$
$$-\frac{1}{2}\xi_3\xi_1\left[\left(\theta_{x3}-\theta_{x1}\right)b_2+\left(\theta_{y3}-\theta_{y1}\right)a_2\right] \qquad (31)$$

$$\theta_x=\xi_1\theta_{x1}+\xi_2\theta_{x2}+\xi_3\theta_{x3} \qquad (32a)$$

$$\theta_y=\xi_1\theta_{y1}+\xi_2\theta_{y2}+\xi_3\theta_{y3}. \qquad (32b)$$

Here θ_{xi}, θ_{yi} are the rotation components at the element vertices (see Fig. 8). Terms in brackets are rotational projections of respective rotation components to the normal on each element side times the side length. Therefore the interpolation is isoparametric for the rotations, while for the displacement function it includes an additional linking

part schematically presented in Fig. 9.

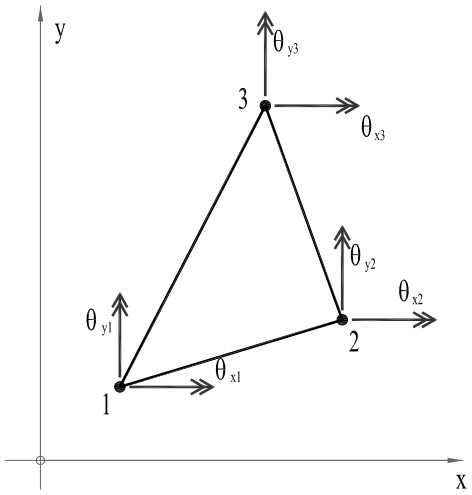

Fig. 8: *Three-node triangular plate element and its nodal rotations. The nodal displacements are perpendicular to the element plane*

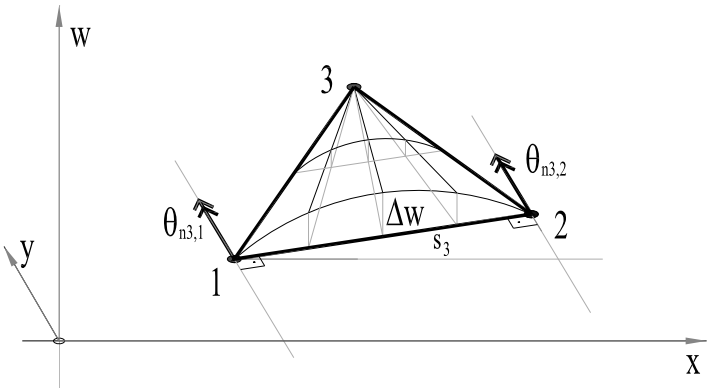

$$\Delta w = -\frac{1}{2}\xi_1\xi_2\left[\left(\theta_{x1}-\theta_{x2}\right)b_3+\left(\theta_{y1}-\theta_{y2}\right)a_3\right]$$

Fig. 9: *Linking part of the shape function on side "1-2" of the element*

The linked interpolation as employed in a two-node Timoshenko beam element can exactly reproduce the quadratic displacement function, and the same should be expected for the 2D interpolation considered here. The finite element developed on this basis will be named T3-U2, denoting the three-node element with the second-order displacement distribution.

5.1.2. Six-node triangular plate element

A six-node linked-interpolation triangular element (Fig. 10) may be defined correspondingly.

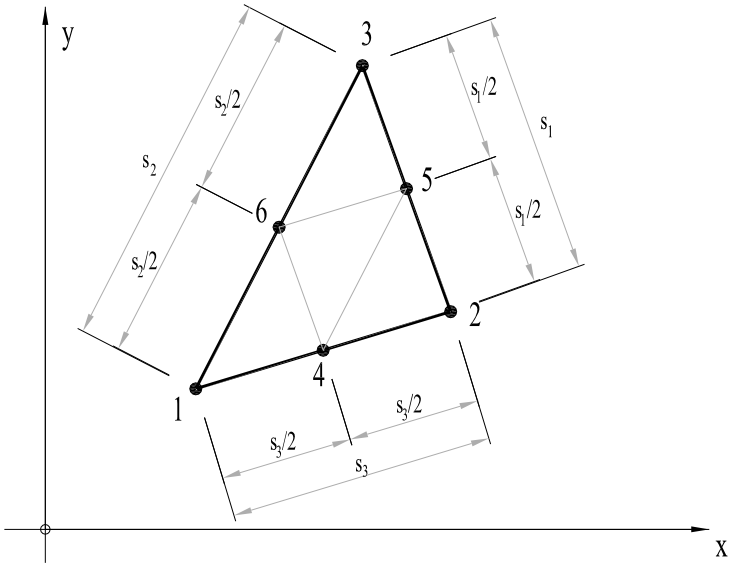

Fig. 10: *Six-node triangular plate element and its geometry.*

Again, if any triangle side k is taken as a beam element, the expressions for the displacement w and the rotation around the in-plane normal θ_n can be derived in the linked form (7), with $i+3$ node located at the middle of the side as in Fig. 11:

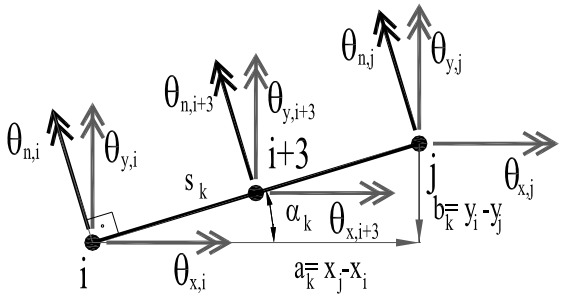

Fig. 11: *Triangular element's side and its rotation degrees of freedom*

$$w=\xi_i(2\xi_i-1)w_i+\xi_j(2\xi_j-1)w_j+4\xi_i\xi_j w_{i+3}-\xi_i\xi_j(\xi_j-\xi_i)\frac{s_k}{3}(-\theta_{n,i}+2\theta_{n,i+3}-\theta_{n,j})=$$
$$=\xi_i(2\xi_i-1)w_i+\xi_j(2\xi_j-1)w_j+4\xi_i\xi_j w_{i+3}-\xi_i\xi_j(\xi_j-\xi_i)\frac{1}{3}[(-\theta_{xi}+2\theta_{x,i+3}-\theta_{xj})b_k+(-\theta_{yi}+2\theta_{y,i+3}-\theta_{yj})a_k]$$

$$\theta_n=\xi_i(2\xi_i-1)\theta_{n,i}+\xi_j(2\xi_j-1)\theta_{n,j}+4\xi_i\xi_j\theta_{n,i+3},$$

since $\xi_k=0$.

Such interpolation may describe a linear moment and shear change along the element side.

The linked interpolation for the displacement field over the whole triangle domain may be now given as

$$w=\xi_1(2\xi_1-1)w_1+\xi_2(2\xi_2-1)w_2+\xi_3(2\xi_3-1)w_3+4\xi_1\xi_2w_4+4\xi_2\xi_3w_5+4\xi_3\xi_1w_6+$$

$$-\xi_1\xi_2(\xi_2-\xi_1)\frac{1}{3}\left[(-\theta_{x1}+2\theta_{x4}-\theta_{x2})b_3+(-\theta_{y1}+2\theta_{y4}-\theta_{y2})a_3\right]$$

$$-\xi_2\xi_3(\xi_3-\xi_2)\frac{1}{3}\left[(-\theta_{x2}+2\theta_{x5}-\theta_{x3})b_1+(-\theta_{y2}+2\theta_{y5}-\theta_{y3})a_1\right]$$

$$-\xi_3\xi_1(\xi_1-\xi_3)\frac{1}{3}\left[(-\theta_{x3}+2\theta_{x6}-\theta_{x1})b_2+(-\theta_{y3}+2\theta_{y6}-\theta_{y1})a_2\right] \quad (33)$$

while the interpolation for the rotations takes the standard Lagrangean form

$$\theta_x=\xi_1(2\xi_1-1)\theta_{x1}+\xi_2(2\xi_2-1)\theta_{x2}+\xi_3(2\xi_3-1)\theta_{x3}+4\xi_1\xi_2\theta_{x4}+4\xi_2\xi_3\theta_{x5}+4\xi_3\xi_1\theta_{x6} \quad (34a)$$

$$\theta_y=\xi_1(2\xi_1-1)\theta_{y1}+\xi_2(2\xi_2-1)\theta_{y2}+\xi_3(2\xi_3-1)\theta_{y3}+4\xi_1\xi_2\theta_{y4}+4\xi_2\xi_3\theta_{y5}+4\xi_3\xi_1\theta_{y6}, \quad (34b)$$

where θ_{xi}, θ_{yi} are the nodal rotation components at the element vertices and midpoints. As before, the displacement and rotation fields are interpolated using the same interpolation functions, but the displacement field has an additional linking part expressed in terms of the rotational components on each element side.

The rotations in (34) have a full quadratic polynomial form, but the displacement field does not have a full cubic polynomial form since expression (33) misses the 10th item in Pascal's triangle with the function that has zero values along all the element sides which cannot be associated with any nodal degree of freedom. To provide the full cubic expansion we need to expand the result from (33) with an independent bubble degree of freedom w_b i.e.

$$w = w_{eqn(33)} + \xi_1\xi_2\xi_3 w_b \tag{35}$$

The finite element developed on this basis will be named T6-U3, denoting the six-node element with the third-order displacement distribution. The same interpolation for the displacements has been applied to the mixed-type six-node triangular plate element in [6].

5.1.3. Ten-node triangular plate element

A ten-node linked-interpolation triangular element (Fig. 12) follows analogously from the linked interpolation for the four-node Timoshenko beam element.

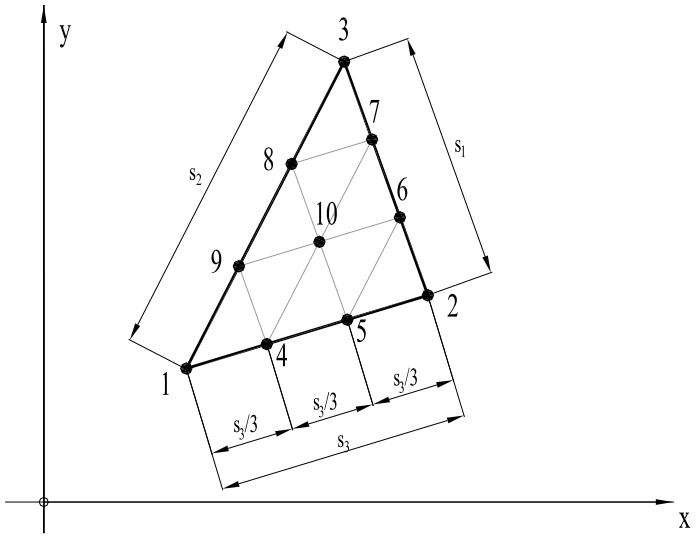

Fig. 12: *Ten-node triangular plate element and its geometry.*

Any triangle side can be taken as a beam element and expressions for w and θ_n can be

expressed in the linked form (7). Completed over the whole triangle, the interpolations for the displacement and the rotations follow as:

$$w=\xi_1(3\xi_1-2)(3\xi_1-1)\frac{1}{2}w_1+\xi_1\xi_2(3\xi_1-1)\frac{9}{2}w_4+\xi_1\xi_2(3\xi_2-1)\frac{9}{2}w_5+$$

$$+\xi_2(3\xi_2-2)(3\xi_2-1)\frac{1}{2}w_2+\xi_2\xi_3(3\xi_2-1)\frac{9}{2}w_6+\xi_2\xi_3(3\xi_3-1)\frac{9}{2}w_7+$$

$$+\xi_3(3\xi_3-2)(3\xi_3-1)\frac{1}{2}w_3+\xi_3\xi_1(3\xi_3-1)\frac{9}{2}w_8+\xi_3\xi_1(3\xi_1-1)\frac{9}{2}w_9+27\xi_1\xi_2\xi_3w_{10}-$$
$$-\xi_1\xi_2(3\xi_1-1)(3\xi_2-1)\frac{1}{8}\left[(-\theta_{x1}+3\theta_{x4}-3\theta_{x5}+\theta_{x2})b_3+(-\theta_{y1}+3\theta_{y4}-3\theta_{y5}+\theta_{y2})a_3\right]$$

$$-\xi_2\xi_3(3\xi_2-1)(3\xi_3-1)\frac{1}{8}\left[(-\theta_{x2}+3\theta_{x6}-3\theta_{x7}+\theta_{x3})b_1+(-\theta_{y2}+3\theta_{y6}-3\theta_{y7}+\theta_{y3})a_1\right]$$

$$-\xi_3\xi_1(3\xi_3-1)(3\xi_1-1)\frac{1}{8}\left[(-\theta_{x3}+3\theta_{x8}-3\theta_{x9}+\theta_{x1})b_2+(-\theta_{y3}+3\theta_{y8}-3\theta_{y9}+\theta_{y1})a_2\right] \quad (36)$$

$$\theta_x=\xi_1(3\xi_1-2)(3\xi_1-1)\frac{1}{2}\theta_{x1}+\xi_1\xi_2(3\xi_1-1)\frac{9}{2}\theta_{x4}+\xi_1\xi_2(3\xi_2-1)\frac{9}{2}\theta_{x5}+$$

$$+\xi_2(3\xi_2-2)(3\xi_2-1)\frac{1}{2}\theta_{x2}+\xi_2\xi_3(3\xi_2-1)\frac{9}{2}\theta_{x6}+\xi_2\xi_3(3\xi_3-1)\frac{9}{2}\theta_{x7}+$$

$$+\xi_3(3\xi_3-2)(3\xi_3-1)\frac{1}{2}\theta_{x3}+\xi_3\xi_1(3\xi_3-1)\frac{9}{2}\theta_{x8}+\xi_3\xi_1(3\xi_1-1)\frac{9}{2}\theta_{x9}+27\xi_1\xi_2\xi_3\theta_{x10} \quad (37a)$$

$$\theta_y=\xi_1(3\xi_1-2)(3\xi_1-1)\frac{1}{2}\theta_{y1}+\xi_1\xi_2(3\xi_1-1)\frac{9}{2}\theta_{y4}+\xi_1\xi_2(3\xi_2-1)\frac{9}{2}\theta_{y5}+$$

$$+\xi_2(3\xi_2-2)(3\xi_2-1)\frac{1}{2}\theta_{y2}+\xi_2\xi_3(3\xi_2-1)\frac{9}{2}\theta_{y6}+\xi_2\xi_3(3\xi_3-1)\frac{9}{2}\theta_{y7}+$$

$$+\xi_3(3\xi_3-2)(3\xi_3-1)\frac{1}{2}\theta_{y3}+\xi_3\xi_1(3\xi_3-1)\frac{9}{2}\theta_{y8}+\xi_3\xi_1(3\xi_1-1)\frac{9}{2}\theta_{y9}+27\xi_1\xi_2\xi_3\theta_{y10}, \quad (37b)$$

where θ_{xi}, θ_{yi} are the nodal rotation components at the element vertices and the mid-side points.

The rotations are expressed as a full cubic polynomial, but the displacement field does not have a full quartic polynomial forms. To extend expression (36) to a full quartic form (with all 15 items in Pascal's triangle), two more parameters are needed and they are related with the functions that have zero values along any element side and at the central point (node with index *10*). Those parameters are some internal bubbles so finally the displacement field may be completed as:

$$w = w_{eqn(36)} + \xi_1\xi_2\xi_3(\xi_1 - \xi_2)w_{b1} + \xi_1\xi_2\xi_3(\xi_2 - \xi_3)w_{b2} \tag{38}$$

The third term that appears to be missing in expression (38) to complete the cyclic triangle symmetry, namely

$$\xi_1\xi_2\xi_3(\xi_3 - \xi_1)w_{b3},$$

is actually linearly dependent on the two other added terms and the 10^{th} term in (36). The finite element developed on the basis of this interpolation will be named T10-U4, denoting the ten-node element with the fourth-order displacement distribution.

A family of triangular elements based on the linked interpolation has been derived in [8] stemming from the requirement of the shear strain in the element being of a prescribed order. The above methodology, in contrast, generates the linked interpolation from the underlying interpolation functions developed for the beam

elements and may be consistently applied to triangular or quadrilateral plate elements of arbitrary order.

5.2. Quadrilateral plate elements

5.2.1. Four-node quadrilateral plate element

Now we turn our attention to a quadrilateral element with four nodal points at the element vertices as in [1-3,7,9,11] (see Fig. 13). At each nodal point i (i=1,2,3,4) there exist three degrees of freedom (displacement w_i, and rotations θ_{xi}, and θ_{yi}). In analogy to (7), the linked interpolation for the displacement field may be now given as

$$w = I_1 w_1 + I_2 w_2 + I_3 w_3 + I_4 w_4 - \frac{a_1}{2}\frac{1-\xi^2}{4}\frac{1-\eta}{2}(\theta^1_{na1} - \theta^2_{na1}) - \frac{a_2}{2}\frac{1-\xi^2}{4}\frac{1+\eta}{2}(\theta^4_{na2} - \theta^3_{na2})$$

$$+ \frac{b_1}{2}\frac{1-\xi}{2}\frac{1-\eta^2}{4}(\theta^1_{nb1} - \theta^4_{nb1}) + \frac{b_2}{2}\frac{1+\xi}{2}\frac{1-\eta^2}{4}(\theta^2_{nb2} - \theta^3_{nb2}), \qquad (39)$$

where ξ and η are the standard natural co-ordinates, a_i and b_i ($i=1,2$) are the lengths of the element sides as shown in Fig. 13, the Lagrangean shape functions are given as $I_1 = \frac{1-\xi}{2}\frac{1-\eta}{2}$, $I_2 = \frac{1+\xi}{2}\frac{1-\eta}{2}$, $I_3 = \frac{1+\xi}{2}\frac{1+\eta}{2}$, $I_4 = \frac{1-\xi}{2}\frac{1+\eta}{2}$ and θ^k_{nai}, θ^k_{nbi} are the rotation components perpendicular to the element side a_i or b_i at node k (see Fig. 14).

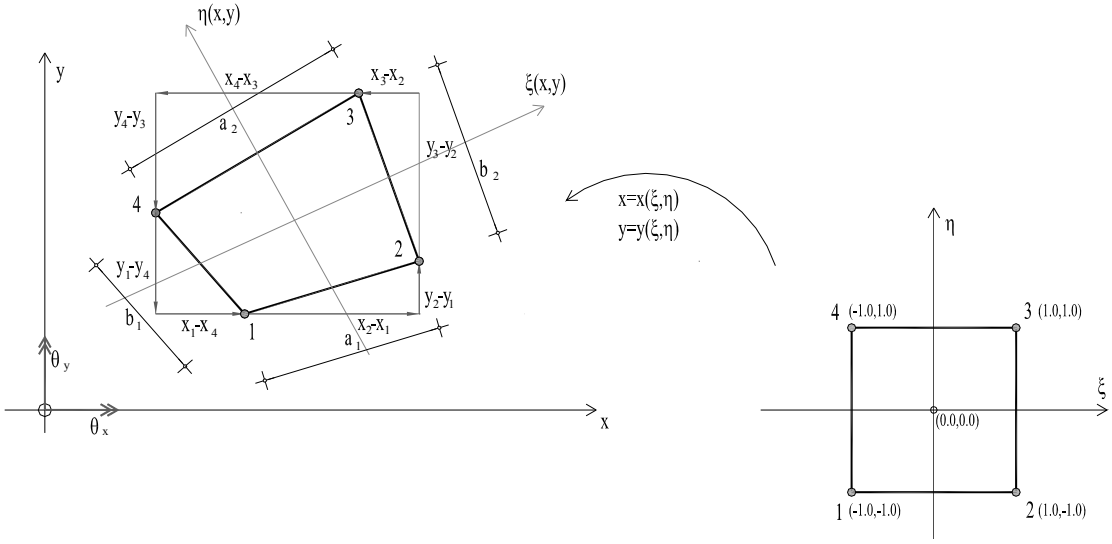

Fig. 13: *Four-node quadrilateral plate element and its geometry. The nodal displacements are perpendicular to the element plane and rotations are oriented in global coordinate directions. The parent domain of the element is a bi-unit square with coordinates ξ and η.*

The interpolation functions for the rotations are given in a usual manner using the standard Lagrangean polynomials:

$$\theta_x = \sum_{i=1}^{4} I_i \theta_{xi}\,, \qquad \theta_y = \sum_{i=1}^{4} I_i \theta_{yi}\,. \tag{40}$$

All the interpolation functions are expressed in natural coordinates ξ and η, which are related to the Cartesian co-ordinates x and y via $x = \sum_{i=1}^{4} I_i x_i$, $y = \sum_{i=1}^{4} I_i y_i$. The normal rotations about an element edge are shown in Fig. 15 and expressed by the global node rotations as $\theta^1_{n\,a1} = -\theta_{x1}\dfrac{y_2 - y_1}{a_1} + \theta_{y1}\dfrac{x_2 - x_1}{a_1}$ and

$$\theta_{na1}^{1}-\theta_{na1}^{2}=-\left(\theta_{x1}-\theta_{x2}\right)\frac{y_2-y_1}{a_1}+\left(\theta_{y1}-\theta_{y2}\right)\frac{x_2-x_1}{a_1}\,.$$

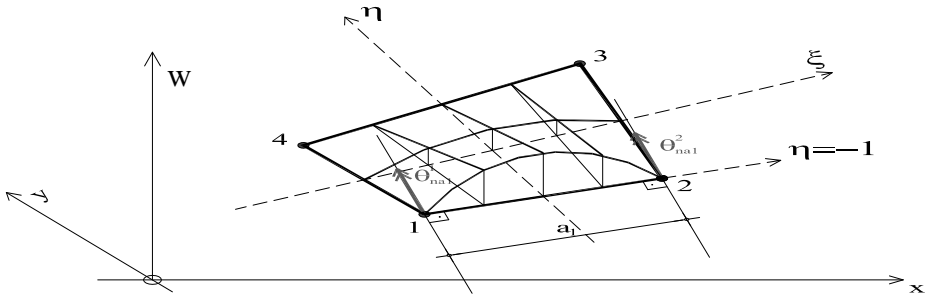

$$-\frac{a_1}{2}\left(\frac{1-\xi^2}{4}\right)\left(\frac{1-\eta}{2}\right)(\theta_{na1}^{1}-\theta_{na1}^{2})$$

Fig. 14: *Linking shape function for normal rotations on the side "1-2" of the element*

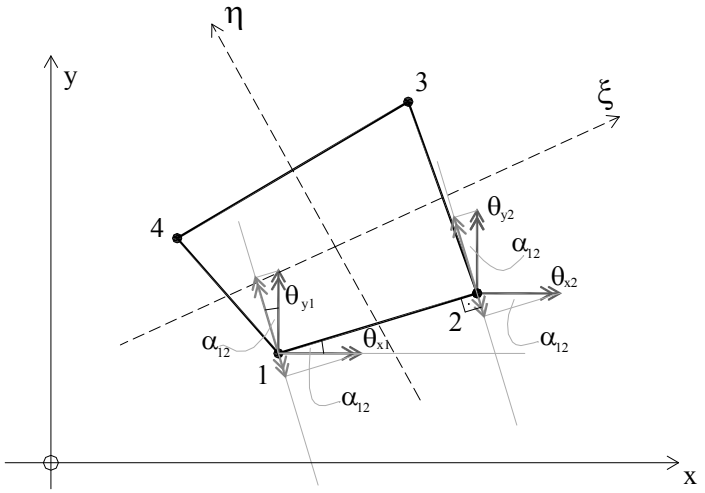

Fig. 15: *Components of the nodal rotations to the normal on the side between nodes 1 and 2*

The linked interpolation as employed in a two-node Timoshenko beam element can

exactly reproduce the quadratic displacement function, and the same should be expected for the 2D interpolation considered here. However, this must be true for any direction, which interpolation (39) cannot satisfy, unless enriched by a bi-quadratic bubble term $\frac{1-\xi^2}{4}\frac{1-\eta^2}{4}w_b$ eventually giving

$$w = w_{eqn(39)} + \frac{1-\xi^2}{4}\frac{1-\eta^2}{4}w_b \tag{41}$$

where $w_{eqn(39)}$ is the displacement interpolation given in equation (39). The displacement and rotational interpolations (41) and (39) can reproduce a constant bending moment and zero shear distribution throughout the arbitrary quadrilateral element.

5.2.2. Nine-node quadrilateral plate element

For a nine-node quadrilateral element the linked interpolation for the displacement field may be defined correspondingly (written in positional order as shown in Fig. 16), i.e.

$$\begin{aligned} w = {} & I_{1\xi}I_{3\eta}w_{3,1} + I_{2\xi}I_{3\eta}w_{3,2} + I_{3\xi}I_{3\eta}w_{3,3} \\ & + I_{1\xi}I_{2\eta}w_{2,1} + I_{2\xi}I_{2\eta}w_{2,2} + I_{3\xi}I_{2\eta}w_{2,3} \\ & + I_{1\xi}I_{1\eta}w_{1,1} + I_{2\xi}I_{1\eta}w_{1,2} + I_{3\xi}I_{1\eta}w_{1,3} \end{aligned}$$

$$+\frac{a_3}{3}\frac{\xi-\xi^3}{4}\frac{1+\eta}{2}\eta(\theta^{3,1}_{na3}-2\theta^{3,2}_{na3}+\theta^{3,3}_{na3})+\frac{a_2}{3}\frac{\xi-\xi^3}{4}4\frac{1+\eta}{2}\frac{1-\eta}{2}(\theta^{2,1}_{na2}-2\theta^{2,2}_{na2}+\theta^{2,3}_{na2})$$
$$-\frac{a_1}{3}\frac{\xi-\xi^3}{4}\eta\frac{1-\eta}{2}(\theta^{1,1}_{na1}-2\theta^{1,2}_{na1}+\theta^{1,3}_{na1})$$

$$+\frac{b_1}{3}\xi\frac{1-\xi}{2}\frac{\eta-\eta^3}{4}(\theta^{1,1}_{nb1}-2\theta^{2,1}_{nb1}+\theta^{3,1}_{nb1})-\frac{b_2}{3}4\frac{1+\xi}{2}\frac{1-\xi}{2}\frac{\eta-\eta^3}{4}(\theta^{1,2}_{nb2}-2\theta^{2,2}_{nb2}+\theta^{3,2}_{nb2})$$
$$-\frac{b_3}{3}\frac{1+\xi}{2}\xi\frac{\eta-\eta^3}{4}(\theta^{1,3}_{nb3}-2\theta^{2,3}_{nb3}+\theta^{3,3}_{nb3}) \qquad (42)$$

where $I_{1\xi}=-\xi\frac{1-\xi}{2}$, $I_{2\xi}=1-\xi^2$, $I_{3\xi}=\xi\frac{1+\xi}{2}$, $I_{1\eta}$, $I_{2\eta}$, $I_{3\eta}$ are the corresponding interpolation functions with natural co-ordinate η, a_k and b_k ($k=1,3$) are the node line lengths in ξ and η directions as shown in Fig. 16. Again, $\theta^{i,j}_{nak}$ and $\theta^{i,j}_{nbk}$ are the components of the nodal rotations to the normal of the respective element line at node (i,j). This time a node has two indices denoting its position (row and column number counted from the lower left corner node).

The interpolation for the rotation fields, in positional order, reads:

$$\theta_x=\sum_{i=1}^{4}\sum_{j=1}^{4}I_{i\eta}I_{j\xi}\theta_{x\,i,j} \qquad (43a)$$

$$\theta_y=\sum_{i=1}^{3}\sum_{j=1}^{3}I_{i\eta}I_{j\xi}\theta_{y\,i,j}\,, \qquad (43b)$$

where $\theta_{xi,j}$ and $\theta_{yi,j}$ denote rotations in the global directions at the node denoted as (i,j). The isoparametric mapping from the natural coordinates ξ and η to the global variables x and y follows the standard rule: $x=\sum_{i=1}^{3}\sum_{j=1}^{3}I_{i\eta}I_{j\xi}x_{i,j}$, $y=\sum_{i=1}^{3}\sum_{j=1}^{3}I_{i\eta}I_{j\xi}y_{i,j}$. In these expressions, the coordinates for nodes *(1,2), (2,3), (3,2)* and *(2,1)* are in the middle between the adjacent nodes and node *(2,2)* is at the element centroid.

As before, in order to reproduce exactly the polynomial of the third order in arbitrary direction, an additional bi-cubic term involving an internal bubble displacement w_b has to be added to displacement interpolation (42). Eventually, therefore, the displacement interpolation reads

$$w = w_{eqn(42)} + \frac{\xi - \xi^3}{4}\frac{\eta - \eta^3}{4} w_b \,. \tag{44}$$

The displacement and rotational interpolations (44) and (43) can reproduce the states of linear bending throughout the arbitrary quadrilateral element.

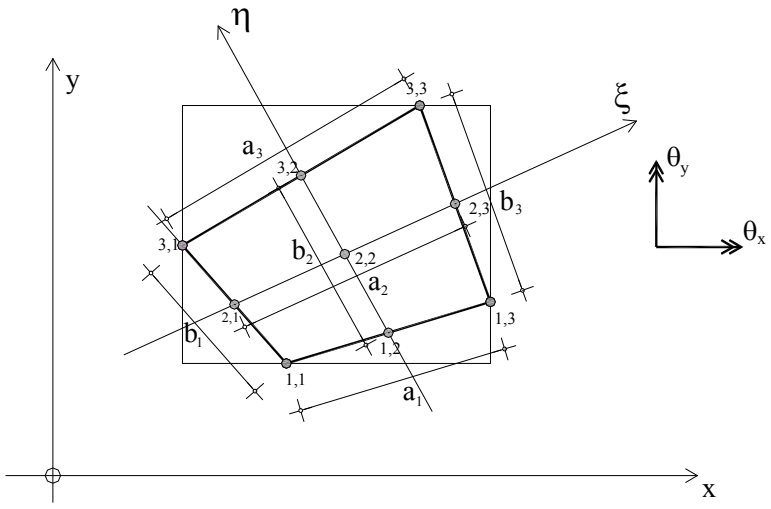

Fig. 16: *Nine-node quadrilateral plate element and its geometry.*

A serendipity-type formulation of a similar sort written in a framework of the hierarchical interpolation has been presented in [2].

5.2.3. Sixteen-node quadrilateral plate element

A sixteen-node (4x4) linked-interpolation quadrilateral element (Fig. 17) may be defined correspondingly.

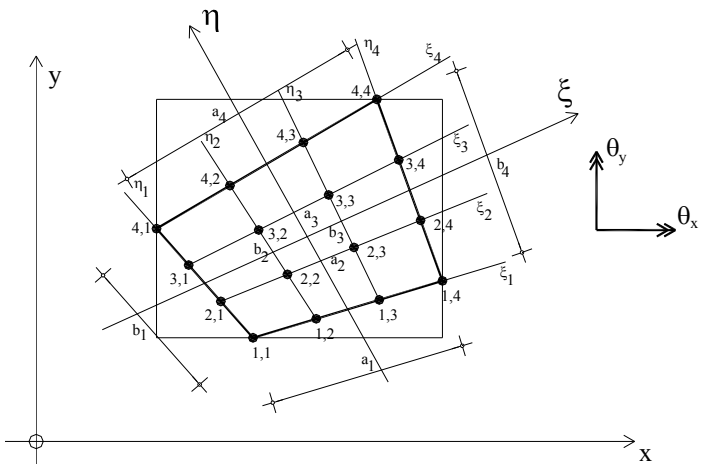

Fig. 17: *Sixteen-node quadrilateral plate element and its geometry.*

The displacement field is defined as

$$w=\sum_{i=1}^{4}\sum_{j=1}^{4} I_{i\eta} I_{j\xi} w_{i,j}$$

$$+ I_{4\eta}\prod_{n=1}^{4} N_{n\xi}\frac{a_4}{4}(\theta_{na4}^{4,1}-3\theta_{na4}^{4,2}+3\theta_{na4}^{4,3}-\theta_{na4}^{4,4}) + I_{3\eta}\prod_{n=1}^{4} N_{n\xi}\frac{a_3}{4}(\theta_{na3}^{3,1}-3\theta_{na3}^{3,2}+3\theta_{na3}^{3,3}-\theta_{na3}^{3,4})$$
$$+ I_{2\eta}\prod_{n=1}^{4} N_{n\xi}\frac{a_2}{4}(\theta_{na2}^{2,1}-3\theta_{na2}^{2,2}+3\theta_{na2}^{2,3}-\theta_{na2}^{2,4}) + I_{1\eta}\prod_{n=1}^{4} N_{n\xi}\frac{a_1}{4}(\theta_{na1}^{1,1}-3\theta_{na1}^{1,2}+3\theta_{na1}^{1,3}-\theta_{na1}^{1,4})$$
$$+ I_{1\xi}\prod_{n=1}^{4} N_{n\eta}\frac{b_1}{3}(\theta_{nb1}^{1,1}-3\theta_{nb1}^{2,1}+3\theta_{nb1}^{3,1}-\theta_{nb1}^{4,1}) + I_{2\xi}\prod_{n=1}^{4} N_{n\eta}\frac{b_2}{3}(\theta_{nb2}^{1,2}-3\theta_{nb2}^{2,2}+3\theta_{nb2}^{3,2}-\theta_{nb2}^{4,2})$$
$$+ I_{3\xi}\prod_{n=1}^{4} N_{n\eta}\frac{b_3}{3}(\theta_{nb3}^{1,3}-3\theta_{nb3}^{2,3}+3\theta_{nb3}^{3,3}-\theta_{nb3}^{4,3}) + I_{4\xi}\prod_{n=1}^{4} N_{n\eta}\frac{b_4}{3}(\theta_{nb4}^{1,4}-3\theta_{nb4}^{2,4}+3\theta_{nb4}^{3,4}-\theta_{nb4}^{4,4}),$$

(45)

where

$$I_{1\xi} = -\frac{9}{16}\left(\xi+\frac{1}{3}\right)\left(\xi-\frac{1}{3}\right)(\xi-1) \qquad I_{1\eta} = -\frac{9}{16}\left(\eta+\frac{1}{3}\right)\left(\eta-\frac{1}{3}\right)(\eta-1)$$

$$I_{2\xi} = +\frac{27}{16}(\xi+1)\left(\xi-\frac{1}{3}\right)(\xi-1) \qquad I_{2\eta} = +\frac{27}{16}(\eta+1)\left(\eta-\frac{1}{3}\right)(\eta-1)$$

$$I_{3\xi} = -\frac{27}{16}(\xi+1)\left(\xi+\frac{1}{3}\right)(\xi-1) \qquad I_{3\eta} = -\frac{27}{16}(\eta+1)\left(\eta+\frac{1}{3}\right)(\eta-1)$$

$$I_{4\xi} = +\frac{9}{16}(\xi+1)\left(\xi+\frac{1}{3}\right)\left(\xi-\frac{1}{3}\right) \qquad I_{4\eta} = +\frac{9}{16}(\eta+1)\left(\eta+\frac{1}{3}\right)\left(\eta-\frac{1}{3}\right)$$

$$\prod_{n=1}^{4} N_{n\xi} = -\frac{9}{32}(\xi+1)\left(\xi+\frac{1}{3}\right)\left(\xi-\frac{1}{3}\right)(\xi-1)$$

$$\prod_{n=1}^{4} N_{n\eta} = -\frac{9}{32}(\eta+1)\left(\eta+\frac{1}{3}\right)\left(\eta-\frac{1}{3}\right)(\eta-1)$$

and where $\theta^{i,j}{}_{nak}$ and $\theta^{i,j}{}_{nbk}$ ($k=1,4$) denote the rotation projections normal to the node line lengths a_k or b_k at node (i,j).

The interpolations for the rotation fields, in positional order, read

$$\theta_x = \sum_{i=1}^{4}\sum_{j=1}^{4} I_{i\eta} I_{j\xi} \theta_{x\,i,j}$$

$$\theta_y = \sum_{i=1}^{4}\sum_{j=1}^{4} I_{i\eta} I_{j\xi} \theta_{y\,i,j}\,, \tag{46}$$

where $\theta_{x\,i,j}$ and $\theta_{y\,i,j}$ denote the rotations in the global directions at node (i,j) and the isoparametric mapping from natural coordinates ξ and η to global variables x and y follows as $x = \sum_{i=1}^{4}\sum_{j=1}^{4} I_{i\eta} I_{j\xi} x_{i,j}$, $y = \sum_{i=1}^{4}\sum_{j=1}^{4} I_{i\eta} I_{j\xi} y_{i,j}$.

In these expressions, the coordinates for the nodes along any element side are equally spaced (a third of lengths a_k and b_k) and the internal nodes follow the same rule along their lines in both directions.

Finally, the bubble term completes the displacement interpolation:

$$\mathrm{w} = \mathrm{w}_{\mathrm{eqn(45)}} + \frac{9}{32}\left(\xi^2 - 1\right)\left(\xi^2 - \frac{1}{9}\right)\frac{9}{32}\left(\eta^2 - 1\right)\left(\eta^2 - \frac{1}{9}\right)\cdot \mathrm{w}_{\mathrm{b}} = w^* + \prod_{n=1}^{3} N_n(\xi)\prod_{n=1}^{3} N_n(\eta)\cdot \mathrm{w}_{\mathrm{b}} \qquad (47)$$

5.3. Finite element stiffness matrix and load vector

The earlier interpolations may be written in matrix form as

$$w = \mathbf{I}_{ww}\mathbf{w} + \mathbf{N}_{w\theta}\boldsymbol{\theta}_{x,y} + \mathbf{N}_{wb}\mathbf{w}_b\,,$$

(48)

$$\begin{Bmatrix}\theta_x\\ \theta_y\end{Bmatrix} = \mathbf{I}_{\theta\theta}\boldsymbol{\theta}_{x,y}\,,$$

(49)

where $\mathbf{I}_{ww}$ is a matrix of all interpolation functions concerning the nodal displacement parameters with the dimension *1* x N_{nd}, where $N_{nd} = n(n+1)/2$ for triangle elements, or $N_{nd}=n^2$ for quadrilateral elements, and n is the number of nodes per element side. Also, $\mathbf{w}$ is the vector of nodal displacement parameters with the dimension N_{nd}: $\mathbf{w}^T = \langle w_1 \cdots w_n \rangle$ for triangles, or $\mathbf{w}^T = \langle w_{1,1} \cdots w_{n,n} \rangle$ for quadrilaterals, $\mathbf{N}_{w\theta}$ is the matrix of all linked interpolation functions with the dimension *1* x $2N_{nd}$ and

$\boldsymbol{\theta}_{x,y}$ is the vector of nodal rotations in global coordinate directions with the dimension $2N_{nd}$: $\boldsymbol{\theta}_{x,y}^T = \langle \theta_{x1}, \theta_{y1} \cdots \theta_{xn}, \theta_{yn} \rangle$ for triangles, or $\boldsymbol{\theta}_{x,y}^T = \langle \theta_{x1,1}, \theta_{y1,1} \cdots \theta_{xn,n}, \theta_{yn,n} \rangle$ for quadrilaterals. Further, $\mathbf{N}_{wb}$ is the matrix of bubble interpolation functions for triangles given in (35) or (38) with the dimension 1xN_b and $\mathbf{w}_b$ is the bubble parameter vector with the dimension $N_b=n-2$: $\mathbf{w}_b^T = \langle w_{b,1} \cdots w_{b,n-2} \rangle$, only for $n \geq 2$. For quadrilaterals N_{wb} is a bubble interpolation function in (41), (44) or (47) and w_b is the bubble parameter (single). $\mathbf{I}_{\theta\theta}$ is again the matrix of all interpolation functions concerning rotational parameters described in (32), (34) or (37) for triangles and in (40), (43) or (46) for quadrilaterals, all with the dimension 2 x $2N_{nd}$.

The formation of the element stiffness matrix and the external load vector for the interpolation functions defined in this way follows the standard finite-element procedure described in text-books e.g. [26,32,33]. A functional of the total energy of the system is given in (15) and from the stationarity condition for the total potential energy of an element, a system of algebraic equations is derived:

$$\begin{bmatrix} \mathbf{K}_{\mathbf{S}ww} & \mathbf{K}_{\mathbf{S}w\theta}^T & \mathbf{K}_{\mathbf{S}wb}^T \\ \mathbf{K}_{\mathbf{S}w\theta} & \mathbf{K}_{\mathbf{B}\theta\theta} + \mathbf{K}_{\mathbf{S}\theta\theta} & \mathbf{K}_{\mathbf{S}b\theta}^T \\ \mathbf{K}_{\mathbf{S}wb} & \mathbf{K}_{\mathbf{S}b\theta} & \mathbf{K}_{\mathbf{S}bb} \end{bmatrix} \begin{bmatrix} \mathbf{w} \\ \boldsymbol{\theta}_{x,y} \\ \mathbf{w}_b \end{bmatrix} = \begin{bmatrix} \mathbf{f}_w \\ \mathbf{f}_\theta \\ \mathbf{f}_b \end{bmatrix}, \tag{50}$$

where vectors $\mathbf{f}_w$, $\mathbf{f}_\theta$ and $\mathbf{f}_b$ are the terms due to external loading. The submatrices in the stiffness matrix follow

$$\mathbf{K}_{\mathbf{B}\theta\theta} = \int_A \left(\mathbf{L}\mathbf{I}_{\theta\theta}\right)^T \mathbf{D}_\mathbf{b} \left(\mathbf{L}\mathbf{I}_{\theta\theta}\right) dA$$

and

$$\begin{aligned}
\mathbf{K}_{\mathbf{S}ww} &= \int_A \left(\nabla \mathbf{I}_{ww}\right)^T \mathbf{D}_\mathbf{s} \left(\nabla \mathbf{I}_{ww}\right) dA \\
\mathbf{K}_{\mathbf{S}bb} &= \int_A (\nabla \mathbf{N}_{wb})^T \mathbf{D}_\mathbf{s} (\nabla \mathbf{N}_{wb}) dA \\
\mathbf{K}_{\mathbf{S}\theta\theta} &= \int_A \left(\mathbf{e}\mathbf{I}_{\theta\theta} + \nabla \mathbf{N}_{w\theta}\right)^T \mathbf{D}_\mathbf{s} \left(\mathbf{e}\mathbf{I}_{\theta\theta} + \nabla \mathbf{N}_{w\theta}\right) dA \\
\mathbf{K}_{\mathbf{S}w\theta} &= \int_A \left(\mathbf{e}\mathbf{I}_{\theta\theta} + \nabla \mathbf{N}_{w\theta}\right)^T \mathbf{D}_\mathbf{s} \left(\nabla \mathbf{I}_{ww}\right) dA \\
\mathbf{K}_{\mathbf{S}wb} &= \int_A (\nabla N_{wb})^T \mathbf{D}_\mathbf{s} \left(\nabla \mathbf{I}_{ww}\right) dA \\
\mathbf{K}_{\mathbf{S}b\theta} &= \int_A (\nabla N_{wb})^T \mathbf{D}_\mathbf{s} \left(\mathbf{e}\mathbf{I}_{\theta\theta} + \nabla \mathbf{N}_{w\theta}\right) dA
\end{aligned} \quad ,$$

where **L** and ∇ are the differential operators from (11) and (10) acting on the interpolation functions in (49) and (48) respectively, while **e** is a transformation matrix given in (10).

After static condensation of the bubble terms in the stiffness matrix of (50), the final element matrix is formed for the element out of plane nodal displacements and rotations (w_i, $\theta_{x,i}$, $\theta_{y,i}$) for all nodes *"i"* included in the element (N_{nd}):

$$\sum_{j=1}^{N_{nd}} \begin{bmatrix} k_{w,w}^{ij} & k_{w,\theta x}^{ij} & k_{w,\theta y}^{ij} \\ k_{\theta x,w}^{ij} & k_{\theta x,\theta x}^{ij} & k_{\theta x,\theta y}^{ij} \\ k_{\theta y,w}^{ij} & k_{\theta y,\theta x}^{ij} & k_{\theta y,\theta y}^{ij} \end{bmatrix} \begin{Bmatrix} w_j \\ \theta_{x,j} \\ \theta_{y,j} \end{Bmatrix} = \begin{Bmatrix} f_{w,i} \\ f_{\theta x,i} \\ f_{\theta y,i} \end{Bmatrix} \tag{51}$$

5.4. Comparison with some similar elements from literature

Here we look more closely into two families of elements, in which linked interpolation has been also employed for element modeling.

5.4.1. Liu - Riggs family of pure displacement-based triangular elements

If arbitrary direction 's' crossing the triangle element is chosen (Fig. 17), the shear strain can be expressed in terms of the shear strains along the directions of the co-ordinate axes x and y *as*

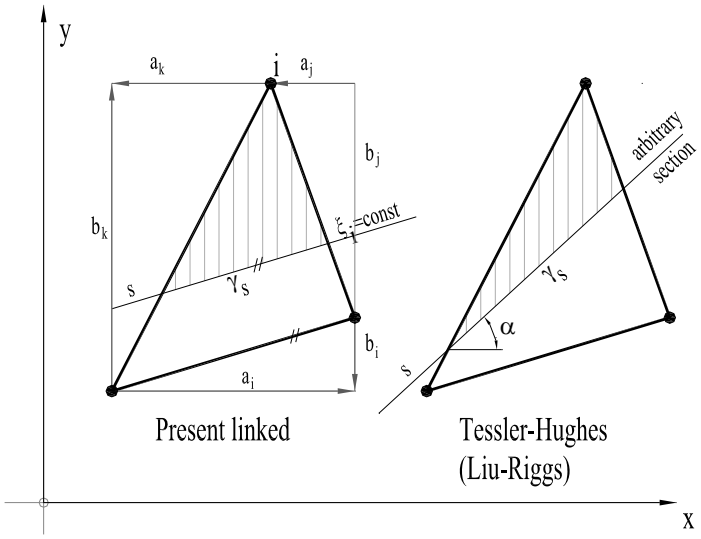

Fig. 17: *Difference in the shear strain condition between the present formulation and the Liu-Riggs formulation [8].*

$$\gamma_s = \gamma_x \cos\alpha + \gamma_y \sin\alpha, \tag{52}$$

where α is the angle between the *s*-direction and the *x*-axis.

In the linked interpolation formulation presented in this work, the expression for the shear along an element side is a polynomial which is two orders lower than the displacement interpolation polynomial. This is also valid for any direction parallel to an element side.

Liu and Riggs [8] have derived the family of triangle elements likewise based purely on displacement interpolations, which eventually, also, turns out to be of the linked type in the sense that the displacement distribution also depends on the nodal rotations. In contrast to the approach presented here, however, the requirement that the authors set is that the shear strain along arbitrary direction *s*, and not only those parallel to the element sides, should satisfy the above condition (Fig. 17), thus imposing the *p*-th derivative of (52) to be zero for arbitrary α, while the displacement interpolation is of the order *p+2* and the interpolation for the rotations is of the order *p+1*.

5.4.1.1.Tessler - Hughes three-node triangular plate element – *MIN3*

Liu and Riggs [8] and Tessler and Hughes [24] before them, have derived interpolation functions for the triangular element named *MIN3* with three nodes and nine degrees of freedom (the same degrees as the *T3-U2* element presented in 6.1.1) from the condition that the shear strain must be constant along any direction within

the element (Tessler and Hughes have additionally introduced a shear-relaxation factor in order to improve the *MIN3* element performance). Their interpolations for the displacement and the rotation fields are:

$$w = N_i w_i + L_i \theta_{xi} + M_i \theta_{yi}, \qquad \theta_x = N_i \theta_{xi} \qquad \text{and} \qquad \theta_y = N_i \theta_{yi} \tag{53}$$

where the interpolation functions are

$$N_i = \xi_i, \quad L_i = \frac{1}{2}\left(b_k \xi_i \xi_j - b_j \xi_k \xi_i\right) \quad \text{and} \quad M_i = -\frac{1}{2}\left(a_j \xi_k \xi_i - a_k \xi_i \xi_j\right) \tag{54}$$

with i, j and k again being the cyclic permutations of 1, 2 and 3. It can be verified that the rigid body conditions are satisfied because

$$\sum_{i=1}^{3} N_i = 1, \qquad \sum_{i=1}^{3} L_i = 0 \qquad \text{and} \qquad \sum_{i=1}^{3} M_i = 0, \tag{55}$$

and it can be also verified by direct calculation that the Liu–Riggs interpolation is the same as the linked interpolation given in 6.1.1. Therefore, for the triangular element with three nodes, in the present formulation the shear strain is also constant in any direction and not only along the directions parallel to the sides of the triangle.

5.4.1.2.Liu - Riggs six-node triangular plate element – *MIN6*

Liu and Riggs in [8] have next derived a family of elements based on upgrading the criteria for the shear strain along an arbitrary direction over the element. The second member of the family is the so-called *MIN6* element with six nodal points. The interpolations are derived to provide linear shear in any direction crossing the element. Interpolations in *MIN6* for the displacement and rotations are again:

$$w = N_i w_i + L_i \theta_{xi} + M_i \theta_{yi}, \qquad \theta_x = N_i \cdot \theta_{xi} \qquad \text{and} \qquad \theta_y = N_i \cdot \theta_{yi}$$

$$\text{for } i=1,2,\ldots 6 \tag{56}$$

where the actual interpolation functions are

$$N_i = \xi_i(2\xi_i - 1), \qquad N_{i+3} = 4\xi_i\xi_j \qquad \text{for } i=1,2,3 \tag{57a}$$

$$L_i = -\xi_i(2\xi_i - 1)\frac{1}{3}(b_k\xi_j - b_j\xi_k), \quad L_{i+3} = -4\xi_i\xi_j\frac{1}{3}\left[b_j\left(\xi_i - \frac{1}{2}\right) - b_i\left(\xi_j - \frac{1}{2}\right)\right] \tag{57b}$$

and $$M_i = -\xi_i(2\xi_i - 1)\frac{1}{3}(a_k\xi_j - a_j\xi_k), \qquad M_{i+3} = -4\xi_i\xi_j\frac{1}{3}\left[a_j\left(\xi_i - \frac{1}{2}\right) - a_i\left(\xi_j - \frac{1}{2}\right)\right]$$

(57c)

It should be stressed that in the expressions for L_{i+3} and M_{i+3} given here a typographic error in the Liu-Riggs original [8] is corrected to satisfy the rigid body conditions:

$$\sum_{i=1}^{6} N_i = 1, \qquad \sum_{i=1}^{6} L_i = 0 \qquad \text{and} \qquad \sum_{i=1}^{6} M_i = 0. \tag{58}$$

The element based on interpolations (56) – denoted as *MIN6* - has been coded in the finite-element programme environment *FEAP* [1] along with the earlier elements *T3-U2, T6-U3* and *T10-U4*. In contrast to *MIN3* (without shear relaxation), which corresponds exactly to the *T3-U2* presented in 6.1.1, the *MIN6* element is different from the *T6-U3* presented in 6.1.2, which has an additional bubble degree of freedom. It can be verified by direct calculation that the Liu–Riggs interpolation for *MIN6* should coincide with the *T6-U3* interpolation given in (35) if the bubble degree of freedom were constrained to

$$w_b = \frac{1}{3}\left[(b_3 - b_2)\theta_{x1} + (a_3 - a_2)\theta_{y1} + (b_1 - b_3)\theta_{x2} + (a_1 - a_3)\theta_{y2} + (b_2 - b_1)\theta_{x3} + (a_2 - a_1)\theta_{y3}\right] +$$

$$+ \frac{2}{3}\left[(b_2 - b_1)\theta_{x4} + (a_2 - a_1)\theta_{y4} + (b_3 - b_2)\theta_{x5} + (a_3 - a_2)\theta_{y5} + (b_1 - b_3)\theta_{x6} + (a_1 - a_3)\theta_{y6}\right]. \tag{59}$$

It should be made clear that the shear strain distribution of a certain order along an arbitrary direction is the basic underlying condition from which the *MINn* family of elements has been derived, while the shear strain distribution of a certain order along a direction parallel to the element sides is a consequence, rather than the origin of the family of triangle elements presented in Section 6.1. The presented methodology generates the linked interpolation from the underlying interpolation functions developed for the beam elements and may be consistently and straight-forwardly applied to triangular plate elements of arbitrary order. In contrast, the *MINn*

methodology requires a symbolic manipulation of algebraic expressions which get progressively more complicated as the order of the element is raised.

5.4.2. Auricchio -Taylor elements based on linked interpolation and mixed approach

Auricchio and Taylor [3,7,12,30] have developed a concept based on mixed approach in designing three- and four-node elements in which they use linked interpolation for displacement and rotations and constrain it using separate interpolation for shear distribution over the element domain, for each element. To constrain deformations with shear they need equal number of bubble parameters and bubble higher order functions in the rotations fields to satisfy the so-called count conditions necessary to perform static condensation of the stiffness matrix for internal bubble and shear terms. These conditions are

$$n_\theta + n_w \geq n_s \qquad \text{and} \qquad n_s \geq n_w ,$$

where n_θ, n_w and n_s are the total number of rotation, displacement and shear-force unknown parameters in the element test or in the patchwork of analysed elements.

The result is an excellent quadrilateral element *Q4-LIM* and slightly poorer triangle elements: *T3BL* and *T3-LIM*, which exhibit no shear locking phenomena in thin limit situations and are very efficient for both thick- and thin-plate cases.

5.4.2.1.Three-node triangular plate element - *T3BL*

The displacement interpolation for this element is actually the same linked interpolation used for our *T3-U2* element and the interpolation for rotations too, but enriched with two bubble terms. The displacement and rotations are written as:

$$w = \mathbf{N}_w \mathbf{w} + \mathbf{N}_{w\theta} \boldsymbol{\theta}_{x,y} = w_{T3U2},$$

$$\boldsymbol{\theta}_{x,y} = \mathbf{N}_\theta \boldsymbol{\theta}_{x,y} + \mathbf{N}_b \boldsymbol{\theta}_b = \boldsymbol{\theta}_{x,y\,T3U2} + \mathbf{N}_b \boldsymbol{\theta}_b \quad \text{(with two bubble terms in rotations).}$$

Here, $\mathbf{N}_w$ and $\mathbf{N}_\theta$ are matrices with Lagrangean interpolation functions and $\mathbf{N}_{w\theta}$ is a matrix of linked functions projected to the global coordinates. $\mathbf{N}_b$ is a matrix of bubble functions with $\boldsymbol{\theta}_b$ vector of two bubble parameters.

The shear force is approximated over the element as constant:

$$\mathbf{S} = \mathbf{N}_s \mathbf{S}_s \quad \text{(with two shear forces: } S_x \text{ and } S_y \text{ at the centroid),}$$

where $\mathbf{N}_s = \begin{bmatrix} 1 & 0 \\ 0 & 1 \end{bmatrix}$.

Interpolation functions for the bubble parameters are the same for both rotation fields:

$$N_{bx} = N_{by} = 27\xi_1\xi_2\xi_3 .$$

5.4.2.2.Four-node quadrilateral plate element - *Q4-LIM*

The notation used for expressing deformation of this quadrilateral element is equal as before. The displacement interpolation is, also the same linked interpolation used for our *Q4-U2* element and the interpolation for rotations are also identical, but for the four bubble terms added to the Lagrangean part. The displacement and rotations are written as:

$$w = \mathbf{N}_w \mathbf{w} + \mathbf{N}_{w\theta} \boldsymbol{\theta}_{x,y} = w_{Q4U2},$$

$$\boldsymbol{\theta}_{x,y} = \mathbf{N}_\theta \boldsymbol{\theta}_{x,y} + \mathbf{N}_b \boldsymbol{\theta}_b = \boldsymbol{\theta}_{x,y_{Q4U2}} + \mathbf{N}_b \boldsymbol{\theta}_b \quad \text{(with four bubble terms in rotations).}$$

The shear force is approximated linearly over the element with four parameters: constant shears for ξ and η directions at the centroid point of the element and two shear slopes in the same directions:

$$\mathbf{S} = \mathbf{N}_s \mathbf{S}_s \quad \text{(with four shear parameters),}$$

with $$\mathbf{N}_s = \begin{bmatrix} J_{11}^0 & J_{21}^0 & J_{11}^0 \eta & J_{21}^0 \xi \\ J_{12}^0 & J_{22}^0 & J_{12}^0 \eta & J_{22}^0 \xi \end{bmatrix}.$$

Matrix of rotation bubble functions is expressed as:

$$\mathbf{N}_b = \frac{(1-\xi^2)(1-\eta^2)}{j}\begin{bmatrix} J_{21}^0 & -J_{11}^0 & J_{21}^0\eta & -J_{11}^0\xi \\ J_{22}^0 & -J_{12}^0 & J_{22}^0\eta & -J_{12}^0\xi \end{bmatrix}.$$

In the above matrices values $J_{11}^0, J_{12}^0, J_{21}^0$ and J_{22}^0 are elements of Jacobian transformation matrix at the element centroid.

5.5. Patch tests

Consistency of the developed elements is tested for the constant strain conditions on the patch example with ten elements, covering a rectangular domain of a plate as shown in Fig. 18. The displacements and rotations for the four internal nodes within the patch are checked for the specific displacements and rotations given at the four external nodes [34, 35]. The plate properties are $E=10^5$, $v=0.25$, $k=5/6$, while two different thicknesses corresponding to a thick and a thin plate extremes are considered: $h= 1.0$ and $h= 0.01$.

Two strain-stress states are analysed [35]:

- Constant bending state

  Displacements and rotations are expressed respectively by

  $$w = (1 + x + 2y + x^2 + xy + y^2)/2, \qquad \theta_x = (2 + x + 2y)/2, \qquad \theta_y = -(1 + 2x + y)/2.$$

  The exact displacements and rotations at the internal nodes and the exact strains and stress resultants at every integration point are expected. The

moments are constant $M_x = M_y = -11111.11\ h^3$, $M_{xy} = -33333.33\ h^3$ and the shear forces vanish ($S_x = S_y = 0$).

- Constant shear state

Displacements and rotations are expressed respectively by

$$w = -\frac{h^2}{5(1-\nu)}(14x+18y) + x^3 + 2y^3 + 3x^2y + 4xy^2, \quad \theta_x = 3x^2 + 8xy + 6y^2,$$

$$\theta_y = -(3x^2 + 6xy + 4y^2).$$

The exact displacements and rotations at the internal nodes and the exact strains and stress resultants at every integration point are expected again. The shear forces are constant $S_x = -124400.0\ h^3$ and $S_y = -160000.0\ h^3$ in every Gauss point and the moments are linearly distributed according to

$$M_x = -\frac{Eh^3}{12(1-\nu^2)}[x(6+8\nu) + y(6+12\nu)], \quad M_y = -\frac{Eh^3}{12(1-\nu^2)}[x(8+6\nu) + y(12+6\nu)]$$

and $$M_{xy} = -\frac{Eh^3}{12(1-\nu^2)}\frac{1-\nu}{2}(12x+16y).$$

The three node triangle element *T3-U2* is tested on the patch given in Fig. 18. For the given values for the displacements and rotations at the external nodes calculated from the above data, the displacements and rotations at the internal nodes as well as the bending and torsional moments and the shear forces at the integration points are calculated and found out to correspond exactly to the analytical results given above for the constant bending test, but not for the constant shear test. It should be noted that the constant shear test performed here is related to a a linear change in curvature

(third-order cylindrical bending) and in fact by definition requires an element to enable cubic distribution of the displacement field and the quadratic distribution of the rotation fields, for which the analysed element is not designed. This test should not be mistaken for the constant shear test with no curvature as a consequence of a suitable choice of distributed moment loadings [9], which the analysed element also passes.

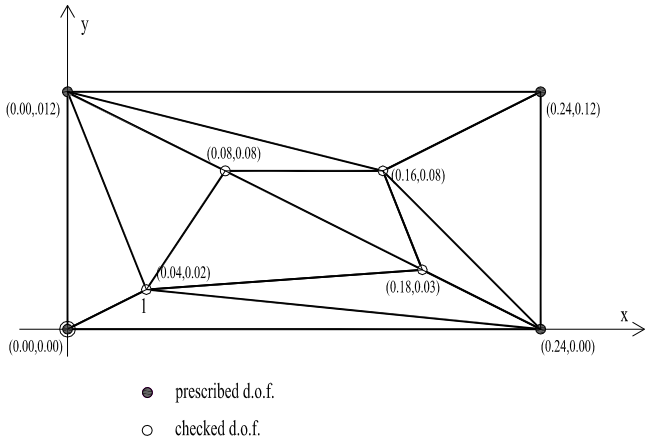

Fig. 18: *Element patch for consistency assessment of three-node elements*

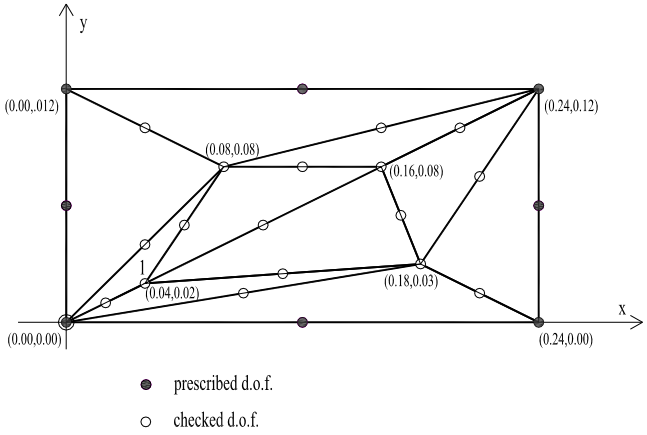

Fig. 19: *Element patch for consistency assessment of six-node elements*

The six node triangle element *T6-U3* is tested on the similar patch example (the mesh is given in Fig. 19). Again, only the displacements and rotations at the boundary nodes are given (8 displacements and 16 rotations), while all the internal nodal displacements and rotations are to be calculated by the finite-element solution procedure. In fact they are calculated exactly for both the constant bending and the constant shear test. The moments and shear forces at the integration points are also exact.

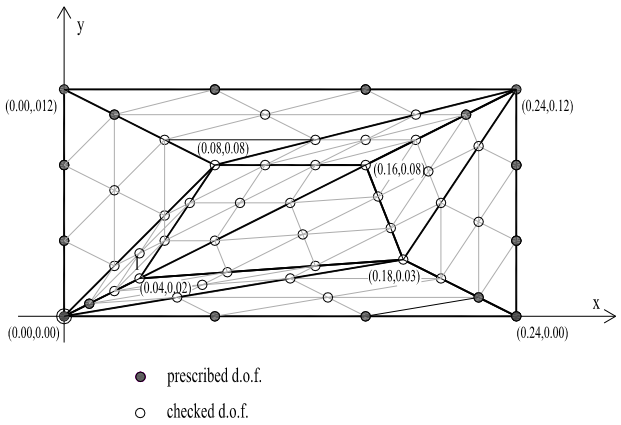

Fig. 20: *Element patch for consistency assessment of ten-node elements*

The same patch tests are also successfully performed by the ten-node elements *T10-U4*, where 48 parameters for the degrees of freedom are prescribed and 108 others are checked (Fig. 20).

The results of the patch tests for all three proposed triangular elements are given in Table 1 for the displacement at node 1 with co-ordinates (0.04, 0.02).

Furthermore, the quartic interpolation for the displacement field would enable the ten-node element *T10-U4* to exactly reproduce even the cylindrical bending of the fourth order.

Table 1: The patch test results for the proposed elements (displacement at point 1: w_1)

Elements	*Patch test for constant curvature*			*Patch test for constant shear*		
	h=1.0	*h=0.01*	*result*	*h=1.0*	*h=0.01*	*result*
T3-U2	0.5414000	0.5414000	pass	-0.2455871	0.000318188	fail
T6-U3	0.5414000	0.5414000	pass	-0.2450933	0.000215467	pass
T10-U4	0.5414000	0.5414000	pass	-0.2450933	0.000215467	pass
Analytical solution	0.5414	0.5414		-0.245093333	0.000215467	

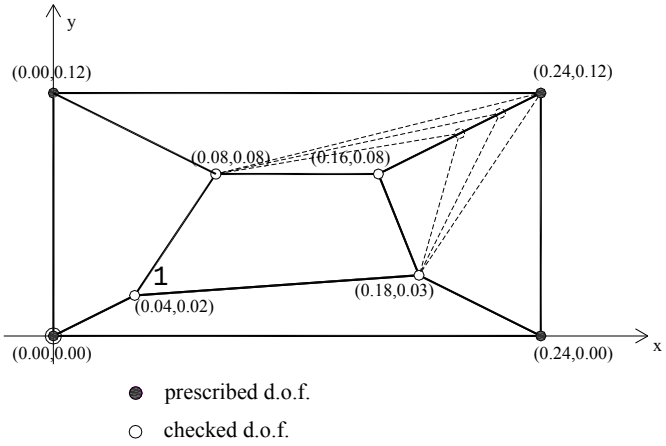

Fig. 21: *Patch for consistency assessment of four-node elements*

The four-node element *Q4U2* is also tested on the patch given in Fig. 21 for constant bending state. For the values of the displacements and rotations at the external nodes calculated from the above data, the displacements and rotations at the internal nodes as well as the bending and torsional moments and the shear forces at the integration points are calculated and again correspond exactly to the analytical results given above. The results are not affected if the internal nodes are defined at a different set of co-ordinates including the case in which one of the internal nodes corresponds with the upper right-hand corner of the patch as shown in Fig. 21. Effectively, the element

naturally degenerates to a triangular element, which is also an observation made in [36].

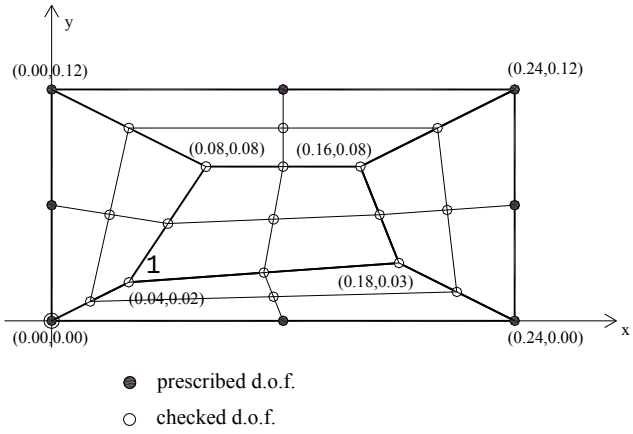

Fig. 22: *Patch for consistency assessment of nine node elements*

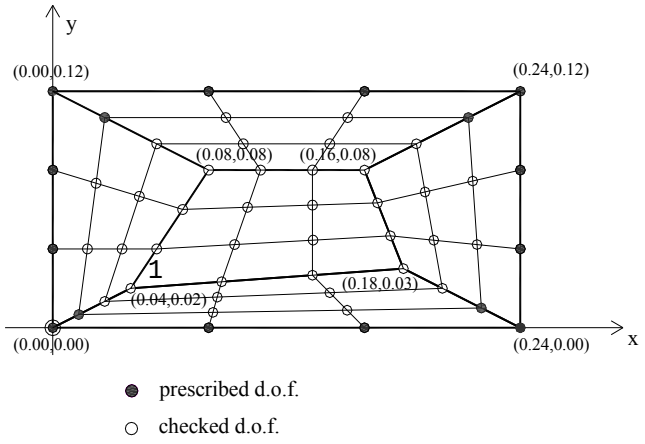

Fig. 23: *Patch for consistency assessment of sixteen node elements*

The nine-node element *Q9-U3* is tested on the same patch examples (the mesh is given in Fig. 22). Only the displacements and rotations at the boundary nodes are given (8 displacements and 16 rotations). All the other nodal displacements and rotations are to be calculated and they are calculated exactly for both the constant

bending and the constant shear tests. The moments and shear forces at the integration points are again exact.

The same patch tests are also successfully performed by five sixteen-node elements *Q16-U4*, where 48 parameters for the degrees of freedom are prescribed and 108 others are checked out (Fig. 23).

The results of the patch tests for all three proposed quadrilateral elements are given the Table 2 for the control displacement at node 1. All elements can pass the patch test for zero shear deformation and only *Q4-U2* fails the test for non-zero constant shear.

Table 2: The patch test results for three proposed elements (control deformation at point 1: w_1)

Elements	*Patch test for zero shear*			*Patch test for non-zero constant shear*		
	h=1.0	*h=0.01*	*result*	*h=1.0*	*h=0.01*	*result*
Q4-U2	0.5414000	0.5414000	pass	-0.2456171	-0.000017896	fail
Q9-U3	0.5414000	0.5414000	pass	-0.2450933	0.000215467	pass
Q16-U4	0.5414000	0.5414000	pass	-0.2450933	0.000215467	pass
Analytical solution	0.5414	0.5414		-0.245093333	0.000215467	

5.6. Test examples for plates

In all the examples to follow the elements presented in this thesis are denoted as triangles *T3-U2* for the three-node, *T6-U3* for the six-node and *T10-U4* for the ten-node element and quadrilaterals *Q4-U2* for the four-node, *Q9-U3* for the nine-node and *Q16-U4* for the sixteen-node element.

The results for triangle elements are compared to the mixed-type element of Auricchio and Taylor denoted as *T3-LIM* [30] and integrated in *FEAP* (A Finite Element Analysis Program) by the same authors, or to the *T3BL* element [12]. Also, comparison is made to *MIN3* and *MIN6* elements [8].

The results for quadrilaterals are compared with the mixed-type element of Auricchio and Taylor [3] denoted as *Q4-LIM* and with the hybrid-type element of de Miranda and Ubertini [9] denoted as *9βQ4*.

5.6.1. Clamped square plate

In this example a quadratic plate with clamped edges is considered. Only one quarter of the plate is modeled with symmetric boundary conditions imposed on the symmetry lines. Two ratios of span versus thickness are analysed, $L/h=10$ representing a relatively thick plate and $L/h= 1000$ representing its thin counterpart. The loading on the plate is uniformly distributed of magnitude $q = 1$. The plate material properties are $E = 10.92$ and $v = 0.3$.

The numerical results are given in Tables 3 and 4 for two different mesh patterns (*a* and *b* in Fig. 24) and compared to the elements presented in [12, 30] based on the mixed approach or using the *T3BL* element [12] from the finite-element analysis programme *FEAP* [1]. The dimensionless results $w^*= w / (qL^4/100D)$ and $M^*=M / (qL^2/100)$, where $D=Eh^3/(12(1-v^2))$ and L is the plate span, given in these tables are

related to the central displacement of the plate and the bending moment at the integration point nearest to the centre of the plate. The number of elements per mesh in these tables is given for one quarter of the structure as shown in Fig. 24 for the *4x4* mesh consisting of 32 elements.

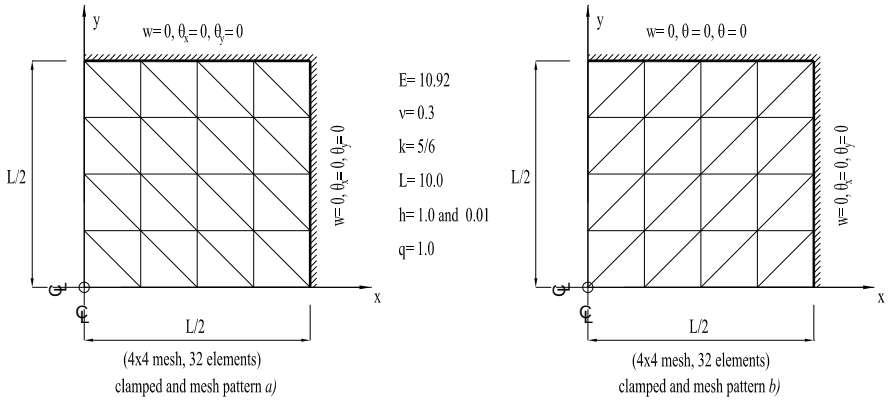

Fig. 24: *A quarter of the square plate under uniform load (32-element mesh)*

Table 3a: Clamped square plate: displacement and moment at the centre using mesh pattern a), *L/h= 10*

Element mesh	*T3-U2 = MIN3*		*T6-U3*		*T10-U4*	
	*w**	*M**	*w**	*M**	*w**	*M**
1x1	0.011905	-	0.109953	2.78382	0.149621	2.24062
2x2	0.093113	1.54908	0.147738	2.44245	0.150373	2.10660
4x4	0.136004	2.14715	0.150250	2.35521	0.150456	2.31965
8x8	0.146780	2.28127	0.1504437	2.32909	0.1504623	2.31997
16x16	0.149521	2.31093	0.1504611	2.32229	0.1504626	2.31998
32x32	0.150224	2.31779	0.1504625	2.32056		
64x64	0.1504021	2.31944				
Ref. sol. [37]	0.150191		0.150191		0.150191	

Element	*T3BL*		*MIN6*	
mesh	*w**	*M**	*w**	*M**
1x1	0.027452	-	0.111003	2.68933
2x2	0.108628	1.706	0.147927	2.43947
4x4	0.139052	2.172	0.150267	2.35489
8x8	0.147453	2.284	0.1504445	2.32907
16x16	0.149685	2.311	0.1504611	2.32229
32x32	0.150264	2.318	0.1504625	2.32056
64x64	0.150412	2.319		
Ref. sol. [37]	0.150191		0.150191	

Clearly, all the new elements converge towards the same solution as the elements from the literature, and the higher-order elements exhibit an expected faster convergence rate. Still, the lowest-order element *T3-U2* is somewhat inferior to *T3BL*, which is not surprising knowing that that element is actually based on the linked interpolation as in T3-*U2* on top of which additional improvements are made. The minute differences between the results of *T6-U3* and *MIN6* are attributed to the slight difference in these elements as explained in Section 6.1.2. The results do not differ considerably between the two mesh patterns (shown in Tables 3a and 3b).

Table 3b: Clamped square plate: displacement and moment at the centre using mesh pattern b), *L/h= 10*

Element	*T3-U2 =MIN3*		*T6-U3*		*T10-U4*	
mesh	*w**	*M**	*w**	*M**	*w**	*M**
1x1	0.023810	-	0.133334	3.31099	0.150650	2.29043
2x2	0.107572	1.67455	0.150247	2.63888	0.150386	2.31564
4x4	0.141724	2.20593	0.150447	2.39797	0.150455	2.31955
8x8	0.148406	2.29114	0.150458	2.33941	0.1504622	2.31996
16x16	0.149959	2.31216	0.1504621	2.32486	0.1504626	2.31998
32x32	0.150339	2.31796	0.1504625	2.32121		
64x64	0.150432	2.31948				
Ref. sol. [37]	0.150191		0.150191		0.150191	

Element	*T3BL* [12]		*MIN6*	
mesh	*w**	*M**	*w**	*M**
1x1			0.128411	3.21000
2x2	0.126275	1.59649	0.150072	2.63367
4x4	0.144973	2.15009	0.150435	2.39768
8x8	0.149114	2.27741	0.150457	2.33937
16x16	0.150131	2.30930	0.1504620	2.32486
32x32	0.150382	2.31734	0.1504625	2.32121
64x64	0.150443	2.31933		
Ref. sol. [37]	0.150191		0.150191	

Convergence of the central displacement for the thick-plate case is presented in Fig. 25, with respect to the number of degrees of freedom (in logarithmic scale). Best convergence with respect to the number of degrees of freedom can be observed in elements with higher-order linked interpolation and it may be concluded that for the thick clamped plate the present elements converge competitively for a comparable number of degrees of freedom.

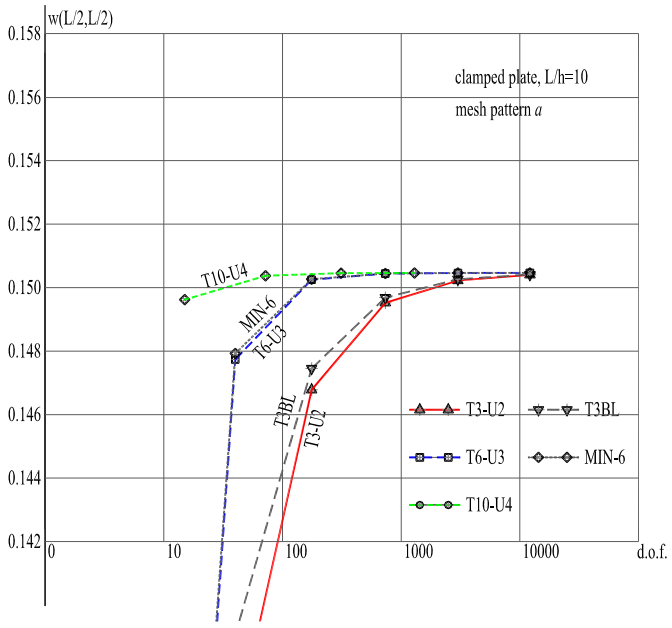

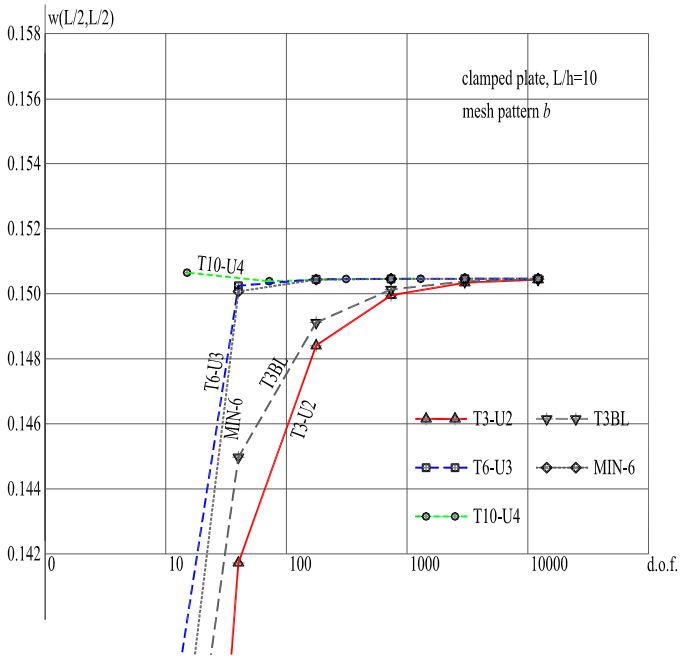

Fig. 25: *Convergence of the transverse displacement at the centre for L/h=10, mesh pattern a and b*

The M_x moment distribution along the x axis is computed at the Gauss points closest to the axis and, beginning from the centre point of the plate, shown in Fig. 26. These results are the same as the results for the moment M_y along the y direction. For *T3-U2* element, the moment is constant across the element, owing to its dependence on the derivatives of rotations (32) in both directions. For elements *T6-U3* and *T10-U4*, the moment distribution is accordingly linear or quadratic, respectively, and the results converge towards the exact distribution fast. Similar observations may be made for the distribution of the shear-stress resultants.

For the thin plate case shown in Tables 4a and 4b, the elements *T3-U2* and *T6-U3* suffer from some shear locking when the meshes are coarse, but as expected they

converge to the correct result. The higher-order elements exhibit an expected faster convergence rate.

A comparison is again made between the two different triangular mesh patterns (Tables 4a and 4b). As for the case of the thick plate, the lowest-order element *T3-U2* is still somewhat inferior to *T3BL*, while *T6-U3* is marginally better than *MIN6*. The results for the mesh pattern *b)* are slightly better than those for the mesh pattern *a)*.

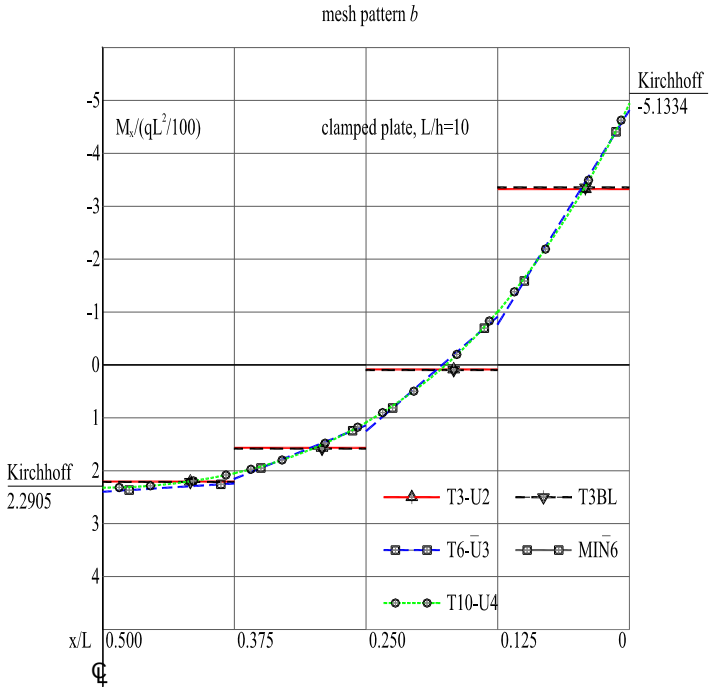

Fig. 26: *Moment M_x distribution along element's Gauss points closest to the x axis on the 4x4 regular mesh for the clamped plate with L/h=10*

Likewise, comparing the triangular linked-interpolation elements to their quadrilateral counterparts [29] shows that for the same number of the degrees of freedom the latter converges a little faster (Table 6).

Table 4a: Clamped square plate: displacement and moment at the centre using mesh pattern a), *L/h = 1000.*

Element	*T3-U2 = MIN3*		*T6-U3*		*T10-U4*	
mesh	*w**	*M**	*w**	*M**	*w**	*M**
1x1	0.000001		0.000057	0.00195	0.113949	2.03147
2x2	0.000052	0.00112	0.080795	1.09704	0.125997	2.28567
4x4	0.001531	0.02764	0.116226	1.87195	0.126515	2.29025
8x8	0.025112	0.38406	0.125363	2.18328	0.1265340	2.29044
16x16	0.100985	1.64321	0.126496	2.27223	0.1265344	2.29050
32x32	0.124358	2.20020	0.1265336	2.28838		
64x64	0.126356	2.28191				
Ref. sol. [11]	0.126532	2.29051	0.126532	2.29051	0.126532	2.29051

Element	*T3BL*		*MIN6*	
mesh	*w**	*M**	*w**	*M**
1x1			0.000048	0.00159
2x2	0.083024	1.624	0.080767	1.09628
4x4	0.113803	2.084	0.116161	1.86944
8x8	0.123452	2.240	0.125316	2.18097
16x16	0.125790	2.278	0.126494	2.27158
32x32	0.126352	2.287	0.1265336	2.28826
64x64	0.126489	2.290		
Ref. sol. [11]	0.126532	2.29051	0.126532	2.29051

Table 4b: Clamped square plate: displacement and moment at the centre using mesh pattern b), *L/h = 1000.*

Element	*T3-U2 = MIN3*		*T6-U3*		*T10-U4*	
mesh	*w**	*M**	*w**	*M**	*w**	*M**
1x1			0.000069	0.00206	0.130198	4.05972
2x2	0.000062	0.00127	0.097869	2.03760	0.126738	2.74752
4x4	0.001793	0.03807	0.121256	2.44562	0.126527	2.34533
8x8	0.028267	0.55913	0.125905	2.38599	0.1265340	2.29246
16x16	0.104428	2.12079	0.1265121	2.31332	0.1265344	2.29055
32x32	0.124820	2.32200	0.1265341	2.29420		
64x64	0.126403	2.29435				
Ref. sol. [11]	0.126532	2.29051	0.126532	2.29051	0.126532	2.29051

Element mesh	*T3BL* [12]		*MIN6*	
	*w**	*M**	*w**	*M**
1x1			0.000061	0.00182
2x2	0.093098	1.40767	0.097850	2.03613
4x4	0.118006	2.10245	0.121205	2.43983
8x8	0.124616	2.24825	0.125878	2.38437
16x16	0.126092	2.28031	0.1265107	2.31409
32x32	0.126429	2.28798	0.1265341	2.29440
64x64	0.126509	2.28987		
Ref. sol. [11]	0.126532	2.29051	0.126532	2.29051

The same example of the clamped plate (Fig. 27) is modeled with presented quadrilateral elements *Q4-U2*, *Q9-U3* and *Q16-U4*.

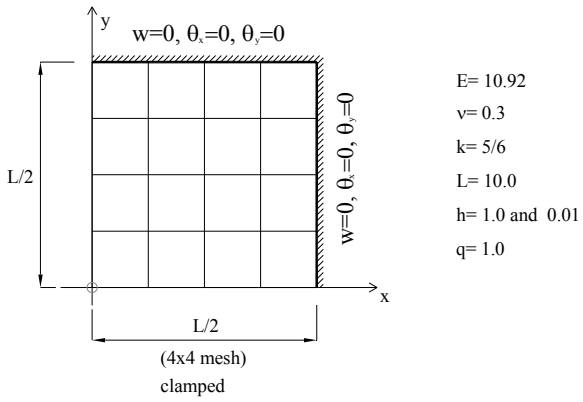

Fig. 27*: A quarter of the square plate under uniform load (16-element mesh)*

Numerical results are given in Tables 5 and 6 and compared to the elements presented in [3,9] based on the mixed approach and with the reference solutions taken from [3]. The number of elements per mesh in these tables relates to one quarter of the structure as shown in Fig. 27 for the mesh of 4x4 elements.

Table 5: Clamped square plate: displacement and moment at the centre with regular meshes, *L/h = 10*

Element mesh	*Q4-U2*		*Q9-U3*		*Q16-U4*	
	*w**	*M**	*w**	*M**	*w**	*M**
1x1	0.02679		0.15059	1.971	0.14974	2.08359
2x2	0.11920	1.63801	0.15046	2.229	0.15041	2.30177
4x4	0.14361	2.16385	0.15044	2.297	0.15046	2.31802
8x8	0.14876	2.28107	0.15046	2.314	0.15046	2.31966
16x16	0.15004	2.31025	0.15046	2.31857		
32x32	0.15036	2.31755	0.15046	2.31963		
64x64	0.15044	2.31938				
Ref. sol. [37]	0.150191		0.150191		0.150191	

Element mesh	*Q4-LIM*		*9βQ4*	
	*w**	*M**	*w**	*M**
1x1	0.12107			
2x2	0.14211	1.660	0.1625190	2.83817
4x4	0.14858	2.157	0.1534432	2.44825
8x8	0.14997	2.279	0.1511805	2.35119
16x16	0.15034	2.310	0.1506379	2.32770
32x32	0.15043	2.317	0.1505061	2.32191
64x64	0.15045	2.319		
Ref. sol. [37]	0.150191		0.150191	

Convergence of the displacement error is presented in Fig. 28, with respect to the number of degrees of freedom in chosen element meshes (in logarithmic scale). Zero error value corresponds to the referent solution taken from [3,17]. Best convergence with respect to the number of degrees of freedom can be observed in elements with higher-order linked interpolation. Table 5 and Fig. 28 show that for the thick clamped plate the present elements converge competitively for a comparable number of degrees of freedom.

In Fig. 29, the M_x moment distribution along the x axis is shown (actually at the Gauss points closest to the axis), beginning from the centre point of the plate (origin of the co-ordinate system of the mesh). These results are the same as the results for the

moment M_y along the y direction. For *Q4-U2* element, moment is distributed linearly across the element, owing to its dependence on the curvatures in both directions for any non-zero value of the Poisson coefficient (12). For ν=0 this moment would be constant as in the Timoshenko beam. For higher-order elements, the moment distribution is accordingly described by higher polynomials, and the results converge towards the exact distribution fast.

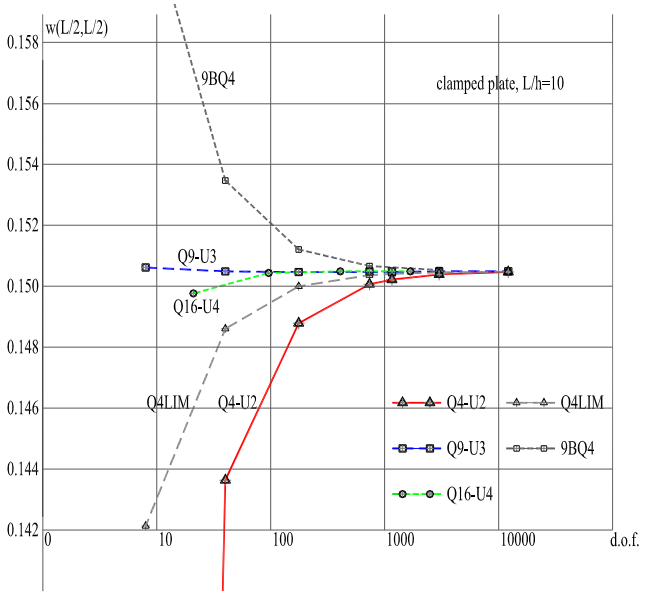

Fig. 28: *Convergence of the transverse displacement error at the centre on regular meshes for clamped plate L/h=10*

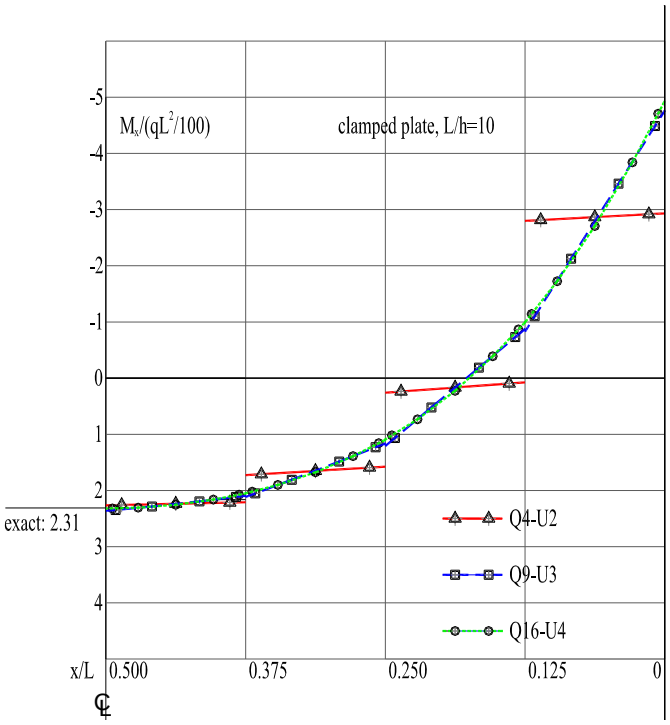

Fig. 29: *Moment M_x distribution along element's Gauss points closest to the x axis on the 4x4 regular mesh for the clamped plate with L/h=10*

In Fig. 30, shear distribution S_x along the x axis is shown (again at the closest Gauss point to the axis), beginning from the centre point of the plate. For *Q4-U2* element, the distribution of S_x along the x axis is linear, but this time due to the internal bubble interpolation function (41) without which it would be constant. The same shear S_x but along the y axis is quadratic due to the linked interpolation functions and their derivatives. For the higher order elements, the distribution is of a correspondingly higher order, and the difference with respect to the exact shear force distribution becomes increasingly smaller.

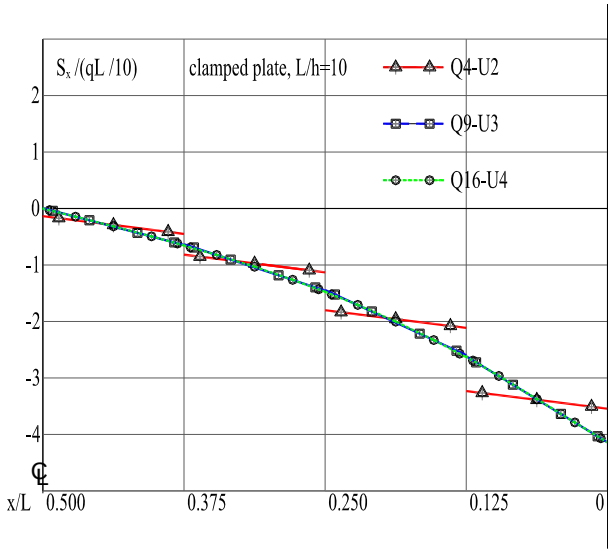

Fig. 30: *Shear force S_x distribution along element's Gauss points closest to the x axis on the 4x4 regular mesh for the clamped plate with L/h=10*

For the thin plate case, the displacement-based elements *Q4-U2* and *Q9-U3* obviously suffer from shear locking when the meshes are coarse (lower order element *Q4-U2*), but they still converge to the correct result competitively fast, in particular the higher-order elements *Q9-U3* and *Q16-U4*.

A comparison is done between full integration rule for deformation energy, and that is 3 by 3 integration points for quadratic interpolations (*Q4-U2*), 4 by 4 integration for cubic interpolations (*Q9-U3*) and 5 by 5 integration for bi-quadratic interpolations (*Q16-U4*), with the reduced ones on the same elements.

Table 6: Clamped square plate: displacement and moment at the centre with regular meshes, $L/h = 1000$. In upper part integration is performed with full integration rule. I lower part the reduced integration is performed.

Element	*Q4-U2*	*G.p.3x3*	*Q9-U3*	*G.p.4x4*	*Q16-U4*	*G.p.5x5*
mesh	*w**	*M**	*w**	*M**	*w**	*M**
1x1	0.0000027		0.0002699	0.0041	0.13241	3.70328
2x2	0.0001284		0.099183	1.998	0.12646	2.40533
4x4	0.0046933	0.10106	0.12112	2.224	0.12653	2.29613
8x8	0.059881	1.17024	0.12621	2.282	0.12653	2.29039
16x16	0.11899	2.16797	0.12653	2.28902		
32x32	0.12600	2.28115	0.12653	2.29016		
64x64	0.12648	2.28948				
Ref. sol.	0.1265319	2.29051	0.1265319	2.29051	0.1265319	2.29051

Element	*Q4-U2*	*G.p.2x2*	*Q9-U3*	*G.p.3x3*	*Q16-U4*	*G.p.4x4*
mesh	*w**	*M**	*w**	*M**	*w**	*M**
1x1	0.0000027		0.00060	0.01432	0.13229	3.46904
2x2	0.0001706	0.00287	0.09832	1.90152	0.12627	2.24644
4x4	0.0105329	0.25856	0.12163	2.23799	0.1265285	2.28636
8x8	0.095705	1.96897	0.12629	2.28926	0.1265344	2.28986
16x16	0.12406	2.26174	0.1265295	2.29105		
32x32	0.12634	2.28730	0.1265344	2.29066		
64x64	0.12650	2.28987				
Ref. sol.	0.1265319	2.29051	0.1265319	2.29051	0.1265319	2.29051

Element	*Q4-LIM*		*9βQ4*	
mesh	*w**	*M**	*w**	*M**
1x1	0.090741			
2x2	0.11469		0.13766768	2.745544
4x4	0.12362	2.120	0.12938531	2.423885
8x8	0.12584	2.248	0.12725036	2.323949
16x16	0.12637	2.280	0.12671406	2.298876
32x32	0.12649	2.288	0.12657946	2.292605
64x64	0.12652	2.290		
Ref. sol.	0.1265319	2.29051	0.1265319	2.29051

The reduced integration in the middle part of table 2 shows some improvement in convergence for low order elements and coarse meshes, but has no importance for higher order elements and dense meshes.

5.6.2. Simply supported square plate

In this example the quadratic plate as before is considered, but this time with the simply supported edges of the type SS2 (displacements and rotations around the normal to the edge set to zero) as shown in Fig. 31. The same elements as before are tested and the results are given in Tables 7 and 8 for the thick and the thin plate, respectively, compared again to the elements presented in [3,30].

The dimensionless results $w^*= w / (qL^4/100D)$ and $M^*=M / (qL^2/100)$ given in these tables are related to the central displacement of the plate and the bending moment at the integration point nearest to the centre of the plate. The number of elements per mesh in these tables relates to one quarter of the structure.

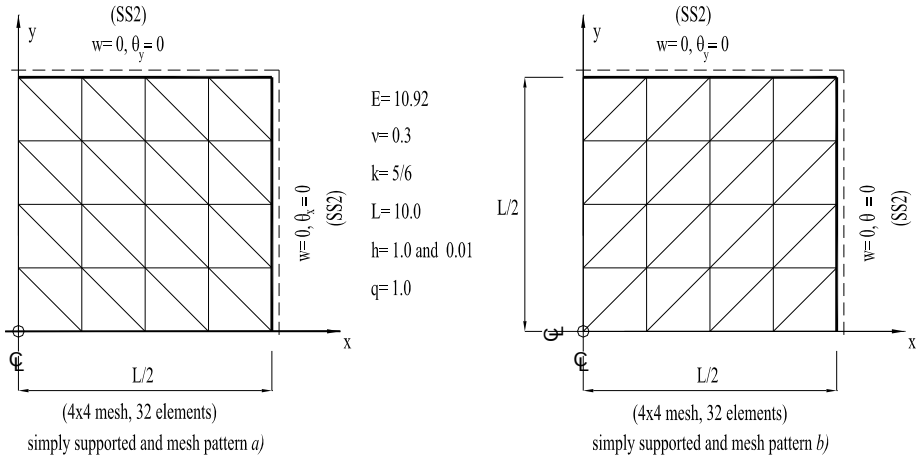

Fig. 31: *A quarter of the square plate under uniform load (32-element mesh)*

Table 7a: Simply supported square plate (SS2) under uniformly distributed load: displacement and moment at the centre using mesh pattern a), *L/h = 10.*

Element	*T3-U2 =MIN3*		*T6-U3*		*T10-U4*	
mesh	*w**	*M**	*w**	*M**	*w**	*M**
1x1	0.337426	3.38542	0.392336	4.67154	0.427715	4.75435
2x2	0.387559	4.24192	0.425236	4.86395	0.427289	4.78646
4x4	0.418375	4.71153	0.427160	4.81585	0.4272843	4.78851
8x8	0.425129	4.78211	0.427276	4.79595	0.4272842	4.78863
16x16	0.426739	4.78913	0.4272837	4.79050	0.4272842	4.78862
32x32	0.427145	4.78913	0.4272842	4.78910		
64x64	0.427249	4.78883				
Navier series Ref. [11]	0.427284	4.78863	0.427284	4.78863	0.427284	4.78863

Element	*T3BL* [12]		*MIN6*		*T3-LIM* [30]	
mesh	*w**	*M**	*w**	*M**	*w**	*M**
1x1			0.394395	4.63782		
2x2	0.403591	4.48351	0.425509	4.85815	0.40786	4.0918
4x4	0.421194	4.74389	0.427183	4.81531	0.42293	4.6063
8x8	0.425688	4.78521	0.427278	4.79591	0.42627	4.7398
16x16	0.426869	4.78940	0.427284	4.79049	0.42704	4.7755
32x32	0.427177	4.78915	0.427284	4.78910	0.42723	4.7852
64x64	0.427257	4.78883				
Navier series Ref. [11]	0.427284	4.78863	0.427284	4.78863	0.427284	4.78863

Table 7b: Simply supported square plate (SS2) under uniformly distributed load: displacement and moment at the centre with mesh pattern b), *L/h = 10.*

Element	*T3-U2 =MIN3*		*T6-U3*		*T10-U4*	
mesh	*w**	*M**	*w**	*M**	*w**	*M**
1x1	0.080445	3.89473	0.436000	6.02777	0.427448	4.82577
2x2	0.352341	4.06337	0.428107	5.07579	0.427286	4.78651
4x4	0.413784	4.64329	0.427349	4.85350	0.4272838	4.78845
8x8	0.424307	4.74712	0.427289	4.80443	0.4272842	4.78862
16x16	0.426574	4.77642	0.4272846	4.79257	0.4272842	4.78862
32x32	0.427111	4.78524	0.4272843	4.78962		
64x64	0.427242	4.78772				
Navier series Ref. [11]	0.427284	4.78863	0.427284	4.78863	0.427284	4.78863

Table 8a: Simply supported square plate (SS2) under uniformly distributed load: displacement and moment at the centre with mesh pattern a), *L/h = 1000.*

Element	*T3-U2 =MIN3*		*T6-U3*		*T10-U4*	
mesh	*w**	*M**	*w**	*M**	*w**	*M**
1x1	0.325522	3.38542	0.325543	2.51970	0.405992	4.53393
2x2	0.325541	3.07155	0.389672	3.56892	0.406198	4.78210
4x4	0.326331	2.67663	0.402526	4.25254	0.406234	4.78844
8x8	0.339027	2.80820	0.405659	4.62852	0.4062373	4.78860
16x16	0.383803	4.01006	0.406211	4.76246	0.4062374	4.78861
32x32	0.403889	4.67235	0.406237	4.78543		
64x64	0.406062	4.77806				
Navier series Ref. [11]	0.406237	4.78863	0.406237	4.78863	0.406237	4.78863

Element	*T3BL* [12]		*MIN6*		*T3-LIM* [30]	
mesh	*w**	*M**	*w**	*M**	*w**	*M**
1x1			0.325542	2.51962		
2x2	0.377793	4.26461	0.389669	3.56861	0.38412	4.0831
4x4	0.399068	4.65804	0.402518	4.25114	0.40114	4.6071
8x8	0.404642	4.76074	0.405646	4.62584	0.40503	4.7408
16x16	0.405871	4.78282	0.406209	4.76157	0.40594	4.7759
32x32	0.406150	4.78747	0.406237	4.78525	0.40616	4.7853
64x64	0.406216	4.78844				
Navier series Ref. [11]	0.406237	4.78863	0.406237	4.78863	0.406237	4.78863

Table 8b: Simply supported square plate (SS2) under uniformly distributed load: displacement and moment at the centre with mesh pattern b), *L/h = 1000.*

Element	*T3-U2 =MIN3*		*T6-U3*		*T10-U4*	
mesh	*w**	*M**	*w**	*M**	*w**	*M**
1x1	0.0000116	-	0.416667	6.49979	0.407968	5.68492
2x2	0.0006793	-	0.409630	5.89979	0.406485	4.99024
4x4	0.0143996	0.18208	0.407029	5.34060	0.406249	4.81505
8x8	0.146596	1.89158	0.406347	4.96262	0.4062375	4.78956
16x16	0.359328	4.79873	0.406244	4.81830	0.4062374	4.78866
32x32	0.402644	4.84606	0.4062376	4.79308		
64x64	0.405975	4.79435				
Navier series Ref. [11]	0.406237	4.78863	0.406237	4.78863	0.406237	4.78863

For the thick plate case, it can be concluded that elements *T6-U3* and *T10-U4* converge considerably faster than elements based on the mixed approach and no locking can be observed on coarse meshes, even for the three-node element *T3-U2*. In the thin plate example, locking on the coarse meshes can be observed for *T3-U2*, but higher order elements, again, show very good convergence rate.

In contrast to the clamped plate problem, here mesh pattern *a)* has slightly better convergence than mesh pattern *b),* where the exact solution for the higher-order elements *T6-U3* and *T10-U4* is approached from the softer side.

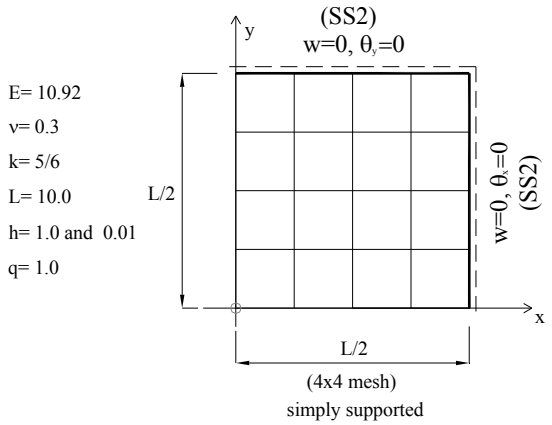

Fig. 32*: A quarter of the square plate under uniform load (16-element mesh)*

The same example of the quadratic plate as before is considered subjected to uniformly distributed pressure, but this time with quadrilateral elements. The results are given in Tables 9 and 10 for the thick and the thin plate, respectively. The model is also analysed for central point load *P*, for various span to thickness ratios and results are given in Table 11.

Table 9: Simply supported square plate (SS2) under uniformly distributed load: displacement and moment at the centre with regular meshes, *L/h = 10*

Mesh	*Q4-U2*		*Q9-U3*		*Q16-U4*	
	*w**	*M**	*w**	*M**	*w**	*M**
1x1	0.26102	1.62404	0.42983	4.443	0.42717	4.66623
2x2	0.41163	4.140	0.42749	4.700	0.42728	4.77762
4x4	0.42448	4.636	0.42730	4.766	0.42728	4.78712
8x8	0.42664	4.751	0.42729	4.783	0.42728	4.78833
16x16	0.42713	4.779	0.42728	4.78722		
32x32	0.42725	4.78629	0.42728	4.78828		
64x64	0.42727	4.78805				
Navier series	0.427284	4.78863	0.427284	4.78863	0.427284	4.78863

Mesh	*Q4-LIM*		*9βQ4*	
	*w**	*M**	*w**	*M**
1x1	0.40562	2.078		
2x2	0.42626	4.125	0.4286943	5.264135
4x4	0.42720	4.623	0.4276333	4.905958
8x8	0.42727	4.747	0.4273690	4.817645
16x16	0.42728	4.778	0.4273052	4.795864
32x32	0.42728	4.786	0.4272895	4.790443
64x64	0.42728	4.788		
Navier series	0.427284	4.78863	0.427284	4.78863

For the thick plate case it can be concluded that elements *Q4-U2* and *Q9-U3* converge a little slower, but element *Q16-U4* shows remarkable accuracy even for a very coarse mesh.

Table 10: Simply supported square plate (SS2) under uniformly distributed load: displacement and moment at the centre with regular meshes, *L/h = 1000*

Element mesh	*Q4-U2*		*Q9-U3*		*Q16-U4*	
	*w**	*M**	*w**	*M**	*w**	*M**
1x1	0.0000008	0.00053	0.35527	3.531	0.41220	5.49186
2x2	0.0031093	0.03396	0.39807	4.609	0.40647	4.85587
4x4	0.055621	0.66535	0.40475	4.751	0.40624	4.79124
8x8	0.29658	3.52362	0.40615	4.782	0.40624	4.78843
16x16	0.39706	4.67709	0.40624	4.78720		
32x32	0.40562	4.77974	0.40624	4.78828		
64x64	0.40619	4.78764				
Navier series	0.406237	4.78863	0.406237	4.78863	0.406237	4.78863

Element mesh	*Q4-LIM*		*9βQ4*	
	*w**	*M**	*w**	*M**
1x1	0.37646	2.018		
2x2	0.40365	4.119	0.4063653	5.241563
4x4	0.40586	4.623	0.4063062	4.904153
8x8	0.40616	4.747	0.4062559	4.817513
16x16	0.40622	4.778	0.4062421	4.795855
32x32	0.40623	4.786	0.4062386	4.790442
64x64	0.40624	4.788		
Navier series	0.406237	4.78863	0.406237	4.78863

For the thin plate case elements *Q4-U2* and *Q9-U3* still suffer from shear locking, but element *Q16-U4* again shows very good convergence rate.

Table 11: Simply supported square plate (SS2) with the central point force: The displacement and the moment at the centre with regular mashes, *L/h = 10:*

Element mesh	*Q4-U2*		*Q9-U3*		*Q16-U4*	
	*w**	*M**	*w**	*M**	*w**	*M**
1x1					1.323308	0.241877
2x2			1.325420	0.250847	1.367704	0.315569
4x4	1.278513	0.205486	1.368758	0.324208	1.402043	0.387595
8x8	1.342758	0.276341	1.403094	0.396356	1.434254	0.459374
16x16	1.384068	0.347739	1.435309	0.468175		
32x32	1.418471	0.419343	1.467002	0.539910		
64x64	1.450823	0.491019				
Navier series	1.346		1.346		1.346	

The displacement and the moment at the centre with regular mashes, *L/h = 100*:

Element mesh	*Q4-U2*		*Q9-U3*		*Q16-U4*	
	*w**	*M**	*w**	*M**	*w**	*M**
1x1					0.1124933	0.207525
2x2			0.1117242	0.216046	0.1155850	0.298162
4x4	0.1032672	0.173925	0.1156059	0.310005	0.1161326	0.380545
8x8	0.1141181	0.264313	0.1161416	0.391813	0.1162576	0.457264
16x16	0.1157769	0.343923	0.1162595	0.466979		
32x32	0.1161476	0.418526	0.1163095	0.539615		
64x64	0.1162663	0.490966				
Navier series	1.160		1.160		1.160	

The displacement and the moment at the centre with regular mashes, *L/h = 1000*:

Mesh	*Q4-U2*		*Q9-U3*		*Q16-U4*	
	*w**	*M**	*w**	*M**	*w**	*M**
1x1					1.108122	0.186094
2x2			1.034215	0.141198	1.147743	0.262474
4x4	0.142801	0.020359	1.128158	0.229189	1.157285	0.341231
8x8	0.802266	0.143671	1.154919	0.328508	1.159517	0.422959
16x16	1.119129	0.278071	1.159353	0.426520		
32x32	1.155844	0.383003	1.160005	0.520375		
64x64	1.159544	0.474917				
Navier series	1.160	∞	1.160	∞	1.160	∞

where is $w^*= w / (PL^2/100D)$ and $M^*=M / P$ in the nearest Gauss point (*Q4-U2*: 3x3, *Q9-U3*: 4x4, *Q16-U4*: 5x5).

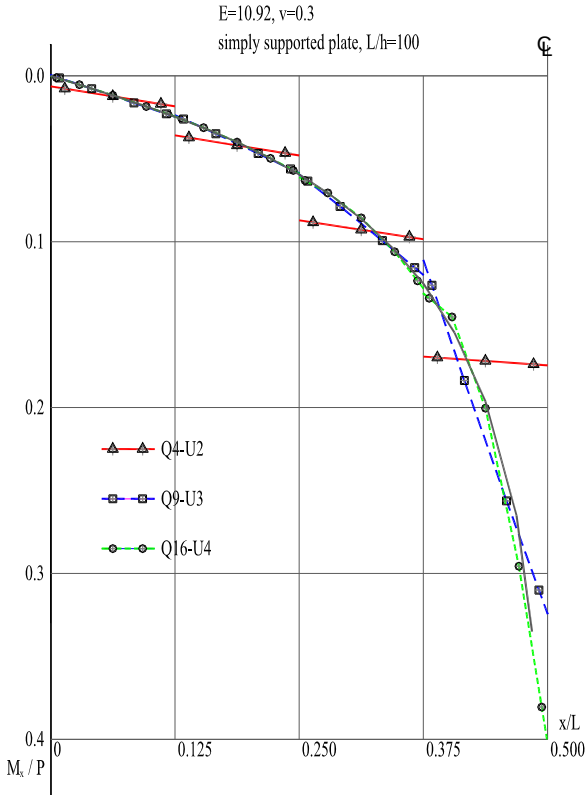

Fig. 33: *Moment M_x distribution along element's Gauss points closest to the x axis on the 4x4 regular mesh for the concentrated force at the midpoint of the simply supported square plate with L/h=100*

The moment distribution for this load case and *L/h=100* and with 4 by 4 element mesh is given in Fig. 33. The moment has singularity at the central point as is well known.

5.6.3. Simply supported skew plate

In this example the rhombic plate is considered with the simply supported edges (this time, of the so-called soft type SS1 [38]) to test performance of the rhombic elements. The problem geometry and material properties are given in Fig. 34, where an example of a 64-element mesh is shown. Three different mesh patterns are tested, as shown in Fig. 35.

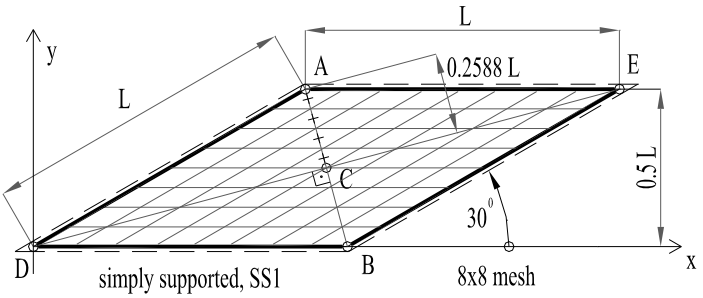

E= 10.92 L= 100.
ν= 0.3 h= 1.0 or 0.10
q= 1.0

Fig. 34: *A simply supported (SS1) skew plate under uniform load*

The same three elements as before are tested and the results are given in Tables 12

and 13 for the thick and the thin plate, respectively. The dimensionless results $w^*= w / (qL^4/10^4D)$, $M_{11}^*=M_{11}/(qL^2/100)$ and $M_{22}^*=M_{22}/(qL^2/100)$ are related to the central displacement of the plate and the principal bending moments in diagonal directions at the integration point nearest to the centre of the plate.

The tested example has two orthogonal axes of symmetry, A-C-B and D-C-E, and only one triangular quarter may be taken for analysis [26,38]. Since there is a singularity in the moment field at the obtuse vertex, this test example is a difficult one. Even more, the analytical solution [38] reveals that moments in the principal directions near the obtuse vertex have opposite signs.

In contrast to the earlier examples, it must be noted that here the new displacement-based elements perform worse than the elements given in [3,12], both for the thick and the thin plate examples. Tables 12c and 13c now reveal slightly more pronounced differences in the results obtained using elements *T6-U3* and *MIN6*, where the latter are somewhat worse, apparently owing to the absence of the internal bubble parameter present in *T6-U3* (see Section 6.1.2). It is interesting to notice that among the presented family of elements with linked interpolation, the best convergence is observed for the mesh pattern a). Also, from Tables 12d and 13d it is apparent that for this test example the new triangular family of linked-interpolation elements is in fact superior to the family of quadrilateral linked-interpolation elements presented in this thesis.

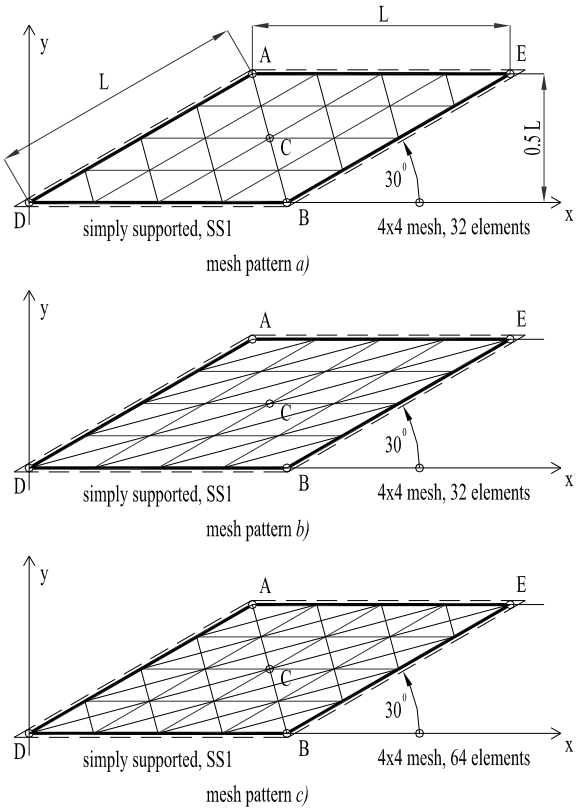

Fig. 35: *A simply supported (SS1) skew plate with three different mesh patterns*

Table 12a: Simply supported skew plate (SS1): displacement and moment at the centre with regular meshes, *L/h = 100.* Mesh pattern a).

Element	*T3-U2 =MIN3*			*T6-U3*			*T10-U4*		
mesh	w^*	M_{22}^*	M_{11}^*	w^*	M_{22}^*	M_{11}^*	w^*	M_{22}^*	M_{11}^*
2x2	0.425288	0.65647	1.35584	0.442337	1.59547	2.48908	0.259711	0.67991	1.29292
4x4	0.393156	1.00823	1.72050	0.391393	1.38415	2.10533	0.410136	1.17851	1.92258
8x8	0.376569	1.11747	1.84630	0.409028	1.18349	1.96100	0.419818	1.12774	1.94013
16x16	0.403524	1.09072	1.87753	0.419769	1.13814	1.95024	0.423207	1.13774	1.95080
24x24	0.412799	1.10360	1.92291	0.422181	1.13934	1.95222			
32x32	0.416390	1.11361	1.93165						
48x48	0.419306	1.12368	1.93948						
Ref. [28]	0.423			0.423			0.423		

Element mesh	*T3-LIM* [30]			*MIN6*		
	w^*	M_{22}^*	M_{11}^*	w^*	M_{22}^*	M_{11}^*
2x2	0.63591	0.9207	1.7827	0.442458	1.61239	2.53454
4x4	0.45819	1.0376	1.8532	0.386472	1.36333	2.10434
8x8	0.43037	1.1008	1.9247	0.405862	1.16617	1.95019
16x16	0.42382	1.1233	1.9376	0.418385	1.13270	1.94618
24x24				0.421307	1.13604	1.94954
32x32	0.42183	1.1284	1.9344			
48x48						
Ref. [28]	0.423			0.423		

Table 12b: Simply supported skew plate (SS1): displacement and moment at the centre with regular meshes, *L/h = 100.* Mesh pattern b).

Node mesh	*D.o.f.*	*T3-U2 = MIN3*		
		w^*	M_{22}^*	M_{11}^*
2x2	19	0.038301	0.10796	0.33128
4x4	59	0.071514	0.18081	0.49677
8x8	211	0.170524	0.39288	0.98827
16x16	803	0.285767	0.67726	1.48281
24x24	1779	0.337019	0.82818	1.67627
32x32	3139	0.362652	0.91441	1.76454
48x48	7011	0.386794	1.00372	1.84209
Ref. [39]		0.423		

Table 12c: Simply supported skew plate (SS1): displacement and moment at the centre with Riggs-Liu meshes, *L/h = 100.* Mesh pattern c),

Element mesh	*D.o.f.*	*T3-U2 = MIN3*			*T6-U3*			*MIN6 (Liu - Riggs)*		
		w^*	M_{22}^*	M_{11}^*	w^*	M_{22}^*	M_{11}^*	w^*	M_{22}^*	M_{11}^*
4x4	107	0.394314	0.99968	1.76770	0.442714	1.57560	2.42260	0.443030	1.58489	2.44230
8x8	403	0.380630	1.09990	1.85008	0.398472	1.29021	1.99636	0.394705	1.28551	1.99557
16x16	1571	0.405027	1.09959	1.90959	0.412030	1.16231	1.93387	0.410138	1.15652	1.92888
Ref. [39]		0.423			0.423			0.423		

Table 12d: *Simply supported skew plate (SS1) under uniformly distributed load: displacement and moment at the centre using quadrilateral linked-interpolation elements [29], L/h= 100*

Element	*Q4-U2*			*Q9-U3*			*Q16-U4*		
mesh	w^*	M_{22}^*	M_{11}^*	w^*	M_{22}^*	M_{11}^*	w^*	M_{22}^*	M_{11}^*
2x2	0.06153	0.1349	0.3763	0.21493	0.4860	1.0536	0.28406	0.8404	1.5335
4x4	0.16287	0.3659	0.9226	0.32974	0.8227	1.6486	0.37778	0.9642	1.8310
8x8	0.29165	0.6870	1.4858	0.38719	1.0083	1.8508	0.40497	1.0681	1.8962
16x16	0.37449	0.9470	1.7959	0.40904	1.0890	1.9094	0.41774	1.1172	1.9345
24x24	0.39633	1.0348	1.8690	0.41554	1.1115	1.9279			
32x32	0.40536	1.0696	1.8890						
48x48	0.41326	1.1028	1.9213						
Ref. [39]	0.423			0.423			0.423		

Mesh	*Q4-LIM*			*9βQ4*		
	w^*	M_1^*	M_2^*	w^*	M_1^*	M_2^*
2x2	0.52729	0.745	1.42			
4x4	0.42571	1.068	1.775	0.502900	1.354215	2.054527
8x8	0.42096	1.140	1.773	0.443176	1.082957	1.956494
16x16	0.42307	1.172	1.858	0.432211	1.149921	1.966940
24x24	0.42494	1.183	1.880			
32x32	0.42619	1.190	1.889	0.426964	1.148682	1.959293
48x48	0.42777	1.196	1.897			
Ref. [39]	0.423			0.423		

In contrast to the earlier examples, it must be noted that here the new displacement-based element perform worse than the elements given in [3,9], both for the thick and the thin plate examples.

The distribution of the principal moments between the obtuse angle at A and the centre-point C is very complex owing to the presence of singularity at A and worth particular consideration. The principal moment M_{11} acting around the in-plane normal to the shorter diagonal converges towards the exact solution satisfactorily, but for the principal moment M_{22} acting around the shorter diagonal it is obvious that this family

of elements finds it difficult to follow the exact moment distribution near the singularity point. These results are shown in Fig. 36 for triangle elements.

Table 13a: Simply supported skew plate (SS1): displacement and moment at the centre with regular meshes, *L/h = 1000.* Mesh pattern a).

Element	*T3-U2 = MIN3*			*T6-U3*			*T10-U4*		
mesh	w^*	M_{22}^*	M_{11}^*	w^*	M_{22}^*	M_{11}^*	w^*	M_{22}^*	M_{11}^*
2x2	0.421115	0.64790	1.33819	0.443104	1.62431	2.52722	0.246108	0.60215	1.16324
4x4	0.393999	1.01757	1.67013	0.348698	1.30423	1.98429	0.356469	1.05704	1.76663
8x8	0.305318	1.11745	1.58532	0.326564	0.86335	1.71994	0.365434	0.95047	1.78325
16x16	0.285607	1.05519	1.61422	0.358165	0.97179	1.80192	0.390331	1.02111	1.85543
24x24	0.309866	1.05211	1.68162	0.376441	0.99480	1.82813			
32x32	0.330657	1.00984	1.72183						
48x48	0.360440	0.96062	1.77377						
Ref. [38]	0.4080	1.08	1.91	0.4080	1.08	1.91	0.4080	1.08	1.91

Element	*T3BL*[12]			*MIN6*		
mesh	w^*	M_{22}^*	M_{11}^*	w^*	M_{22}^*	M_{11}^*
2x2	0.537100	0.74915	1.44018	0.443109	1.62421	2.52671
4x4	0.420881	0.95544	1.72257	0.348478	1.30308	1.98405
8x8	0.415286	1.09045	1.89280	0.324182	0.83373	1.70398
16x16	0.413626	1.10028	1.91234	0.354328	0.93747	1.78247
24x24				0.373069	0.97850	1.81691
32x32	0.412734	1.09998	1.91781			
48x48						
64x64	0.412062	1.10022	1.91790			
Ref. [38]	0.4080	1.08	1.91	0.4080	1.08	1.91

Table 13b: Simply supported skew plate (SS1): displacement and moment at the centre with regular meshes, *L/h = 1000.* Mesh pattern b).

Element	*D.o.f.*	*T3-U2 = MIN3*		
mesh		w^*	M_{22}^*	M_{11}^*
2x2	19	0.035848	0.10398	0.32325
4x4	59	0.016994	0.09510	0.29664
8x8	211	0.034444	0.13982	0.42144
16x16	803	0.105405	0.25184	0.67616
24x24	1779	0.166415	0.38001	0.95930
32x32	3139	0.216686	0.49628	1.18776
48x48	7011	0.283740	0.66654	1.47484
Ref. [38]		0.4080	1.08	1.91

Table 13c: Simply supported skew plate (SS1): displacement and moment at the centre with Riggs-Liu meshes, *L/h = 1000.* Mesh pattern c).

Element mesh	D.o.f.	*T3-U2 = MIN3*			*T6-U3*			*MIN6*		
		w^*	M_{22}^*	M_{11}^*	w^*	M_{22}^*	M_{11}^*	w^*	M_{22}^*	M_{11}^*
4x4	107	0.390176	0.99889	1.75653	0.443535	1.62871	2.54207	0.443541	1.62901	2.54279
8x8	403	0.332815	1.01588	1.70789	0.362133	1.23772	1.91453	0.361659	1.23760	1.91465
16x16	1571	0.323598	0.90943	1.67572	0.349185	0.93963	1.76645	0.346320	0.92433	1.75660
Ref. [38]		0.4080	1.08	1.91	0.4080	1.08	1.91	0.4080	1.08	1.91

Table 13d: Simply supported skew plate (SS1) under uniformly distributed load: displacement and moment at the centre using quadrilateral linked-interpolation elements [29], *L/h= 1000.*

Element mesh	*Q4-U2*			*Q9-U3*			*Q16-U4*		
	w^*	M_{22}^*	M_{11}^*	w^*	M_{22}^*	M_{11}^*	w^*	M_{22}^*	M_{11}^*
2x2	0.00087	0.0018	0.0048	0.15198	0.2596	0.5436	0.24947	0.7742	1.4298
4x4	0.00940	0.0222	0.0604	0.24245	0.5181	1.0542	0.32983	0.8966	1.7738
8x8	0.08101	0.1991	0.5320	0.31048	0.7569	1.5423	0.35493	0.9036	1.7595
16x16	0.20304	0.4738	1.1403	0.35670	0.9010	1.7574	0.37775	0.9730	1.8191
24x24	0.27309	0.6451	1.4369	0.37401	0.9595	1.8097			
32x32	0.31365	0.7544	1.5910						
48x48	0.35353	0.8802	1.7386						
Ref. [38]	0.4080	1.08	1.91	0.4080	1.08	1.91	0.4080	1.08	1.91

Mesh	*Q4-LIM*			*9βQ4*		
	w^*	M_1^*	M_2^*	w^*	M_1^*	M_2^*
2x2	0.52154	0.962	1.927			
4x4	0.41851	1.083	1.830	0.501994	1.352235	2.056188
8x8	0.40941	1.128	1.772	0.442198	1.079937	1.955570
16x16	0.40725	1.134	1.819	0.430832	1.149342	1.964564
24x24	0.40759	1.135	1.835			
32x32	0.40803	1.138	1.843	0.424505	1.143222	1.953153
48x48	0.40898	1.143	1.851			
Ref. [3]	0.4080	1.08	1.91	0.4080	1.08	1.91

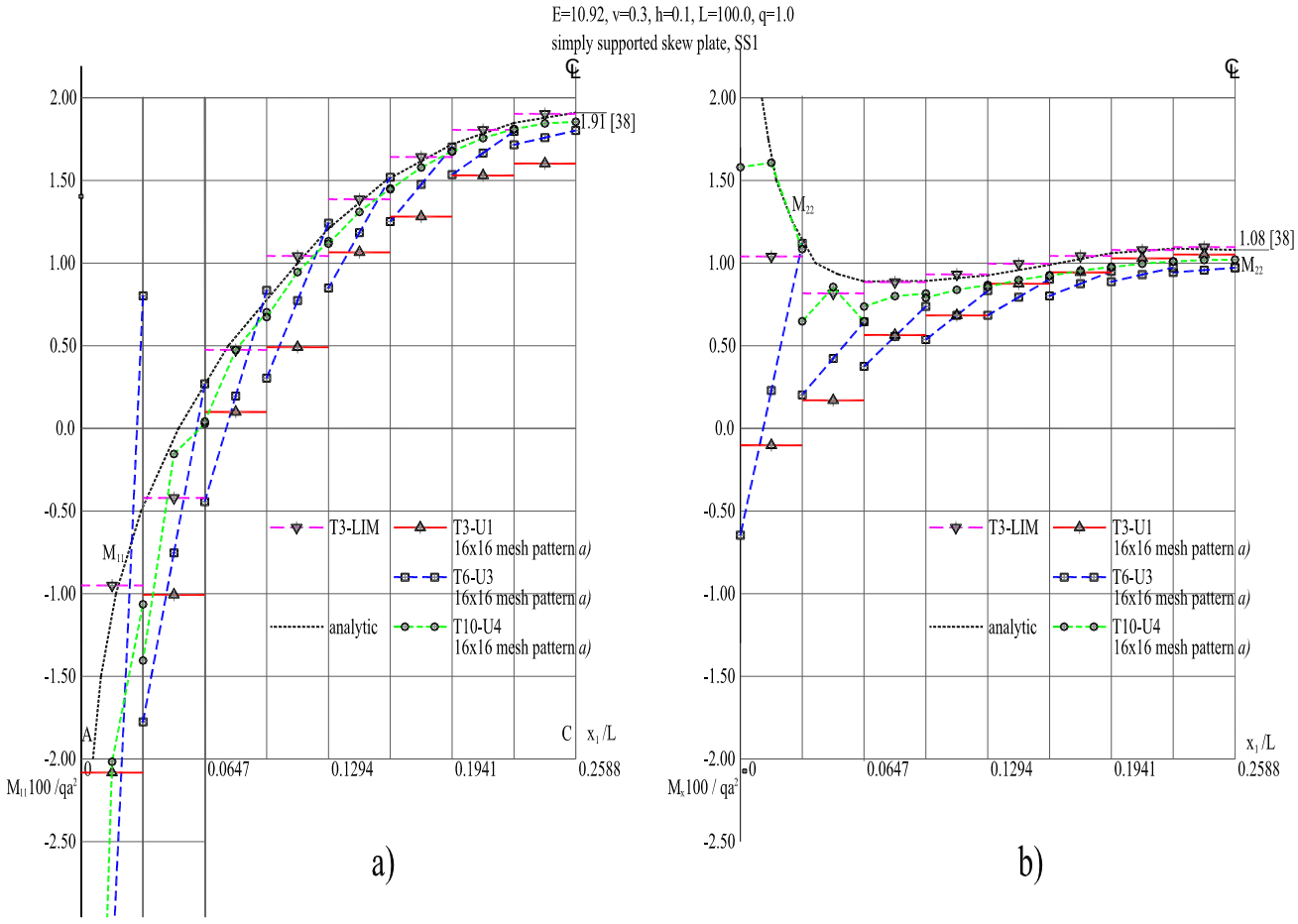

Fig. 36: *Simply supported skew plate under uniform load - a) principal moment M_{11} distribution between points A and C – b) principal moment M_{22} distribution between points A and C*

It should be noted that near the singularity point the moments are getting high values of opposite signs, and there even a small relative difference between the exact result and the finite-element solution in one of the principal moments may strongly influence the other principal moment since they are related via Poisson's coefficient (ν= 0.3 in this case) as shown in (12). Specifically, even though the finite-element

solutions for the principal moment M_{11} recognise the monotonous trend of the exact solution, the fact that, as absolute values, these moments are overestimated makes it difficult for the element to provide a solution for M_{22} which would recognise the change in sign, slope and curvature evident in the exact solution. Of course, there exist techniques to reduce the error in M_{11} which, as a result, would also correct this anomaly in M_{22}, e.g. the shear correction factor concept (see e.g. Fig. 14 in [24]), an idea that has not been followed up in this paper (see [8] for evidence).

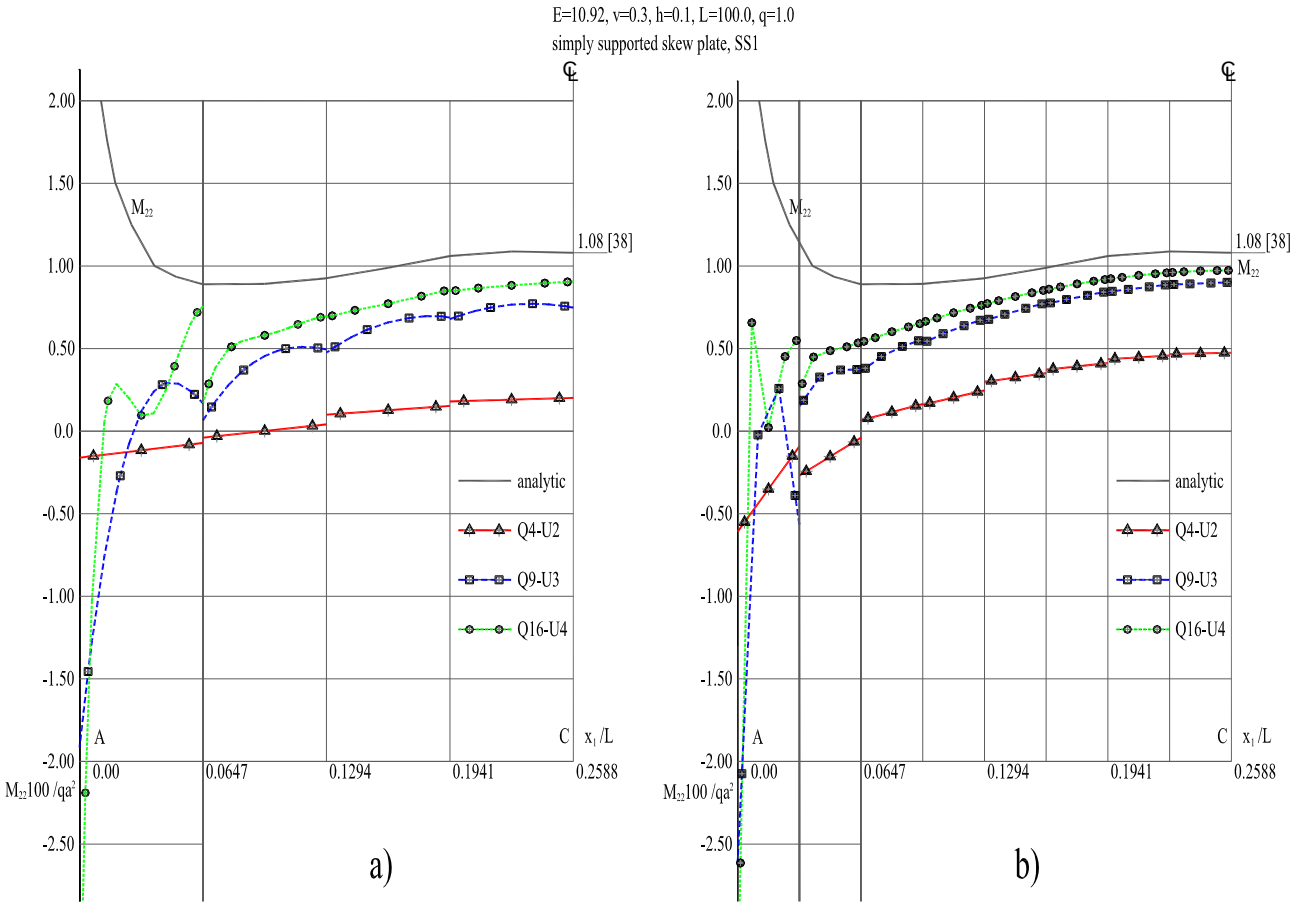

Fig. 37: *Simply supported skew plate under uniform load – principal moment in D-C-E direction (M_{22}) distribution in Gauss points along diagonal A-C using: a) 8 x 8 element mesh, b) 16 x 16 element mesh for the whole plate*

For the quadrilaterals, the moment for direction "D-C-E" in Fig. 37 for the Gauss points on the diagonal from vertex A to the central point C of the plate shows that this family of elements struggles to follow the exact moment distribution near the singularity point.

5.6.4. Simply supported circular plate

The circular plate with the simply supported edges is analysed next. The element mesh is here irregular and the influence of such irregularity is studied on the element family in consideration.

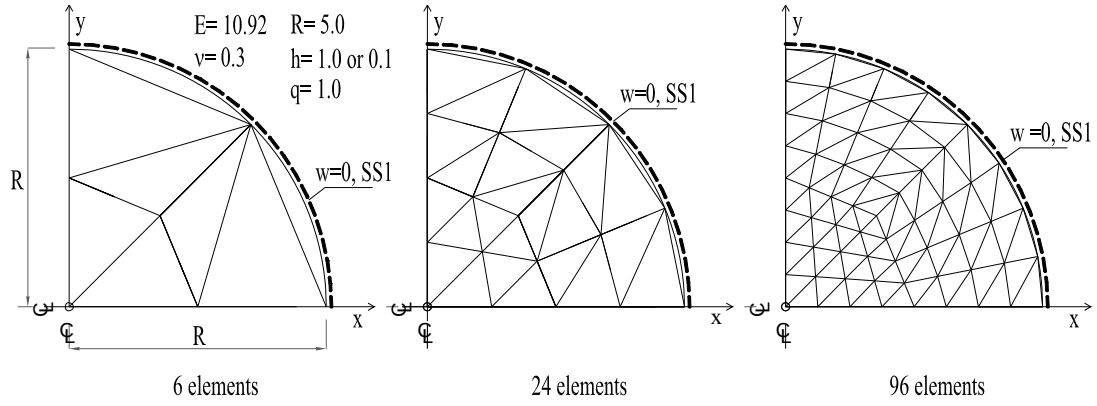

Fig. 38: *A simply supported (SS1) ¼ of the circular plate under uniform load. Three meshes used in analysis in Tables 14 and 15.*

$$w_c^* = \frac{w_c}{q}\frac{100D}{(2R)^4}, \qquad D = \frac{Eh^3}{12(1-\nu^2)}$$

$M_x=M_y=M_c$ – moment at the central point and $M_c^* = \frac{M_c}{q}\frac{100}{(2R)^2}$ (at closest Gauss point)

Additionally, not only the vertex nodes, but also the side nodes of the higher-order elements (six-node *T6-U3* and ten-node *T10-U4*) are now placed on the circular boundary. The edge elements are not following the straight line rule, so they must behave as curvilinear transformed triangles for which linked interpolation does not solve the patch test exactly (unless the elements become infinitesimally small). Only the transverse displacements of the nodes on the circular plate boundary are restrained and the rotations remain free (SS1 boundary condition).

The results are given in Tables 14 and 15a for the thick and the thin plate, respectively. The problem geometry and material properties are given in Fig. 38 (only one quarter of the plate is analysed), where examples of the three node element mesh is shown. A comparison with the linked-interpolation quadrilateral elements [29] is given in Table 15b.

Table 14a: Simply supported circular plate (SS1) with uniform load on meshes from Fig. 38: displacement and moment at the centre, *R/h = 5*.

Element mesh	*T3-U2 = MIN3*			*T6-U3*			*T10-U4*		
	d.o.f.	w_c^*	M_c^*	*d.o.f.*	w_c^*	M_c^*	*d.o.f.*	w_c^*	M_c^*
6	12	0.401654	4.7169	42	0.415578	5.44937	72	0.415956	5.1564
24	42	0.411726	5.0351	156	0.415978	5.23677	270	0.416000	5.1567
96	156	0.414989	5.1280	600	0.415999	5.17735	1044	0.415991	5.1573
384	600	0.415747	5.1497						
Ref. [9]		0.415994	5.1563		0.415994	5.1563		0.415994	5.1563

Element mesh	*T3BL* [12]	
	*w**	*M**
6	0.411627	4.72366
24	0.414296	5.02944
96	0.415555	5.12392
384	0.415891	5.14840
1536	0.415971	5.15445
6144	0.415989	5.15586
Ref. [9]	0.415994	5.1563

Table 14b: Simply supported circular plate (SS1) with uniform load: displacement and moment at the centre, *R/h = 5,* using quadrilateral linked-interpolation elements [29]. Quadrilateral mesh pattern joins two triangles to form a quadrilateral.

Element mesh	*Q4-U2*		*Q9-U3*		*Q16-U4*	
	w_c*	M_c*	w_c*	M_c*	w_c*	M_c*
3	0.410450	4.9346	0.415679	5.2185	0.416237	5.1547
12	0.414462	5.1251	0.415977	5.1831	0.416028	5.1552
48	0.415615	5.1494	0.415992	5.1641		
192	0.415893	5.1546				
768						
Ref. [9]	0.415994	5.1563	0.415994	5.1563	0.415994	5.1563

Element mesh	*Q4-LIM* [3]		*9βQ4* [9]	
	w_c*	M_c*	w_c*	M_c*
3	0.42191	4.8010	0.2812290	5.11686
6	0.41760	5.0682		
12	0.41641	5.1337	0.4133307	5.16833
24	0.41610	5.1505		
48	0.41602	5.1548	0.4153994	5.16188
192			0.4158536	5.15782
768			0.4159633	5.15669
Ref. [9]	0.415994	5.1563	0.415994	5.1563

Table 15a: Simply supported circular plate (SS1) with uniform load on meshes from Fig. 38: displacement and moment at the centre, *R/h = 50.*

Element	*T3-U2 = MIN3*			*T6-U3*			*T10-U4*		
mesh	*d.o.f.*	w_c*	M_c*	*d.o.f.*	w_c*	M_c*	*d.o.f.*	w_c*	M_c*
6	12	0.341539	3.7043	42	0.396171	5.5157	72	0.396469	5.1413
24	42	0.379082	4.6686	156	0.398321	5.2512	270	0.397956	5.1505
96	156	0.393800	5.0691	600	0.398257	5.1758	1044	0.398176	5.1617
384	600	0.397745	5.1462						
Ref. [9]		0.398315	5.1563		0.398315	5.1563		0.398315	5.1563

Element	*T3BL* [12]	
mesh	*w**	*M**
6	0.394319	4.70841
24	0.396576	5.03098
96	0.397848	5.12424
384	0.398200	5.14859
1536	0.398287	5.15448
6144	0.398308	5.15586
Ref. [9]	0.398315	5.1563

Table 15b: Simply supported circular plate (SS1) with uniform load: displacement and moment at the centre, *R/h = 50,* using quadrilateral linked-interpolation elements [29].

Element	*Q4-U2*		*Q9-U3*		*Q16-U4*	
mesh	w_c*	M_c*	w_c*	M_c*	w_c*	M_c*
3	0.3486007	3.85988	0.3904531	5.10265	0.397474	5.1484
12	0.3828163	4.82198	0.3981520	5.17865	0.398265	5.1553
48	0.3968067	5.12375	0.3982781	5.16337		
192	0.3981513	5.15283				
768						
Ref. [9]	0.398315	5.1563	0.398315	5.1563	0.398315	5.1563

Element mesh	*Q4-LIM* [3]		*9βQ4* [9]	
	w_c*	M_c*	w_c*	M_c*
3	0.40576	4.7980	0.2692074	5.10642
6	0.40027	5.0670		
12	0.39881	5.1335	0.3959145	5.14593
24	0.39844	5.1505		
48	0.39835	5.1548	0.3977919	5.16070
192			0.3981935	5.15773
768			0.3982894	5.15668
Ref. [9]	0.398315	5.1563	0.398315	5.1563

Again, here the displacement-based elements presented converge very quickly towards the exact solution, in particular the nine-node *Q9-U3* element and the 16-node *Q16-U4* element, which provides better results than the other elements for the comparable number of the degrees of freedom.

In Table 16 the results for the simply supported circular plate subject to a concentrated load at the center point are given. The geometry and material properties are identical to the problem from Fig. 38. For the thin plate situation (*R/h=50*) the exact solution for the central displacement is known [9], while the bending moment at the centre has a singularity.

Table 16: Simply supported circular plate (SS1) with the point load at the centre.
Displacement and moment at the centre, *R/h = 50.*

Element mesh	*T3-U2 = MIN3*			*T6-U3*			*T10-U4*		
	d.o.f.	w_c*	M_c*	*d.o.f.*	w_c*	M_c*	*d.o.f.*	w_c*	M_c*
6	12	0.904743	0.101126	42	1.235808	0.279935	72	1.256633	0.366285
24	42	1.125456	0.184045	156	1.258859	0.348196	270	1.262771	0.431803
96	156	1.230098	0.273531	600	1.263289	0.420456	1044	1.264680	0.503816
384	600	1.257735	0.352032						
Ref. [9]		1.262528	∞		1.262528	∞		1.262528	∞

With: $w_c^* = \frac{w_c}{P}\frac{100D}{4R^2}$, $M_c^* = \frac{M_c}{P}$ (at closest Gauss point)

5.6.5. Clamped circular plate

In this example the same elements, on the same meshes subjected to uniformly distributed loading are tested, only this time with the clamped boundary conditions. Results are given in Table 10 for the thin plate only (*R/h=50*) where the exact solution for central displacement is known [9].

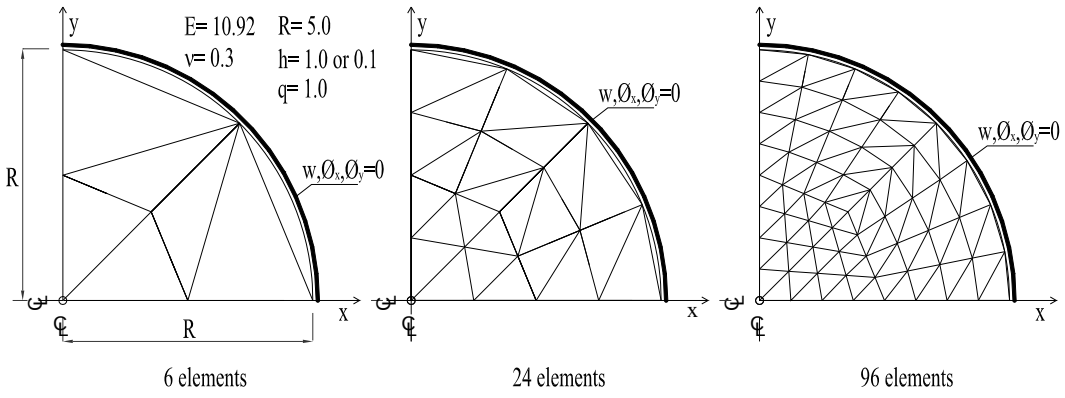

Fig. 39: *Clamped ¼ of the circular plate under uniformly distributed loading. Three meshes used in analysis in Table 17*

Table 17: Clamped circular plate (SS1) with uniform load on meshes from Fig. 39: displacement and moment at the centre, *R/h = 50*.

Element mesh	*T3-U2 = MIN3*			*T6-U3*			*T10-U4*		
	d.o.f.	w_c*	M_c*	*d.o.f.*	w_c*	M_c*	*d.o.f.*	w_c*	M_c*
6	8	0.004279	0.0977	40	0.110847	2.53527	60	0.095840	2.00680
24	34	0.049480	1.1886	140	0.097711	2.11270	246	0.097697	2.02936
96	140	0.089996	1.9073	568	0.097755	2.04355	996	0.097843	2.03233
384	568	0.096739	2.0157						
Ref. [9]		0.097835	2.03125		0.097835	2.03125		0.097835	2.03125

Element mesh	*T3BL* [12]	
	*w**	*M**
6	0.0604946	1.21883
24	0.0877499	1.81886
96	0.0952366	1.97714
384	0.0970870	2.01702
1536	0.0975353	2.02667
6144	0.0978474	2.03163
Ref. [9]	0.0978348	2.03125

In all this axisymmetric problems with irregular meshes, the response of the elements is similar and the convergence is quite good on all element types. Higher order elements converge faster, but low order elements do not exhibit significant locking phenomena with coarse meshes.

6. Plate element as a facet shell element

In the plate theory considered so far, just three degrees of freedom are needed to describe the plate behavior. Nevertheless, the presented elements could be used as spatial elements, e.g. in shell type structures composed of flat parts. In this case, the nodal displacements and rotations related to the local element coordinate system must be transformed to the global coordinates in order to define the assembly matrix of the space model. Additionally, the strain energy due to membrane (in-plane) effects must be included, too.

6.1. Stiffness of the facet element in local coordinates

As it is well known [1], the behavior of the shell model is strongly affected by in-plane effects which may become dominant over the bending and shear ones coming from the plate theory. Therefore, those effects must be taken into account and the in-plane (membrane) stiffness should be derived together with the in-plane nodal forces. Again, this can be performed through appropriate choice of displacement interpolations.

Since our plate elements are derived to satisfy the constant bending state over an arbitrary patch of elements and the higher order elements can even satisfy the constant shear patch tests exactly, the membrane displacement interpolations should be chosen in the way to satisfy the constant in-plane stress patch tests. This can be easily

achieved by interpolating the in-plane displacements using just the Lagrangean isoparametric forms, because the in-plane stresses depend only on the first derivatives of the displacements. The in-plane constant-stress state is achieved by interpolating the displacement in two local plane directions ($\bar{x}$, $\bar{y}$), without the need of including the sixth degree of freedom – the drilling rotation, over the element:

$$\bar{u} = \sum_{i=1}^{N} I_i \bar{u}_i \qquad \text{and} \qquad \bar{v} = \sum_{i=1}^{N} I_i \bar{v}_i ,$$

where, $\bar{u}_i$ and $\bar{v}_i$ are the in-plane nodal displacements and I_i are the Lagrangean interpolation functions.

The membrane equilibrium equations can be, also, derived from the stationarity condition for the potential of membrane energy functional over an element

$$\Pi_{memb}(\bar{u},\bar{v}) = \frac{1}{2}\int \left\langle \varepsilon_{\bar{x}\bar{x}} \quad \varepsilon_{\bar{y}\bar{y}} \quad \gamma_{\bar{x}\bar{y}} \right\rangle \begin{Bmatrix} \sigma_{\bar{x}\bar{x}} \\ \sigma_{\bar{y}\bar{y}} \\ \tau_{\bar{x}\bar{y}} \end{Bmatrix} dA + \Pi_{ext} =$$

$$= \frac{1}{2}\int \left\langle \bar{u} \quad \bar{v} \right\rangle \begin{bmatrix} \frac{\partial}{\partial \bar{x}} & 0 & \frac{\partial}{\partial \bar{y}} \\ 0 & \frac{\partial}{\partial \bar{y}} & \frac{\partial}{\partial \bar{x}} \end{bmatrix} \frac{Eh}{1-\nu^2} \begin{bmatrix} 1 & \nu & 0 \\ \nu & 1 & 0 \\ 0 & 0 & \frac{1-\nu}{2} \end{bmatrix} \begin{bmatrix} \frac{\partial}{\partial \bar{x}} & 0 \\ 0 & \frac{\partial}{\partial \bar{y}} \\ \frac{\partial}{\partial \bar{y}} & \frac{\partial}{\partial \bar{x}} \end{bmatrix} \begin{Bmatrix} \bar{u} \\ \bar{v} \end{Bmatrix} dA + \Pi_{ext} , \qquad (60)$$

where the last term describes the potential energy of the distributed and boundary in-plane loading. In expression (60) the material is described with the same quantities like in (12) and (13) for the plate behavior and the membrane differential matrix

operator is introduced acting on the displacements in the local in-plane directions. Finally, the equilibrium equations over the membrane element can have a form

$$\sum_{j=1}^{N}\begin{bmatrix} k^{ij}_{\bar{u},\bar{u}} & k^{ij}_{\bar{u},\bar{v}} \\ k^{ij}_{\bar{v},\bar{u}} & k^{ij}_{\bar{v},\bar{v}} \end{bmatrix}\begin{Bmatrix} \bar{u}_j \\ \bar{v}_j \end{Bmatrix} = \begin{Bmatrix} \bar{f}_{\bar{u},i} \\ \bar{f}_{\bar{v},i} \end{Bmatrix}, \tag{61}$$

where $\bar{f}_{\bar{u},i}$ and $\bar{f}_{\bar{v},i}$ are the in-plane nodal forces in $\bar{u}$ and $\bar{v}$ local directions while the coefficients $k^{ij}_{\bar{u},\bar{u}}$, $k^{ij}_{\bar{u},\bar{v}} = k^{ij}_{\bar{v},\bar{u}}$ and $k^{ij}_{\bar{v},\bar{v}}$ are the stiffness coefficients.

When this result is combined with (51), the two sets of equations build the stiffness matrix of the facet shell element expressed by five d.o.f. per element node:

$$\sum_{j=1}^{N}\begin{bmatrix} k^{ij}_{\bar{u},\bar{u}} & k^{ij}_{\bar{u},\bar{v}} & 0 & 0 & 0 & 0 \\ k^{ij}_{\bar{v},\bar{u}} & k^{ij}_{\bar{v},\bar{v}} & 0 & 0 & 0 & 0 \\ 0 & 0 & k^{ij}_{\bar{w},\bar{w}} & k^{ij}_{\bar{w},\theta\bar{x}} & k^{ij}_{\bar{w},\theta\bar{y}} & 0 \\ 0 & 0 & k^{ij}_{\theta\bar{x},\bar{w}} & k^{ij}_{\theta\bar{x},\theta\bar{x}} & k^{ij}_{\theta\bar{x},\theta\bar{y}} & 0 \\ 0 & 0 & k^{ij}_{\theta\bar{y},\bar{w}} & k^{ij}_{\theta\bar{y},\theta\bar{x}} & k^{ij}_{\theta\bar{y},\theta\bar{y}} & 0 \\ 0 & 0 & 0 & 0 & 0 & 0 \end{bmatrix}\begin{Bmatrix} \bar{u}_j \\ \bar{v}_j \\ \bar{w}_j \\ \theta_{\bar{x},j} \\ \theta_{\bar{y},j} \\ \theta_{\bar{z},j} \end{Bmatrix} = \begin{Bmatrix} \bar{f}_{\bar{u},i} \\ \bar{f}_{\bar{v},i} \\ \bar{f}_{\bar{w},i} \\ \bar{f}_{\theta\bar{x},i} \\ \bar{f}_{\theta\bar{y},i} \\ 0 \end{Bmatrix}. \tag{62}$$

The above formulation is valid for any shape of element (triangles, quadrilaterals or higher order elements) and it demonstrates that the in-plane and out-of-plane effects are independent. This independence would not be valid after assembly of non coplanar elements is undertaken in global coordinates.

Only in a special case where plane segments of a model allow an assembly of plane elements in some nodal points, the solving program must be able to eliminate the drilling rotation from the global matrix.

6.2. Transformation to global coordinates

The element stiffness matrix, as well as the vector of nodal forces in (62) are formed in a 'reference plane' of local coordinates $(\bar{x},\bar{y},\bar{z})$. To assemble the equilibrium equations of the structure, a transformation of the nodal local unknowns and loading is needed via transformation of coordinates to a common global system (x,y,z). Initially all nodes are defined in global coordinates, so the 'reference plane' is found and inverse transformation from the global to the local coordinates is first needed. If the transformation of the unknowns and loading from global to local coordinates is described by matrix $\boldsymbol{T}$ as:

$$\overline{\mathbf{a}}_i = \mathbf{T}\mathbf{a}_i \qquad \text{and} \qquad \overline{\mathbf{f}}_i = \mathbf{T}\mathbf{f}_i ,$$

where $\overline{\mathbf{a}}_i$ and $\mathbf{a}_i$ denote the vector of nodal unknowns in local and global coordinates respectively, and $\overline{\mathbf{f}}_i$ and $\mathbf{f}_i$ denote the six component load vector in the two co-ordinate systems. Equation (62) now reads

$$\sum_{j=1}^{N} \overline{\mathbf{K}}_e^{ij} \overline{\mathbf{a}}_j = \overline{\mathbf{f}}_i \tag{63}$$

and the transformation matrix has a six by six form

$$\mathbf{T} = \begin{bmatrix} \mathbf{\Lambda} & \mathbf{0} \\ \mathbf{0} & \mathbf{\Lambda} \end{bmatrix},$$

with $\mathbf{\Lambda}$ being a 3x3 matrix of direction cosines between the two sets of coordinate axes, that is

$$\mathbf{\Lambda} = \begin{bmatrix} \cos(\bar{x},x) & \cos(\bar{x},y) & \cos(\bar{x},z) \\ \cos(\bar{y},x) & \cos(\bar{y},y) & \cos(\bar{y},z) \\ \cos(\bar{z},x) & \cos(\bar{z},y) & \cos(z,z) \end{bmatrix} = \begin{bmatrix} \Lambda_{\bar{x},x} & \Lambda_{\bar{x},y} & \Lambda_{\bar{x},z} \\ \Lambda_{\bar{y},x} & \Lambda_{\bar{y},y} & \Lambda_{\bar{y},z} \\ \Lambda_{\bar{z},x} & \Lambda_{\bar{z},y} & \Lambda_{\bar{z},z} \end{bmatrix},$$

where $\cos(\bar{x},x)$ is the cosine of the angle between $\bar{x}$ - axis and x – axis, and so on. By the rules of orthogonal transformation the inverse of $\mathbf{T}$ is given by its transpose:

$$\mathbf{a}_i = \mathbf{T}^T \overline{\mathbf{a}}_i \qquad \text{and} \qquad \mathbf{f}_i = \mathbf{T}^T \overline{\mathbf{f}}_i .$$

Substituting this transformation into (63) eventually gives the element equilibrium in the global coordinate system as

$$\sum_{j=1}^{N} \mathbf{K}_e^{ij} \mathbf{a}_j = \mathbf{f}_i \tag{64}$$

with $\mathbf{K}_e^{ij} = \mathbf{T}^T \overline{\mathbf{K}}_e^{ij} \mathbf{T}$.

6.3. Test examples for shells

In all the examples to follow the elements presented are denoted as triangles: *T3-U2* for the tree-node element, *T6-U3* for the six-node element and *T10-U4* for the ten-node element and quadrilaterals: *Q4-U2* for the four-node element. The results are compared to the *SHELL* element by Taylor [1] incorporated in his *FEAP* program. All the new elements have been added to *FEAP* as user-defined elements.

6.3.1. Folded plate structure example

In the following example a folded symmetrical structure is chosen to illustrate the behavior of the developed shell elements in which the flat finite element representation is physically exact. The structure is a plate folded in the manner illustrated in Fig. 40 and has two planes of symmetry – one containing the vertical rib, and other passing perpendicularly to the structure's crown. The structure is supported vertically along the horizontal edges and on the rigid diaphragm along the front edges. Other geometrical and load data are given in Fig. 40.

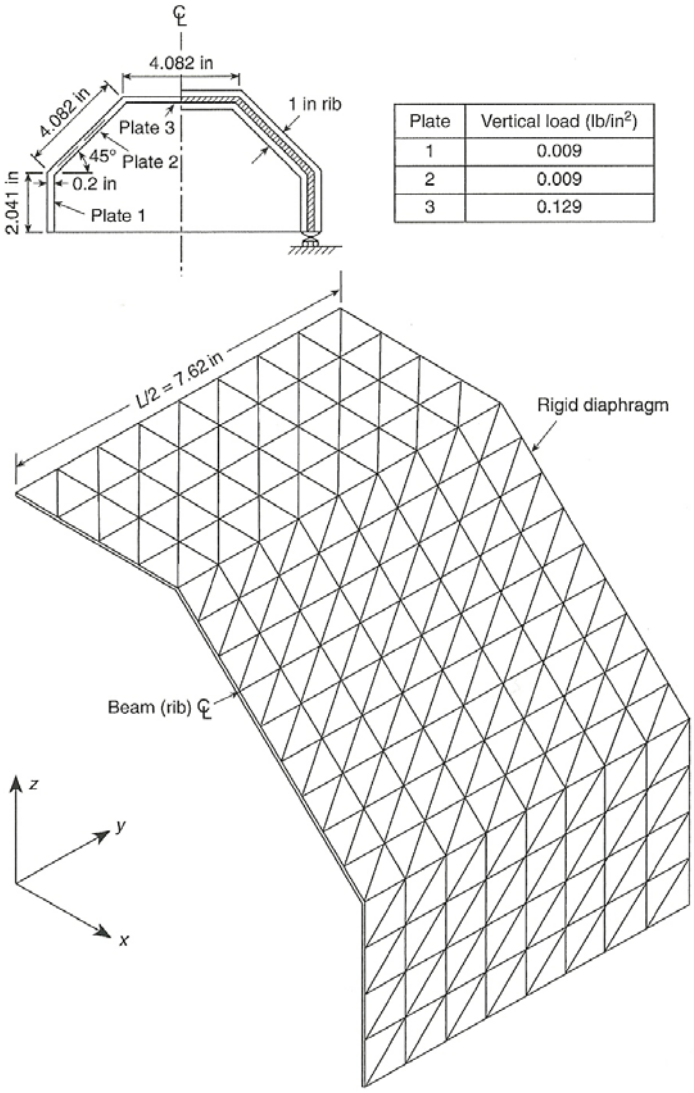

Plate	Vertical load (lb/in^2)
1	0.009
2	0.009
3	0.129

Fig. 40 [1]: *Folded plate structure – model geometry, loading and mesh, E=3560, v=0.43*

The same model is analysed with various element types: all triangle elements in the family (three-node, six-node, and ten-node) and quadrilateral element with four nodes. The resulting displacements are then compared with those obtained using *SHELL* element from *FEAP* program. In Fig. 41.a-c, the displacements are given in contour graphs, and in Table 18 the numerical results are given for two control displacements both located in the vertical plane in the middle between the beam rib and the rigid diaphragm, the vertical one at the crown and the horizontal displacement at the bottom edge.

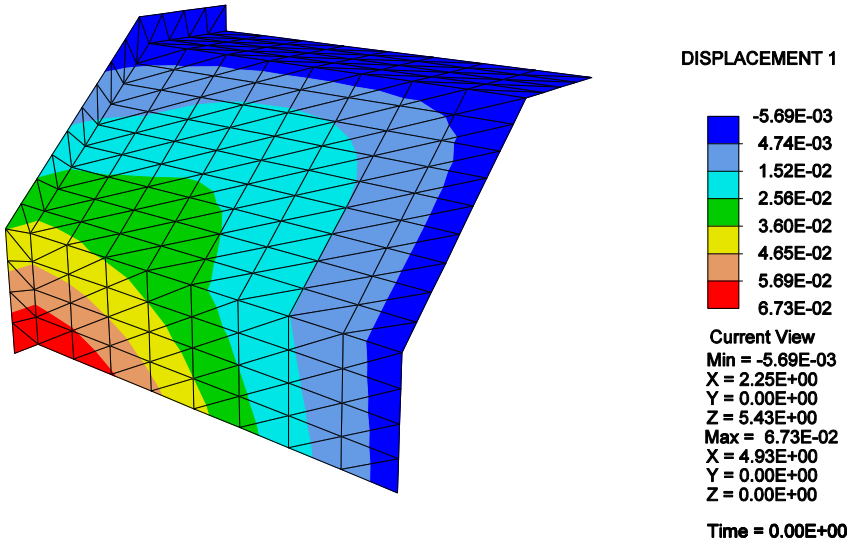

Fig. 41.a*: A folded plate structure – transverse displacements of the model*

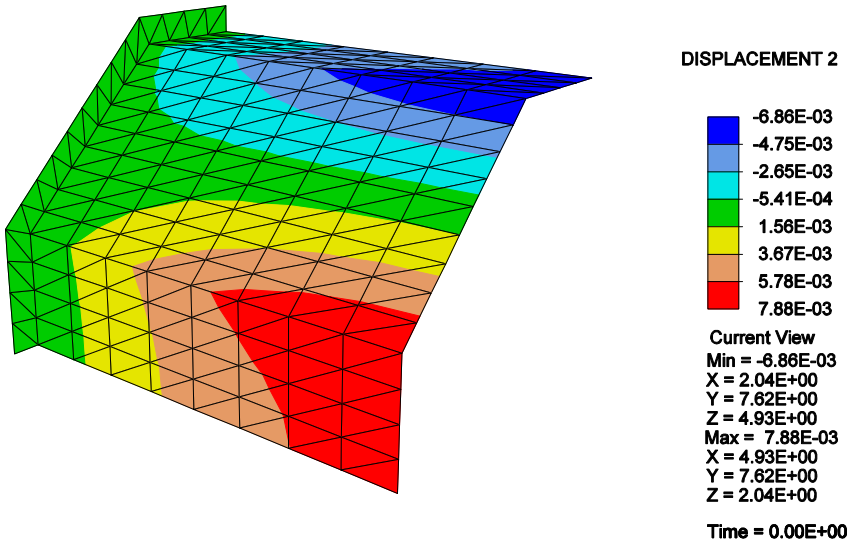

Fig. 41.b: *A folded plate structure – longitudinal displacements of the model*

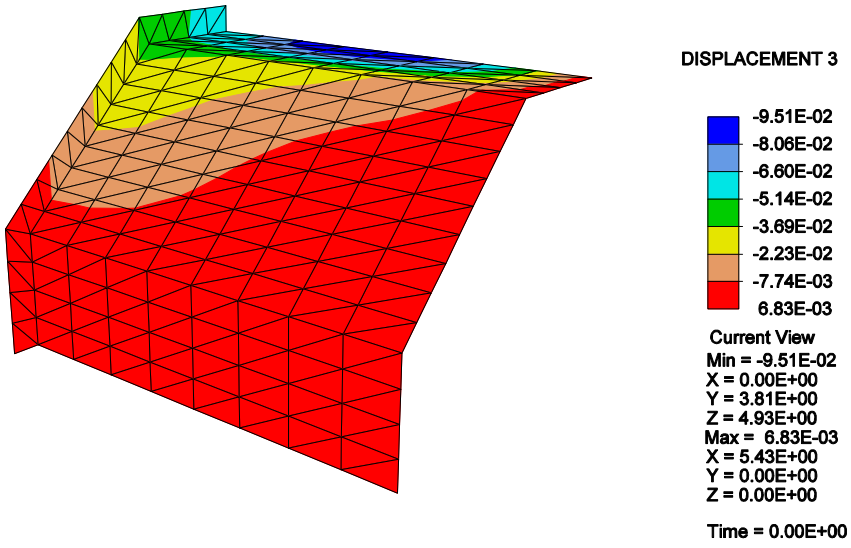

Fig. 41.c: *A folded plate structure – vertical displacements of the model*

Table 18: Folded plate structure: numerical results for control displacements of the midpoint at the crown (w_c is vertical) and at the edge (w_e is transverse horizontal)

Element type	Number of elements	d.o.f.	Control displacements w_c	w_e
T3-U2	272 544	1030 3474	-0.09513 -0.09879	0.03929 0.03944
T6-U3	64 128	1161 3860	-0. 10067 -0. 10153	0.04065 0.04066
T10-U4	42 84	1026 1485	-0.10480 -0.10070	0.04076 0.04067
Q4-U2	136 272	1030 3474	-0. 09884 -0. 10077	0.04036 0.04048
SHELL element from FEAP	136 272	1030 3474	-0.10024 -0.09992	0.04040 0.04062

All the results converge toward the result using *SHELL* element from *FEAP*, but better convergence can be observed with the higher order elements.

6.3.2. Scordelis-Lo roof

The Scordelis-Lo roof [40] is a standard test example for examining the behavior of shell elements and can be found in most textbooks on the topic. It is a shell of the barrel vault form with two planes of symmetry and only one constant curvature as it is shown in Fig. 42.

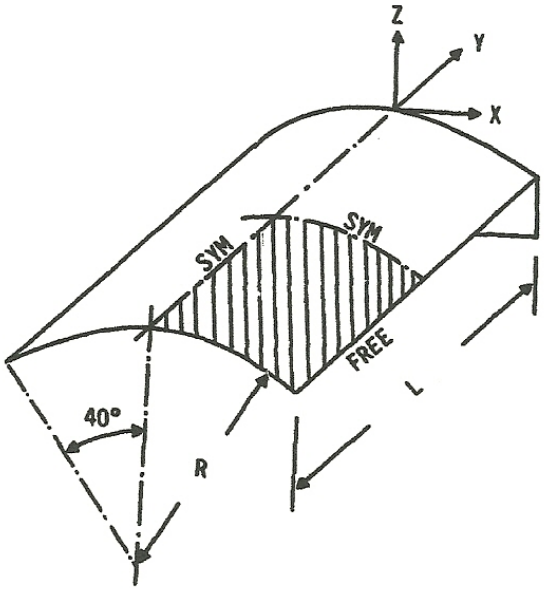

Fig. 42 [40]: *Scordelis-Lo roof. Radius = 25.0; length = 50.0; thickness=0.25; $E=4.32\cdot10^{8}$; v=0.00; loading= 90.0 per unit area in –Z direction; $u_x= u_z= 0$ on curved edges: N x N on shaded area.*

The test result for this problem is usually the vertical displacement at the midpoint of the free edge. In Table 19 this control displacement is calculated for various meshes and for all element types used. The theoretical value for this result is -0.3086 [40] but most elements converge to a slightly lower value. MacNeal [40] uses the value -0.3024 for normalization of his results.

In Fig. 43.a. b. and c displacements are shown for vertical and both horizontal directions over the whole model divided into 8 by 8 triangular element mesh.

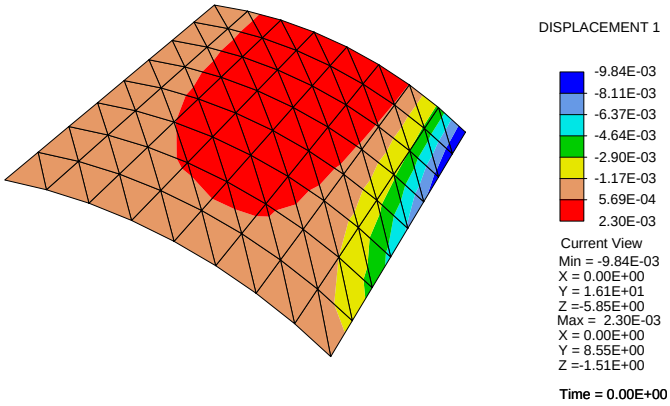

Fig. 43.a: *A Scordelis-Lo roof: longitudinal displacements of the model.*

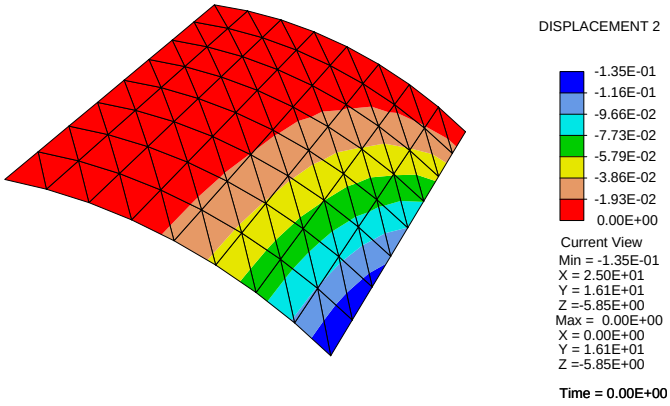

Fig. 43.b: *A Scordelis-Lo roof: transverse displacements of the model.*

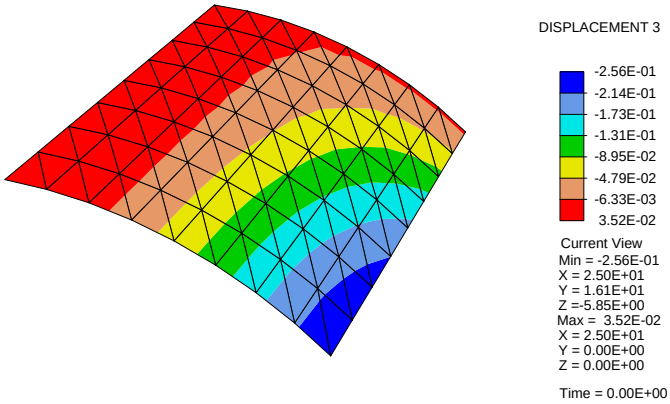

Fig. 43.c: *A Scordelis-Lo roof: vertical displacements of the model with 8 nodes per edge.*

Table 19: Scordelis-Lo roof: numerical results for control vertical displacement at the middle point of the free edge

Number of nodes per side	*T3-U2*	*T6-U3*	*T10-U4*	*Q4-U2*	*SHELL element from FEAP*
3			-0.9810		
4	-0.1827	-0.3492		-0.2375	-0.3169
6	-0.2294	-0.3113	-0.3582	-0.2772	-0.3068
8	-0.2558	-0.3045		-0.2895	-0.3039
12	-0.2797	-0.3023	-0.3058	-0.2987	-0.3020
Reference [40]	-0.3024	-0.3024	-0.3024	-0.3024	-0.3024

A good convergence can be observed for the higher order elements even though they can not model curved geometry exactly with their interior nodes, because they are designed as facet elements. Convergence of the *T6-U3* element is even better then for the *SHELL* element from *FEAP*.

6.3.3. Hemi-spherical shell example

The hemi-spherical shell problem is also a standard test example for examining the behavior of shell elements from the textbooks [40]. Its form is doubly curved representing a hemi-sphere with a hole within 18º degrees at the pole. Only one quadrant is analysed in the model and loaded with two opposite unit loads at equatorial nodes intersecting both symmetrical planes (Fig. 44).

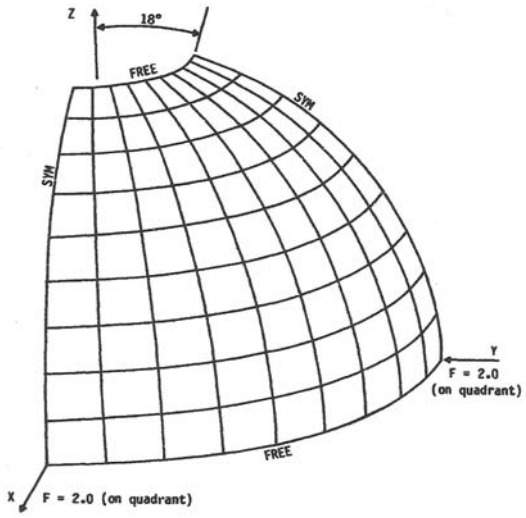

Fig. 44 [40]: *A spherical shell problem. Radius = 10.0; thickness=0.04; E=6.825·10^7; v=0.30; loading: concentrated forces as shown; mesh: N x N on quadrant.*

The test results for this problem are the horizontal displacements at the force points on the equator which is free-edged (they are equal and opposite). In Table 20 this control displacement is calculated for various meshes and element types used. The theoretical

value for this result is 0.0924 [40] in the case where the hole at the centre is not present. MacNeal [40] uses the value 0.0940 for normalizations of his results.

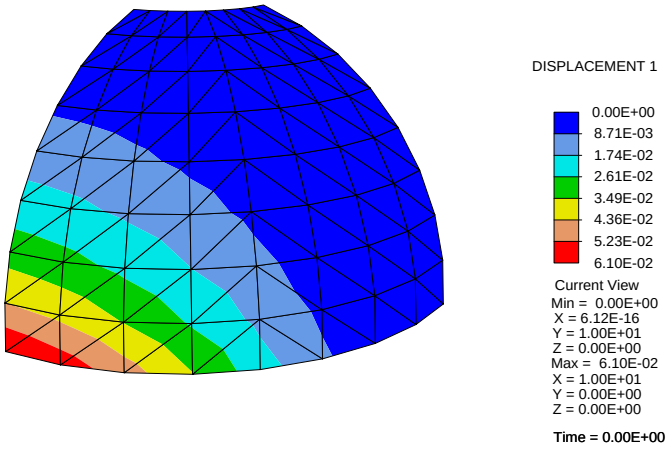

Fig. 45.a: *A spherical shell problem: x-displacements of the model.*

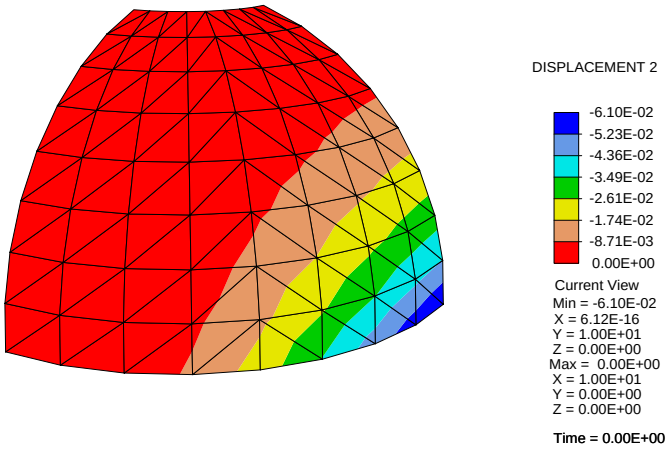

Fig. 45.b: A *spherical shell problem: y-displacements of the model.*

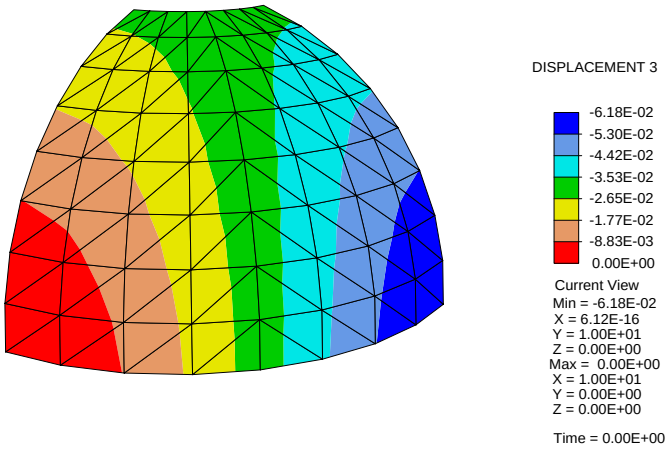

Fig. 45.c: *A spherical shell problem: vertical displacements of the model with 8 nodes per edge.*

In Fig. 45.a. b. and c displacements are shown, for vertical and both horizontal directions over the whole model divided into 8 by 8 element triangular mesh.

Table 20: A spherical shell problem: numerical results for control horizontal displacements at the force points of the equator

Number of nodes per side	*T3-U2*	*T6-U3*	*T10-U4*	*Q4-U2*	*SHELL element from FEAP*
2					
4	0.0179			0.0119	0.0865
6			0.0323		
8	0.0610	0.0145		0.0610	0.0942
10					
12	0.0803	0.0208	0.0364	0.0828	0.0937
16	0.0867	0.0363		0.0889	0.0935
Reference [40]	0.0940	0.0940	0.0940	0.0940	0.0940

This example shows that using higher-order facet shells in modeling double-curved geometries, makes little sense as any improvement in accuracy of the elements is more then off-set by their inherent inability to describe curved geometries.

7. Bubble-enriched basic elements with linked interpolation

As the three-node and four-node elements are very simple to describe in a structural model compared to higher order elements with ten or sixteen nodes, they are widely used in practical problems. Here we present an idea of enriching the basic elements with bubble functions coming from higher-order interpolations for displacements and rotations. The new enriched elements are incompatible with the adjacent elements except at the nodal points, but they do not contain zero-energy modes and they are extremely accurate in describing deformations and stress resultants even in extremely demanding bench-marks with singularities in stress resultants.

We start by considering the conditions necessary to enrich the linked interpolation presented in 6.1.1, with additional bubble function that satisfies the zero shear patch test (constant bending test) in the displacement field.

For example, the standard linked interpolation for the *T3-U2* element may be enriched with the bubble-function in the displacement field with a parameter w_b:

$$w = w_{T3U2} + f_b(\xi_1, \xi_2, \xi_3)w_b, \tag{65}$$

where f_b is arbitrary function of an order higher than the existing interpolation for w_{T3U2} (cubic or higher). The rotation interpolations are assumed to remain unchanged:

$$\theta_x = \theta_{xT3U2},$$

$$\theta_y = \theta_{yT3U2}\,. \tag{66}$$

In (65) and (66) index "*T3U2*" denotes the original reference value of the basic triangle element *T3-U2*. The expressions for shear (10) and curvature (11) will now have the following forms:

$$\boldsymbol{\Gamma} = \begin{Bmatrix} \gamma_{xz} \\ \gamma_{yz} \end{Bmatrix} = \begin{Bmatrix} \theta_y + \dfrac{\partial w}{\partial x} \\ -\theta_x + \dfrac{\partial w}{\partial y} \end{Bmatrix} = \begin{bmatrix} 0 & 1 \\ -1 & 0 \end{bmatrix} \begin{Bmatrix} \theta_{xT3U2} \\ \theta_{yT3U2} \end{Bmatrix} + \begin{Bmatrix} \dfrac{\partial}{\partial x} \\ \dfrac{\partial}{\partial y} \end{Bmatrix} \left(w_{T3U2} + f_{bi} w_{bi} \right) =$$

$$= \mathbf{B}_{\mathbf{S},T3U2}\mathbf{p}_n + \begin{Bmatrix} \dfrac{\partial f_{bi}}{\partial x} \\ \dfrac{\partial f_{bi}}{\partial y} \end{Bmatrix} w_b = \mathbf{B}_{\mathbf{S},T3U2}\mathbf{p}_n + \mathbf{B}_{\mathbf{S},b} w_b = \boldsymbol{\Gamma}_{T3U2} + \boldsymbol{\Gamma}_b$$

and $\boldsymbol{\kappa} = \mathbf{B}_{\mathbf{B},T3U2}\mathbf{p}_n = \boldsymbol{\kappa}_{T3U2}$ (unchanged).

In the above expressions $\mathbf{B}_{\mathbf{S},T3U2}$ is a shear-strain displacement matrix of the interpolations for basic *T3U2* element, $\mathbf{B}_{\mathbf{S},b}$ is a shear-strain displacement matrix of the bubble interpolation and from it, $\boldsymbol{\Gamma}_b$ is the shear-strain contribution due to the enriched bubble term.

The formation of the element stiffness matrix and the external load vector for the interpolation functions defined in this way follows the standard finite-element procedure. From the stationarity condition for the total potential energy functional (15) over an element, a system of algebraic equations is derived:

$$\begin{bmatrix} \mathbf{K}_{\mathbf{S}w\theta} + \mathbf{K}_{\mathbf{B}w\theta} & \mathbf{K}_{\mathbf{S}w\theta,b}^{T} \\ \mathbf{K}_{\mathbf{S}w\theta,b} & k_{\mathbf{S}b} \end{bmatrix} \begin{bmatrix} \mathbf{p}_n \\ w_b \end{bmatrix} = \begin{bmatrix} \mathbf{f}_{w\theta,q} \\ f_{b,q} \end{bmatrix}, \tag{67a}$$

where $\mathbf{K}_{\mathbf{S}w\theta} = \int_A \left(\mathbf{B}_{\mathbf{S},T3U2}\right)^T \mathbf{D}_{\mathbf{S}} \mathbf{B}_{\mathbf{S},T3U2} dA$ and $\mathbf{K}_{\mathbf{B}w\theta} = \int_A \left(\mathbf{B}_{\mathbf{B},T3U2}\right)^T \mathbf{D}_{\mathbf{B}} \mathbf{B}_{\mathbf{B},T3U2} dA$

$$\mathbf{K}_{\mathbf{S}w\theta,b} = \int_A \left(\mathbf{B}_{\mathbf{S},b}\right)^T \mathbf{D}_{\mathbf{S}} \mathbf{B}_{\mathbf{S},T3U2} dA$$

$$\mathbf{K}_{\mathbf{S}b} = \int_A \left(\mathbf{B}_{\mathbf{S},b}\right)^T \mathbf{D}_{\mathbf{S}} \mathbf{B}_{\mathbf{S},b} dA$$

and where $\mathbf{p}_n$ is a vector of all nodal parameters (nodal displacement and rotations) and w_b is a internal bubble parameter.

To satisfy the zero shear condition over a patchwork of elements, for the corresponding nodal deformations defined at the boundary nodes and in the absence of external loading ($f_{b,q}=0$), a bubble parameter has to vanish. In expression (67a) the following part should therefore vanish:

$$\mathbf{K}_{\mathbf{S}w\theta,b} \mathbf{p}_n + k_{\mathbf{S}b} w_b = 0\,. \tag{67b}$$

Here, w_b will be equal to zero if $k_{\mathbf{S}b}$ is non zero, because $\mathbf{K}_{\mathbf{S}w\theta,b} \mathbf{p}_n = 0$ for $\boldsymbol{\Gamma}_{T3U2} = \mathbf{B}_{\mathbf{S},T3U2} \mathbf{p}_n = \mathbf{0}$ in the standard zero shear patch test. The condition is thus

$$\mathbf{K}_{\mathbf{S}w\theta,b} \mathbf{p}_n = \int_A \begin{Bmatrix} \dfrac{\partial f_{bi}}{\partial x} \\ \dfrac{\partial f_{bi}}{\partial y} \end{Bmatrix}^T \mathbf{D}_{\mathbf{S}} \mathbf{B}_{\mathbf{S},T3U2} dA \cdot \mathbf{p}_n = 0\,. \tag{67c}$$

If more then one bubble parameter is taken in to consideration, together with corresponding independent bubble functions, $k_{\mathbf{S}b}$ is replaced with matrix $\mathbf{K}_{\mathbf{S}b}$ and for the same reason this matrix should be invertible ($det\mathbf{K}_{Sb}\neq 0$) and a vector of all bubble parameters $\mathbf{w}_b$ will be equal to zero.

The condition (67c) is obviously satisfied for **any function** f_b in (65). There is no restriction in their selection, but, as already mentioned this functions have sense only if they are cubic or higher order.

Likewise we may ask ourselves if it is possible to enrich the basic interpolations of the triangle element with bubble functions in the rotation fields, so as to satisfy the zero shear patch test (constant bending test) as before.

The bubble-functions in the rotation fields, with bubble parameters θx_b and θy_b are expressed as:

$$\theta_x = \theta_{xT3U2} + f_b(\xi_1, \xi_2, \xi_3)\theta_{xb}$$

$$\theta_y = \theta_{yT3U2} + f_b(\xi_1, \xi_2, \xi_3)\theta_{yb}, \tag{68}$$

while $w = w_{T3U2}$ remains unchanged. (69)

This interpolation makes both the shear and the curvature to change

$$\boldsymbol{\Gamma} = \begin{Bmatrix} \gamma_{xz} \\ \gamma_{yz} \end{Bmatrix} = \begin{Bmatrix} \theta_y + \dfrac{\partial w}{\partial x} \\ -\theta_x + \dfrac{\partial w}{\partial y} \end{Bmatrix} = \begin{bmatrix} 0 & 1 \\ -1 & 0 \end{bmatrix} \begin{Bmatrix} \theta_{xT3U2} + f_b \theta_{xb} \\ \theta_{yT3U2} + f_b \theta_{yb} \end{Bmatrix} + \begin{Bmatrix} \dfrac{\partial}{\partial x} \\ \dfrac{\partial}{\partial y} \end{Bmatrix} w_{T3U2} =$$

$$= \mathbf{B}_{\mathbf{S},T3U2}\mathbf{p}_n + \begin{bmatrix} 0 & 1 \\ -1 & 0 \end{bmatrix} \begin{Bmatrix} f_b \theta_{xb} \\ f_b \theta_{yb} \end{Bmatrix} = \mathbf{B}_{\mathbf{S},T3U2}\mathbf{p}_n + \mathbf{B}_{\mathbf{S},b}\boldsymbol{\theta}_b = \boldsymbol{\Gamma}_{T3U2} + \boldsymbol{\Gamma}_b$$

$$\boldsymbol{\kappa} = \begin{Bmatrix} \kappa_x \\ \kappa_y \\ \kappa_{xy} \end{Bmatrix} = \begin{Bmatrix} \dfrac{\partial \theta_y}{\partial x} \\ -\dfrac{\partial \theta_x}{\partial y} \\ \dfrac{\partial \theta_y}{\partial y} - \dfrac{\partial \theta_x}{\partial x} \end{Bmatrix} = \begin{bmatrix} 0 & \dfrac{\partial}{\partial x} \\ -\dfrac{\partial}{\partial y} & 0 \\ -\dfrac{\partial}{\partial x} & \dfrac{\partial}{\partial y} \end{bmatrix} \begin{Bmatrix} \theta_{xT3U2} + f_b \theta_{xb} \\ \theta_{yT3U2} + f_b \theta_{yb} \end{Bmatrix} =$$

$$= \mathbf{B}_{\mathbf{B},T3U2}\mathbf{p}_n + \begin{bmatrix} 0 & \dfrac{\partial f_{bi}}{\partial x} \\ -\dfrac{\partial f_{bi}}{\partial y} & 0 \\ -\dfrac{\partial f_{bi}}{\partial x} & \dfrac{\partial f_{bi}}{\partial y} \end{bmatrix} \begin{Bmatrix} \theta_{xb} \\ \theta_{yb} \end{Bmatrix} = \mathbf{B}_{\mathbf{B},T3U2}\mathbf{p}_n + \mathbf{B}_{\mathbf{B},b}\boldsymbol{\theta}_b = \boldsymbol{\kappa}_{T3U2} + \boldsymbol{\kappa}_b \,.$$

In the above expressions $\mathbf{B}_{\mathbf{S},T3U2}$ and $\mathbf{B}_{\mathbf{S},b}$ are shear-strain displacement matrices as before and $\mathbf{B}_{\mathbf{B},T3U2}$ and $\mathbf{B}_{\mathbf{B},b}$ are bending-strain displacement counterparts. Follows that $\boldsymbol{\Gamma}_b$ and $\boldsymbol{\kappa}_b$ are the shear-strain and bending contributions due to the enriched bubble terms in rotational fileds.

The following system of algebraic equations is derived like before:

$$\begin{bmatrix} \mathbf{K}_{\mathbf{S}w\theta} + \mathbf{K}_{\mathbf{B}w\theta} & \mathbf{K}^T_{\mathbf{S}w\theta,b} + \mathbf{K}^T_{\mathbf{B}w\theta,b} \\ \mathbf{K}_{\mathbf{S}w\theta,b} + \mathbf{K}_{\mathbf{B}w\theta,b} & \mathbf{K}_{\mathbf{S}b} + \mathbf{K}_{\mathbf{B}b} \end{bmatrix} \begin{bmatrix} \mathbf{p}_n \\ \boldsymbol{\theta}_b \end{bmatrix} = \begin{bmatrix} \mathbf{f}_{w\theta} \\ \mathbf{f}_b \end{bmatrix}, \tag{70a}$$

where $\boldsymbol{\theta}_b = \begin{Bmatrix} \theta_{xb} \\ \theta_{yb} \end{Bmatrix}$. The parts of the stiffness matrix are:

$$\mathbf{K}_{\mathbf{S}w\theta} = \int_A \left(\mathbf{B}_{\mathbf{S},T3U2}\right)^T \mathbf{D}_{\mathbf{S}} \mathbf{B}_{\mathbf{S},T3U2} dA \quad \text{and} \quad \mathbf{K}_{\mathbf{B}w\theta} = \int_A \left(\mathbf{B}_{\mathbf{B},T3U2}\right)^T \mathbf{D}_{\mathbf{B}} \mathbf{B}_{\mathbf{B},T3U2} dA$$

$$\mathbf{K}_{\mathbf{S}w\theta,b} = \int_A \left(\mathbf{B}_{\mathbf{S},b}\right)^T \mathbf{D}_{\mathbf{S}} \mathbf{B}_{\mathbf{S},T3U2} dA \quad \text{and} \quad \mathbf{K}_{\mathbf{B}w\theta,b} = \int_A \left(\mathbf{B}_{\mathbf{B},b}\right)^T \mathbf{D}_{\mathbf{B}} \mathbf{B}_{\mathbf{B},T3U2} dA$$

$$\mathbf{K}_{\mathbf{S}b} = \int_A \left(\mathbf{B}_{\mathbf{S},b}\right)^T \mathbf{D}_{\mathbf{S}} \mathbf{B}_{\mathbf{S},b} dA \quad \text{and} \quad \mathbf{K}_{\mathbf{B}b} = \int_A \left(\mathbf{B}_{\mathbf{B},b}\right)^T \mathbf{D}_{\mathbf{B}} \mathbf{B}_{\mathbf{B},b} dA$$

Again, to satisfy the zero shear condition over a patchwork of elements, the following should vanish:

$$\left(\mathbf{K}_{\mathbf{S}w\theta,b} + \mathbf{K}_{\mathbf{B}w\theta,b}\right)\mathbf{p}_n + \left(\mathbf{K}_{\mathbf{S}b} + \mathbf{K}_{\mathbf{B}b}\right)\boldsymbol{\theta}_b = \mathbf{0}\,. \tag{70b}$$

As before $\boldsymbol{\theta}_b$ is equal to zero, if $\left(\mathbf{K}_{\mathbf{S}b} + \mathbf{K}_{\mathbf{B}b}\right)$ is invertible an if

$$\left(\mathbf{K}_{\mathbf{S}w\theta,b} + \mathbf{K}_{\mathbf{B}w\theta,b}\right)\mathbf{p}_n = \mathbf{0}\,,$$

i.e. $\left(\mathbf{K}_{\mathbf{S}w\theta,b} + \mathbf{K}_{\mathbf{B}w\theta,b}\right)\mathbf{p}_n =$

$$= \left(\int_A \begin{bmatrix} 0 & f_b \\ -f_b & 0 \end{bmatrix}^T \mathbf{D}_{\mathbf{S}} \mathbf{B}_{\mathbf{S},T3U2} dA + \int_A \begin{bmatrix} 0 & \frac{\partial f_b}{\partial x} \\ -\frac{\partial f_b}{\partial y} & 0 \\ -\frac{\partial f_b}{\partial x} & \frac{\partial f_b}{\partial y} \end{bmatrix}^T \mathbf{D}_{\mathbf{B}} \mathbf{B}_{\mathbf{B},T3U2} dA \right) \cdot \mathbf{p}_n = 0$$

The first part of the sum is obviously equal to zero for any bubble function f_b since $\boldsymbol{\Gamma}_{T3U2} = \mathbf{B}_{\mathbf{S},T3U2}\mathbf{p}_n = \mathbf{0}$, but the second part will be zero only if the folowing condition on the function f_b is satisfied:

$$\begin{bmatrix} 0 & \int_A \frac{\partial f_b}{\partial x} dA \\ -\int_A \frac{\partial f_b}{\partial y} dA & 0 \\ -\int_A \frac{\partial f_b}{\partial x} dA & \int_A \frac{\partial f_b}{\partial y} dA \end{bmatrix} = 0, \tag{71}$$

since $\mathbf{D}_\mathbf{B}\boldsymbol{\kappa}_{T3U2} = const$. In other words the conditions on f_b are

$$\int_A \frac{\partial f_b}{\partial x} dA = 0 \quad \text{and} \quad \int_A \frac{\partial f_b}{\partial y} dA = 0. \tag{72}$$

As before, more pairs of bubble functions can be chosen to enrich the rotations θ_x and θ_y if they satisfy the condition (72) and if they are of quadratic order of higher, because the basic interpolation for rotations is linear (Lagrangean).

7.1. Bubble-enriched three-node triangle

According to the conditions derived, a set of bubble functions, together with the associated bubble parameters can be generated to enrich the basic linked interpolation of *T3U2* element. This bubble functions must be of the greater polynomial order then the basic ones, so increasing the order by one we can take:

$$w = w_{T3U2} - \frac{2}{3}\xi_1\xi_2(\xi_2 - \xi_1)w_{b1} - \frac{2}{3}\xi_2\xi_3(\xi_3 - \xi_2)w_{b2} - \frac{2}{3}\xi_3\xi_1(\xi_1 - \xi_3)w_{b3} + \frac{2}{3}\xi_1\xi_2\xi_3 w_{b4}\,, \tag{73}$$

to complete the full form of a third order polynomial in the displacement field. The rotations of the basic element can be enriched using

$$\theta_x = \theta_{xT3U2} + (4\xi_1\xi_2 + 4\xi_2\xi_3 + 4\xi_3\xi_1)\theta_{xb5} + 27\xi_1\xi_2\xi_3\theta_{xb7}$$

$$\theta_y = \theta_{yT3U2} + (4\xi_1\xi_2 + 4\xi_2\xi_3 + 4\xi_3\xi_1)\theta_{yb6} + 27\xi_1\xi_2\xi_3\theta_{yb8}\,, \tag{74}$$

to satisfy condition (72) in quadratic polynomial order and to enrich it with the cubic term as it was done with Auricchio-Taylor‘s triangle element *T3BL*. Coefficients associated with bubble functions are retained to resemble higher order functions of *T6-U3* element. Even higher order terms can be added in both, displacement and rotational field.

7.2. Patch tests

The patch test from Section 5.5, for constant moment condition (zero shear state) is obviously satisfied with all combinations of bubble functions used to enrich the basic triangle element, because the new elements are developed to satisfy this condition. The results from Table 1 of Section 6 along with the results for the bubble-enriched elements are given in Table 21.

Table 21: The patch test results for the triangular elements (control deformation at point 1: w_1, see Fig.18)

Elements	*Patch test for zero shear*			*Patch test for non-zero constant shear*		
	h=1.0	*h=0.01*	*result*	*h=1.0*	*h=0.01*	*result*
T3-U2	0.5414000	0.5414000	pass	-0.2455871	0.000318188	fail
T3-U2+2bub	0.5414000	0.5414000	pass	-0.2455697	0.000198963	fail
T3-U2+6bub	0.5414000	0.5414000	pass	-0.2453268	0.000227389	fail
T3-U2+8bub	0.5414000	0.5414000	pass	-0.2450938	0.000131686	fail
T6-U3	0.5414000	0.5414000	pass	-0.2450933	0.000215467	pass
T10-U4	0.5414000	0.5414000	pass	-0.2450933	0.000215467	pass
Analytical solution	0.5414	0.5414		-0.245093333	0.000215467	

7.3. Clamped square plate

The example of Section 5.6.1 is numerically analysed with various number of bubble terms added to the basic T3-U2 triangular element and results are presented in Tables 21 and 22. The results should be compared with the corresponding results from Table 3b and 4b.

Table 21: Clamped square plate: displacement and moment at the centre with mesh pattern b), *L/h = 10.*

Element	*T3-U2+3 bubbles on w*		*T3-U2+2 bubbles on θx and θy*		*T3-U2+6 bubbles*		*T3-U2+8 bubbles*	
mesh	*w**	*M**	*w**	*M**	*w**	*w**	*w**	*M**
1x1	0.069500	-					0.069500	0.000
2x2	0.255266	1.843	0.117795	1.89529	0.190160	2.347	0.255266	1.866
4x4	0.201662	2.317	0.144223	2.26204	0.174075	2.585	0.201662	2.251
8x8	0.165679	2.337	0.149040	2.30613	0.157546	2.439	0.165679	2.302
16x16	0.154444	2.329	0.150118	2.31601	0.152318	2.356	0.154444	2.315
32x32	0.151471	2.324	0.150379	2.31893	0.150934	2.330	0.151471	2.319
64x64	0.150716	2.321	0.150442	2.31972	0.150581	2.322	0.150716	2.320
Ref. sol. [11]	0.150191		0.150191		0.150191		0.150191	

Reprint of Table 3b: Clamped square plate: displacement and moment at the centre using mesh pattern b), *L/h= 10*

Element	*T3-U2 =MIN3*		*T6-U3*		*T10-U4*	
mesh	*w**	*M**	*w**	*M**	*w**	*M**
1x1	0.023810	-	0.133334	3.31099	0.150650	2.29043
2x2	0.107572	1.67455	0.150247	2.63888	0.150386	2.31564
4x4	0.141724	2.20593	0.150447	2.39797	0.150455	2.31955
8x8	0.148406	2.29114	0.150458	2.33941	0.1504622	2.31996
16x16	0.149959	2.31216	0.1504621	2.32486	0.1504626	2.31998
32x32	0.150339	2.31796	0.1504625	2.32121		
64x64	0.150432	2.31948				
Ref. sol. [37]	0.150191		0.150191		0.150191	

Table 22: Clamped square plate: displacement and moment at the centre with mesh pattern b), *L/h = 1000.*

Element	*T3-U2+4 bubbles on w*		*T3-U2+2 bubbles on θx and θy*		*T3-U2+6 bubbles*		*T3-U2+8 bubbles*	
mesh	*w**	*M**	*w**	*M**	*w**	*w**	*w**	*M**
1x1								
2x2	0.000088	0.00173	0.000100	0.00196	-0.002356		-0.002770	0.0069
4x4	0.002803	0.06056	0.002259	0.04371	0.004719	-	0.004595	0.0098
8x8	0.042227	0.8621	0.030990	0.58596	0.054766	0.9689	0.054734	1.040
16x16	0.113035	2.254	0.105644	2.12630	0.116354	2.186	0.116365	2.278
32x32	0.125597	2.312	0.124889	2.32005	0.125810	2.269	0.125834	2.306
64x64	0.126449	2.292	0.126408	2.29411	0.126511	2.267	0.126535	2.294
Ref. sol. [11]	0.126532	2.29051	0.126532	2.29051	0.126532	2.29051	0.126532	2.29051

Reprint of Table 4b: Clamped square plate: displacement and moment at the centre using mesh pattern b), *L/h = 1000.*

Element	*T3-U2 = MIN3*		*T6-U3*		*T10-U4*	
mesh	*w**	*M**	*w**	*M**	*w**	*M**
1x1			0.000069	0.00206	0.130198	4.05972
2x2	0.000062	0.00127	0.097869	2.03760	0.126738	2.74752
4x4	0.001793	0.03807	0.121256	2.44562	0.126527	2.34533
8x8	0.028267	0.55913	0.125905	2.38599	0.1265340	2.29246
16x16	0.104428	2.12079	0.1265121	2.31332	0.1265344	2.29055
32x32	0.124820	2.32200	0.1265341	2.29420		
64x64	0.126403	2.29435				
Ref. sol. [11]	0.126532	2.29051	0.126532	2.29051	0.126532	2.29051

While for the relatively thick clamped plate model, the new elements do not show

improvement, better behavior can be observed for the thin counterpart even if only a few bubbles are involved.

7.4. Simply supported skew plate

The example of Section 5.6.3 is also numerically analysed with enriched basic T3-U2 triangular element and the results are presented in Tables 23 and 24. The results should be compared with the corresponding results from Tables 12a and 13a.

Table 23: Simply supported skew plate (SS1): displacement and moment at the centre with regular meshes, *L/h = 100.* Mesh pattern a).

Element	*T3-U2+ 4 bubbles on w + 4 bubbles on θ*		
mesh	w^*	M_{22}^*	M_{11}^*
2x2	0.4810901	0.6757	1.407
4x4	0.4446013	1.007	1.803
8x8	0.4469407	1.159	1.982
16x16	0.4402608	1.154	1.982
24x24	0.4356977	1.153	1.976
32x32	0.4328037	1.152	1.972
48x48	0.4294810	1.1529	1.9675
Ref. [39]	0.423		

Reprint of Table 12a: Simply supported skew plate (SS1): displacement and moment at the centre with regular meshes, *L/h = 100.* Mesh pattern a).

Element	*T3-U2 =MIN3*			*T6-U3*			*T10-U4*		
mesh	w^*	M_{22}^*	M_{11}^*	w^*	M_{22}^*	M_{11}^*	w^*	M_{22}^*	M_{11}^*
2x2	0.425288	0.65647	1.35584	0.442337	1.59547	2.48908	0.259711	0.67991	1.29292
4x4	0.393156	1.00823	1.72050	0.391393	1.38415	2.10533	0.410136	1.17851	1.92258
8x8	0.376569	1.11747	1.84630	0.409028	1.18349	1.96100	0.419818	1.12774	1.94013
16x16	0.403524	1.09072	1.87753	0.419769	1.13814	1.95024	0.423207	1.13774	1.95080
24x24	0.412799	1.10360	1.92291	0.422181	1.13934	1.95222			
32x32	0.416390	1.11361	1.93165						
48x48	0.419306	1.12368	1.93948						
Ref. [39]	0.423			0.423			0.423		

Table 24: Simply supported skew plate (SS1): displacement and moment at the centre with regular meshes, *L/h = 1000*. Mesh pattern a).

Element	*T3-U2 + 2 bubbles on θ*			*T3-U2 + 3 bubbles on w*			*T3-U2+ 4 bubbles on w + 2 bubbles on θ*		
mesh	w^*	M_{22}^*	M_{11}^*	w^*	M_{22}^*	M_{11}^*	w^*	M_{22}^*	M_{11}^*
2x2									
4x4	0.394037	1.0176	1.6705	0.393946	1.017	1.671			
8x8	0.307325	1.1218	1.5932	0.308300	1.110	1.610	0.331507	1.154	1.677
16x16	0.296483	1.1266	1.6596	0.296772	1.037	1.628	0.353312	1.293	1.846
24x24	0.321440	1.1303	1.7299	0.321833	1.020	1.703	0.374427	1.195	1.869
32x32	0.341737	1.0623	1.7599	0.342898	0.9862	1.745	0.388913	1.106	1.873
48x48	0.369785	0.9909	1.8031	0.370433	0.9737	1.802	0.403554	1.082	1.896
Ref. [38]	0.4080	1.08	1.91	0.4080	1.08	1.91	0.4080	1.08	1.91

Element	*T3-U2+ 4 bubbles on w + 4 bubbles on θ*		
mesh	w^*	M_{22}^*	M_{11}^*
2x2	0.419517	0.645	1.342
4x4	0.394242	1.015	1.676
8x8	0.335814	1.172	1.710
16x16	0.358933	1.319	1.866
24x24	0.378839	1.2161	1.8842
32x32	0.392434	1.1223	1.8849
48x48	0.406097	1.0939	1.9047
Ref. [38]	0.4080	1.08	1.91

Reprint of Table 13a: Simply supported skew plate (SS1): displacement and moment at the centre with regular meshes, *L/h = 1000*. Mesh pattern a).

Element	*T3-U2 = MIN3*			*T6-U3*			*T10-U4*		
mesh	w^*	M_{22}^*	M_{11}^*	w^*	M_{22}^*	M_{11}^*	w^*	M_{22}^*	M_{11}^*
2x2	0.421115	0.64790	1.33819	0.443104	1.62431	2.52722	0.246108	0.60215	1.16324
4x4	0.393999	1.01757	1.67013	0.348698	1.30423	1.98429	0.356469	1.05704	1.76663
8x8	0.305318	1.11745	1.58532	0.326564	0.86335	1.71994	0.365434	0.95047	1.78325
16x16	0.285607	1.05519	1.61422	0.358165	0.97179	1.80192	0.390331	1.02111	1.85543
24x24	0.309866	1.05211	1.68162	0.376441	0.99480	1.82813			
32x32	0.330657	1.00984	1.72183						
48x48	0.360440	0.96062	1.77377						
Ref. [38]	0.4080	1.08	1.91	0.4080	1.08	1.91	0.4080	1.08	1.91

Again for the thick skew plate model, the new elements do not show much improvement (the convergence is equal as for the basic model, but coming from the upper side). For the thin skew plate, however, better behavior can be observed even for just a few bubbles involved and convergence is better than with the higher-order elements.

8. Conclusions

A displacement-based linked-interpolation concept for designing triangular and quadrilateral Mindlin plate and facet shell finite elements has been presented and numerically verified. The idea has been presented in its general form applicable to elements of any order, but the numerical results have been provided for the first three elements of the family, i.e. the three-, six- and ten-node triangular and four-, nine- and sixteen-node quadrilateral plate elements. In all the elements from the family the leading design principle is borrowed from the underlying family of Timoshenko beam elements. Thus the original shear strain condition of a certain order imposed along the beam has been applied to the plate element edges leading to 2D generalisation of the beam-type linked interpolation for the displacement field, whereby, both nodal rotations contribute to the element out-of-plane displacements. Unlike Timoshenko's beam element, the resulting solutions are just approximations to the true solution problem.

It has been shown that, for the triangular elements with more than two nodes per side, additional internal degrees of freedom are required in order to provide full polynomial expansion of certain order. The number of these degrees of freedom is linearly growing by one, beginning with no internal degrees of freedom for the lowest-order three-node member of the family. For quadrilaterals, the number of bubble terms in displacement field is always one. The elements developed in this way give exact result for cylindrical bending of a corresponding order, e.g. quadratic distribution of

the out-of-plane displacements for the two-nodes-per-side elements, cubic for the three-nodes-per-side elements and so on. However, in contrast to beams, the developed elements still suffer from shear-locking for very coarse meshes of the lowest-order element types.

Performance of these elements has been numerically analysed and it has been found out that they perform well for a number of standard benchmark tests. It has to be stressed, however, that the well-known Morley's skewed plate example turns out to be rather demanding. For this test, the proposed design principle cannot compete with the mixed-type approach. Otherwise, the higher-order members of the element family turn out to be successful when compared to the lower-order elements from literature for the problems with the same total number of the degrees of freedom.

When applied to shell models, these elements also perform competitively for a number of standard benchmark tests as the finite-element mesh is refined. Especially good performance can be observed for spatially folded plate models with significant thickness and dominant bending-shear effects over the membrane deformations. In general, as for the thick plates, for this kind of structures the higher order elements perform better then the low order ones.

On the other hand, for geometrically curved models, especially for double curved thin shells, presented elements have difficulty to converge as fast as the standard shell elements and the higher order elements, can not adapt to the actual curved model geometry with their inner nodes, so results of their performance is poorer then that of the basic three-node triangle or four-node quadrilateral. This difficulty can be

overcome if the higher order elements are designed as full shell elements.

Improvement of basic elements in the family may be achieved by adding higher-order bubble functions to the basic interpolation that pass the constant moment patch test. Both triangles with three nodes and quadrilaterals with four nodes can be enriched in this way. Excellent results are achieved for the thin limit situations on model plates, but improvements in the thick situations are not noticeable.

9. References

[1] O.C. Zienkiewicz, R.L. Taylor, *The Finite Element Method for Solid and Structural Mechanics,* Elsevier Butterworth-Heinemann, Oxford, 2005.

[2] A. Ibrahimbegović, *Quadrilateral finite-elements for analysis of thick and thin plates*, Computer Methods in Applied Mechanics and Engineering, **110**: 195-209, 1993.

[3] F. Auricchio, R.L. Taylor, *A shear deformable plate element with an exact thin limit*, Computer Methods in Applied Mechanics and Engineering, **118**: 393-412, 1994.

[4] C. Chinosi, F. Lovadina, *Numerical analysis of some mixed finite element methods for Reissner-Mindlin plate,* Computational Mechanics **16**: 36-44, 1995.

[5] F. Auricchio, C. Lovadina, *Analysis of kinematic linked interpolation methods for Reissner-Mindlin plate problem*, Computer Methods in Applied Mechanics and Engineering **190**: 2465-2482, 2001.

[6] R.L. Taylor, S. Govindjee, *A quadratic linked plate element with an exact thin plate limit,* Report No. UCB/SEMM-2002/10, University of California at Berkeley, Department of Civil and Environmental Engineering, Berkeley, 2002.

[7] F. Auricchio, R.L. Taylor, *A new family of quadrilateral thick plate finite elements based on linked interpolation*, Report No. UCB/SEMM-93/10, University of California at Berkeley, Department of Civil Engineering, Berkeley, 1993.

[8] Y.J. Liu, H.R Riggs, *The MIN-N family of pure-displacement, triangular, Mindlin plate elements,* Structural Engineering and Mechanics **19:** 297-320, 2005.

[9] S. de Miranda, F. Ubertini, *A simple hybrid stress element for shear deformable plates,* International Journal for Numerical Methods in Engineering **65**: 808-833, 2006.

[10] M.A. Crisfield, *Finite Elements and Solution Procedures for Structural Analysis,* Pineridge Press, Swansea, 1986.

[11] O.C. Zienkiewicz, Z. Xu, L.F. Zeng, A. Samuelsson, N.E. Wiberg, *Linked interpolation for Reissner-Mindlin plate elements: Part I - A simple quadrilateral,* International Journal for Numerical Methods in Engineering **36**: 3043-3056, 1993.

[12] R.L. Taylor, F. Auricchio, *Linked interpolation for Reissner-Mindlin plate elements: Part II - A simple triangle,* International Journal for Numerical Methods in Engineering **36**: 3057-3066, 1993.

[13] Z. Xu, O.C. Zienkiewicz, L.F. Zeng, *Linked interpolation for Reissner-Mindlin plate elements: Part III - An alternative quadrilateral*, International Journal for Numerical Methods in Engineering **37**: 1437-1443, 1994.

[14] W.J. Chen, Y.K. Cheung, *Refined quadrilateral element based on Mindlin/Reissner plate theory,* International Journal for Numerical Methods in Engineering **47**: 605-627, 2000.

[15] W.J. Chen, Y.K. Cheung, *Refined 9-dof triangular Mindlin plate elements*, International Journal for Numerical Methods in Engineering **51**: 1259-1281, 2001.

[16] W.J. Chen, Y.K. Cheung, *Refined discrete quadrilateral degenerated shell element by using Timoshenko's beam function,* International Journal for Numerical Methods in Engineering **63**: 1203-1227, 2005.

[17] A. Tessler, S.B. Dong, *On a hierarchy of conforming Timoshenko beam elements,* Computers and Structures **14:** 335-344, 1981.

[18] G. Jelenić, E. Papa, *Exact solution of 3D Timoshenko beam problem using linked interpolation of arbitrary order,* Archive of Applied Mechanics 18: 171-183, 2011.

[19] J. Przemieniecki, *Theory of Matrix Structural Analysis*, McGraw-Hill, New York, 1968.

[20] J. Rakowski, *The interpretation of the shear locking in beam elements*, Computers and Structures **37**: 769-776, 1990.

[21] L. Yunhua, *Explanation and elimination of shear locking and membrane locking with field consistence approach*, Computer Methods in Applied Mechanics and Engineering **162**: 249-269, 1998.

[22] J.N. Reddy, *On locking-free shear deformable beam finite elements*, Computer Methods in Applied Mechanics and Engineering **149**: 113-132, 1997.

[23] S. Mukherjee, J.N. Reddy, C.S. Krishnamoorthy, *Convergence properties and derivative extraction of the superconvergent Timoshenko beam finite element*, Computer Methods in Applied Mechanics and Engineering **190**: 3475-3500, 2001.

[24] A. Tessler, T.J.R. Hughes, *A three-node Mindlin plate element with improved transverse shear*, Computer Methods in Applied Mechanics and Engineering **50**: 71-101, 1985.

[25] J.C. Simo, M.S. Rifai, *A class of mixed assumed-strain methods and the method of incompatible modes,* International Journal for Numerical Methods in Engineering **29**: 1595-1638, 1990.

[26] T.J.R. Hughes, *The Finite Element Method. Linear Static and Dynamic Finite Element Analysis,* Dover Publications inc., Mineola, New York, 2000.

[27] S. Timoshenko, S. Woinowsky-Krieger, *Theory of plates and shells,* McGraw-Hill, London, 1959.

[28] Z. Zhu, *A thick-thin triangular plate element,* International Journal for Numerical Methods in Engineering **33:** 963-973, 1992.

[29] D. Ribarić, G. Jelenić, *Higher-order linked interpolation in quadrilateral thick plate finite elements*, Finite Elements in Analysis and Design **51**: 67-80, 2012.

[30] F. Auricchio, R.L. Taylor, *A triangular thick plate finite element with an exact thin limit,* Finite Elements in Analysis and Design **19**: 57-68, 1995.

[31] C.M. Wang, J.N. Reddy, K.H. Lee, *Shear deformable beams and plates,* Elsevier, Oxford, 2000.

[32] K.J. Bathe, *Finite Element Procedures,* Prentice Hall, New Jersey, 1989.

[33] O.C. Zienkiewicz, R.L. Taylor, J.Z. Zhu, *The Finite Element Method. Its Basis and Fundamentals,* Elsevier Butterworth-Heinemann, Oxford, 2005.

[34] W.J. Chen, *Enhanced patch test of finite element methods*, Science in China, Series G: Physics, Mechanics & Astronomy, Vol. **49**, No 2, 213-227, 2006.

[35] W.J. Chen, J.Z. Wang & J.Zhao, *Functions for patch test in finite element analysis of the Mindlin plate and the thin cylindrical shell*, Science in China, Series G: Physics, Mechanics & Astronomy, Vol. **52**, No 5, 762-767, 2009.

[36] F. Kikuchi, K. Ishii, *An improved 4-node quadrilateral plate bending element of the Reissner-Mindlin type,* Computer Methods in Applied Mechanics and Engineering **195**: 3448-3460, 2006.

[37] K. Naumenko, J. Altenbach, H. Altenbach, V.K. Naumenko, *Closed and approximate analytical solution for rectangular Mindlin plates*, Acta Mechanica 147 (2001): 153-172.

[38] L.S.D. Morley, *Bending of simply supported rhombic plate under uniform normal loading*, Quarterly Journal of Mechanics and Applied Mathematics Vol. **15**, 413-426, 1962.

[39] I. Babuška, T. Scapolla, *Benchmark computation and performance evaluation for a rhombic plate bending problem,* International Journal for Numerical Methods in Engineering **28:** 155-179, 1989.

[40] R.H. MacNeal, R.L. Harder, *A proposed standard set of problems to test finite element accuracy,* Finite Elements in Analysis and Design 1 (1985): 2-20.

[41] T.J.R. Hughes, T.E. Tezduyar, *Finite elements based upon Mindlin plate theory with particular reference to the four-node bilinear isoparametric element*. Journal of Applied Mechanics **48**: 587-596, 1981.

[42] *M.A. Crisfield, A quadratic Mindlin element using shear constraints, Computers and Structures **18:** 833-852, 1984.*